Report No. 172 / UILU ENG-95-4056

F. E. M. Study of Fatigue Crack Growth and Closure Under Double Slip

by

Kenneth Allen Gall

B.S., University of Illinois at Urbana-Champaign, 1995

THESIS

**Submitted in partial fulfillment of the requirements
for the degree of Master of Science in Mechanical Engineering
in the Graduate College of the
University of Illinois at Urbana-Champaign, 1996**

Urbana, Illinois

Acknowledgments

The research was supported by the Fracture Control Program, Department of Mechanical and Industrial Engineering, College of Engineering, University of Illinois at Champaign-Urbana. The computer simulations were run on the SGI Power Challenge Computer (ODIN) through grants from the National Center for Supercomputing Applications, University of Illinois.

Great appreciation is expressed to my advisor, Professor Huseyin Sehitoglu. His guidance and motivation proved to be infinitely valuable in obtaining my Masters of Science. Thanks are also given to Dr. Yavuz Kadioglu for his work on the formulation of the finite element code and his helpful discussions.

The work herein is dedicated to my parents. Without their support, I would not have advanced to this point in my studies.

Table of Contents

List of Figures

1. Introduction

1.1 Background

Over a period extending some 20 years following the discovery of crack closure by Elber [1971] in the early 70's, researchers have laid down a solid foundation for the understanding of closure mechanisms and implications. It is well understood that closure reduces the stress intensity range at the tip of a growing fatigue crack through premature crack face contact. There are several mechanisms that can cause this premature crack face contact. Currently, the premature contact of crack surfaces is grouped under several primary categories: (1) Plasticity-Induced Closure [Elber 1971], (2) Roughness-Induced Closure [Adams 1972], (3) Oxide-Induced closure [Ritchie et al. 1980], and (4) Transformation-Induced Closure. The actual closure level of a particular crack is governed by a combination of one or more of these mechanisms. However, in this analysis, only plasticity induced closure will be modeled.

Crack closure results have provided justification for a wide array of fatigue crack growth phenomenon such as overload effects, fatigue thresholds, stress ratio effects, short crack behavior, and material effects. In recent studies, much attention has been given to the behavior of microstructurally short cracks. Since short cracks lie within single grains, or several grains, their behavior is highly dependent on the microstructure. This dependence on microstructure causes some exclusive phenomenon to occur in short crack growth. Along with others, Morris [1977] has documented that closure in short cracks, or micro cracks, does occur. Closure in micro cracks has been deemed responsible for variability in short crack fatigue crack growth rates, increased short crack growth rates, and growth below the long crack stress intensity threshold [Morris 1977, Morris and James 1983, De Los Rios et al. 1985, Tokaji et al. 1987, Liaw 1988, Larson et al. 1988, Lee and Sharpe 1988, Tanaka 1989, Miller 1991]. The variability in growth rates is attributed to different closure levels for different grain orientations and "grain boundary" effects, while the latter effects are seen because short cracks have lower opening levels than long cracks at the same applied stress intensity.

1.2 Current Needs

As a crack propagates through a material it travels through hundreds of grains, or single crystals, with different orientations. Each time the crack passes through a particular grain, it may respond differently. One grain may allow the crack to pass through quickly while another will inhibit growth severely. This difference in growth rates arises because of the anisotropic behavior of single grains. Grains with different orientations may cause cracks to experience different degrees of crack tip plasticity, crack tip opening displacement (C.O.D.), and closure. Since long cracks pass through many grains, and their crack tip plastic zones span several grains, the effects of individual grains may be ignored. A continuum approach may be readily used to describe this type of growth. Previous isotropic finite element analyses which have ignored the effect of microstructure have done an excellent job matching experimental crack growth results [McClung and Davidson, 1991]. However when the crack length or plastic zone are on the order of the grain size, the microstructural effects can no longer be ignored. McClung et al. [1991] recognized this problem in their results when they found that a finite element simulation of short cracks under predicted the strain ranges behind the crack tip for an experimental short crack. For that matter, the results of any finite element model of microstructurally short cracks which does not account for microstructural phenomenon may be suspect.

To properly model cracks on the order of the grain size, one needs to consider the anisotropic behavior of single grains. Within the single crystal framework, elastic and plastic deformation are highly directional. Plastic flow, or slip, is only allowed on certain planes. This constraint becomes particularly important at the crack tip where plastic flow causes crack advance and plasticity induced closure. To form a valid finite element model, plasticity must be constrained to certain planes. It should be noted that it is not only important to consider this anisotropic behavior when modeling "short cracks". If the grain size is sufficiently large, as in single grained materials, single crystal properties will have to be considered in long cracks also. The crack length and plastic zone with *respect to the grain size* are the important factors here. A finite element simulation which implements single crystal constitutive relationships can help explain the "short crack" growth rates, and variability. Additionally, since both short and long fatigue

cracks propagate through grains, this type of modeling can give insight into the propagation mechanisms involved in both types of cracks.

1.3 Scope of Present Study

To study the effect of crack closure on cracks influenced by microstructure, a double slip finite element program which models plasticity induced crack closure will be used here. Asaro and coworkers [1978, 1983, 1991] have laid down much of the foundation into the modeling of single crystal microstructures to be used here. The elastic-plastic finite element crack growth simulation program, originally written by Lalor [1986] and updated by Sehitoglu and McClung [1989 I-II], has been converted into a double slip finite element simulation. The double slip finite element model uses elastic and plastic constitutive equations which account for the directionality of elastic deformation and plastic flow, or dislocation motion, in single crystals. Using these laws, the finite element mesh is modeled as a single cracked grain with microscopic slip constrained along two directions. As in a real fatigue crack, [McEvily 1963, Laird 1967, Tomkins 1968, Pelloux 1969, Neumann 1974] slip in the model occurs along two planes emanating from the crack tip. The orientation of the crystal, or the angle between the microscopic slip planes can both be varied to model different grain orientations or materials. This allows one to observe the dependence of closure levels and fatigue crack growth parameters on grain orientation and slip plane direction. Doing so will help one more realistically model the crack tip behavior of short and long fatigue cracks with "small" plastic zones, and properly explain the variability in short fatigue crack growth rates. When compared to experimental results, this information will prove to be extremely valuable.

2. *Single Crystal Behavior Constitutive Law Formulation*

2.1 Background

All solid materials have some degree of ordered structure. This order, or arrangement of atomic particles, is referred to as a crystal structure. Crystalline structures are usually defined using unit cells, see Figure 1. Each unit cell is a repeated arrangement of atoms interlocking in the same way, and having the same orientation. Most engineering metals have

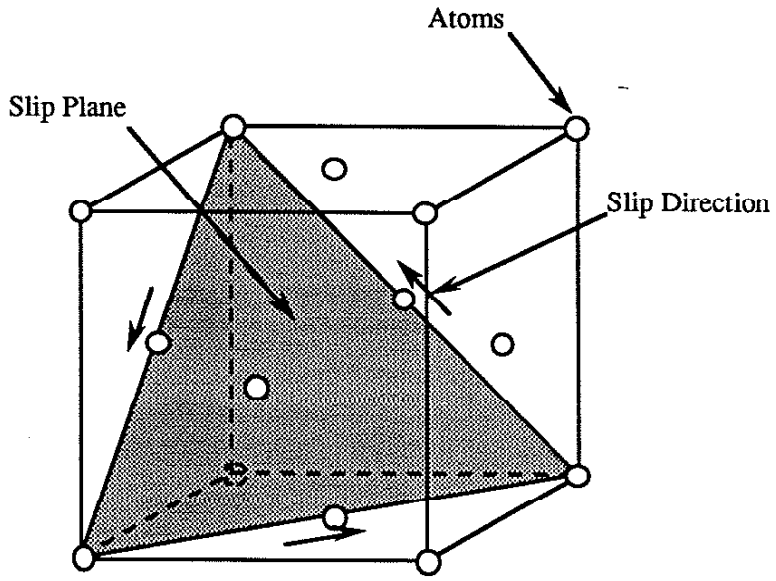

Figure 1: Diagram of an FCC slip system. The slip plane is a {111} plane while the three slip directions are <110> types. Dislocation motion primarily occurs along the drawn directions.

one of three unit cell structures; body-centered-cubic, face-centered-cubic, or hexagonal-close-packed. The properties of all of these structures depend on the direction of measurement, or orientation of the crystal. Hence, single crystals behave anisotropically.

A given portion of material with one crystal structure and oriented in only one direction, is also referred to as a grain. Some, but not all, of the materials used in engineering applications are multi-granular. These multi-granular, or polycrystalline, materials have many small grains with different

orientations joined together by grain boundaries. On the macroscopic level these materials behave isotropically. However, if one is concerned with highly localized behavior this is not the case. Within a grain the material behaves anisotropically. Considering this behavior is important when one is analyzing microscopic phenomenon such as short crack growth in fatigue. Since these cracks have plastic zones on the order of the grain size, they grow through highly anisotropic mediums. The stress strain behavior of single crystals cannot be described using isotropic methods. Different methods, which account for directional microstructural phenomenon must be considered. It is interesting to note that single crystals exhibit some of the same stress-strain behavior as polycrystalline materials. Namely, elastic deformation, yielding, and hardening.

2.2 Elastic Behavior

When a crystal is stressed in it's elastic region, the relationship between stresses and strains is linear, or Hookean. As in isotropic materials, elastic deformation in single crystals is recoverable. Elastic deformation is the stretching of atomic bonds, without breaking them or causing dislocation motion. There are simple relationships developed to relate stresses and strains for single crystals in the elastic region. Assuming shear stress symmetry, the stress and strain tensors (σ_{ij} and ε_{ij}) can be written as;

$$\sigma_{ij} = \begin{pmatrix} \sigma_{11} & \sigma_{12} & \sigma_{13} \\ . & \sigma_{22} & \sigma_{23} \\ . & . & \sigma_{33} \end{pmatrix} \qquad \varepsilon_{ij} = \begin{pmatrix} \varepsilon_{11} & \varepsilon_{12} & \varepsilon_{13} \\ . & \varepsilon_{22} & \varepsilon_{23} \\ . & . & \varepsilon_{33} \end{pmatrix}$$

For plane strain, $\varepsilon_{13}, \varepsilon_{23}$, and ε_{33} are equal to zero. The stresses can be related to the strains through the compliance matrix, [S], while the strains can be related to the stresses through the stiffness matrix, [C]. In equation form;

$$\varepsilon_{ij} = S_{ijkl}\sigma_{kl} \qquad \text{or} \qquad \sigma_{ij} = C_{ijkl}\varepsilon_{kl} \qquad (1,2)$$

The general [S] and [C] matrices have 36 components. However, the number of constants can be reduced to three using strain energy arguments and crystal

symmetry. For a cubic unit cell structure (BCC or FCC), with the primary loading axis oriented in the [100] direction, we have;

$$[C]=\begin{pmatrix} C_{11} & C_{12} & C_{12} & 0 & 0 & 0 \\ . & C_{11} & C_{12} & 0 & 0 & 0 \\ . & . & C_{11} & 0 & 0 & 0 \\ . & . & . & C_{44} & 0 & 0 \\ . & . & . & . & C_{44} & 0 \\ . & . & . & . & . & C_{44} \end{pmatrix}$$

This matrix can be numerically inverted to find the [S] matrix. For this analysis, the elastic relationship will also have three values in the unrotated coordinate system.

2.3 Plastic Behavior

The plastic behavior of single crystals is much more complicated than it's elastic counterpart. Plastic deformation in a single crystal is primarily the movement of dislocations (defects) within the crystal lattice [Hosford, 1993]. These dislocations usually move on certain planes, called slip planes, in the crystal when a sufficient stress is applied to the crystal. The slip planes are the closest packed crystallographic planes. Figure 1 demonstrates this concept. One can see that along the drawn slip directions, the atoms are very close together. When a stress tensor is applied to this FCC crystal, dislocation movement will occur along one of these three directions, or on one of it's 9 counterparts. A "slip system" is the combination of a slip plane and a slip direction. Each slip plane can form several slip systems with characteristic unit vectors **m** and **s**. The vector along the slip direction is denoted **s**, while **m** is the unit normal to the slip plane. As dislocations move along prescribed planes, they begin to pile up at obstacles like grain boundaries. This accumulation of dislocations is the microstructural cause of work hardening. It is also possible for dislocations to move from one slip plane to another slip plane when encountering motion inhibiting obstacles. This process is know as cross slip, and will not be considered in this modeling. Experimental evidence indicates that the effects of cross slip are small. The only type of plastic deformation permitted here will be Schmid law deformation.

The Schmid law states that plastic deformation will occur on a certain slip plane when the resolved shear stress, $\lambda^{(\alpha)}$, on that particular plane exceeds the critical resolved shear stress of the material, λ_o. The resolved shear stress on any given slip system in the crystal is given by:

$$\lambda^{(\alpha)} = P^{(\alpha)}:\sigma \tag{3}$$

Where $P^{(\alpha)}:\sigma$ is shorthand for $P_{ji}^{(\alpha)}\sigma_{ij}$, σ is the applied stress tensor, and P is the Schmid orientation tensor defined as:

$$P_{ij}^{(\alpha)} = \frac{1}{2}\left(m_i^{(\alpha)}s_j^{(\alpha)} + s_i^{(\alpha)}m_j^{(\alpha)}\right) \tag{4}$$

Once this resolved shear stress reaches the critical value, plastic flow will begin. The incremental magnitude of plastic flow can be calculated with the following expression:

$$\dot{\gamma}^{(\alpha)} = \frac{\dot{\lambda}^{(\alpha)}}{h} \tag{5}$$

If more that one slip system is active, then the rate of flow stress on an active slip system can be written as:

$$\dot{\lambda}^{(\alpha)} = \sum_{\beta=1}^{N} h^{(\alpha\beta)}\dot{\gamma}^{(\beta)} \tag{6}$$

Where N is the number of active slip systems and $h^{(\alpha\beta)}$ is the hardening modulus matrix.

2.4 Constitutive Law

To perform a finite element analysis on single crystals, a constitutive law needs to be formed. However, a full three dimensional law modeling BCC or FCC crystals would take considerable effort. The lesser of the two, has 12 different slip systems. A simpler plane strain model involving two slip systems is implemented here. Asaro [1978] stated that in both face centered cubic and body centered cubic crystals, lattice rotations make symmetric

double slip a common phenomenon in crystal plasticity. Additionally, Neumann [1974] has shown that double slip plays an important role in fatigue crack growth. The geometry to be used in this analysis is shown

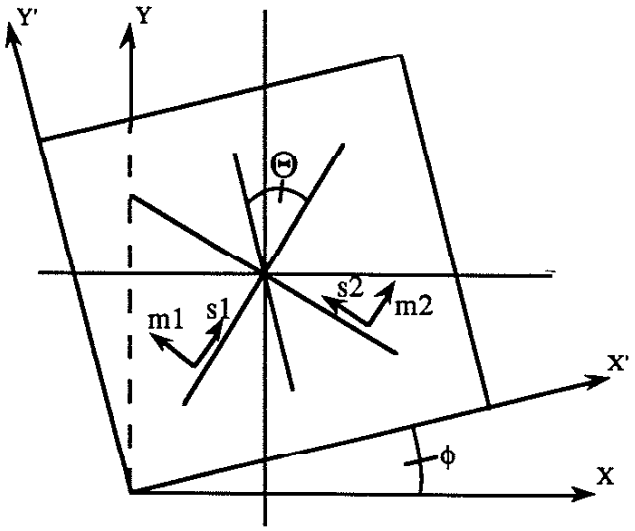

Figure 2: Nomenclature used is symmetric double slip plane model. The slip directions are denoted s1 and s2, while the slip normals are m1 and m2. Rotation of the crystal is accomplished by changing ϕ, while the angle between the symmetric slip planes is varied through Θ.

in Figure 2. The box represents a single crystal, with slip constrained along two slip planes characterized by unit vectors (s1,m1) and (s2,m2). The unit vectors are defined in the X-Y coordinate system through trigonometric functions of the two angles, Θ and ϕ. The angle between either slip plane and the vertical normal of the crystal is called Θ, and the orientation of the crystal with respect to the horizontal (X-direction) is called ϕ. Both slip directions and slip plane normals lie in the plane of the drawing. The model has been successfully used to model the tensile deformation of both BCC and FCC crystals [Asaro, 1978]. For BCC crystals, Θ takes on an approximate value of 60° while for FCC crystals Θ is about 30°.

One important preliminary decision to be made concerns the hardening matrix, $h^{(\alpha\beta)}$. Several different linear hardening matrices have been proposed. Taylor [1938a, 1938b] proposed that the hardening matrix could take the following form:

$$h^{(\alpha\beta)} = \begin{pmatrix} h & h_l \\ h_l & h \end{pmatrix} \tag{7}$$

Where h = h_l = constant, and the h_l terms represent latent hardening. Latent hardening is the hardening on one slip plane caused by slip caused on another. However, new evidence compelled the experimenters to use a different matrix. Koiter [1953] proposed a hardening matrix that did not include latent hardening:

$$h^{(\alpha\beta)} = \begin{pmatrix} h & 0 \\ 0 & h \end{pmatrix} \tag{8}$$

Although this matrix does not include latent hardening, it does a good job correlating with experimental results. Bassani et al. [1991] stated that experimental evidence indicates that latent hardening is much smaller than primary hardening when two or more slip planes are active. They even concluded that a latent hardening ratio ($q=h_l/h$) of zero is reasonable. Using the hardening matrix given in equation 8, a constitutive law can now be formed for the double slip crystal.

Combining equations 3 and 6 for N slip planes, one can write:

$$P^{(\alpha)} : \dot{\sigma} = \sum_{\beta=1}^{N} h^{(\alpha\beta)} \dot{\gamma}^{(\beta)} \tag{9}$$

On the other hand, the general form for the constitutive equation is given as:

$$\dot{\sigma} = L^e : (\dot{\varepsilon} - \dot{\varepsilon}^p) \tag{10}$$

L^e is the fourth order elastic stiffness tensor transformed into the global stress-strain coordinates. In other words, as ϕ is changed, the inputted stiffness values, [C], are changed to accompany the rotation and the new matrix is denoted L^e. Additionally, $\dot{\sigma}$, $\dot{\varepsilon}$, and $\dot{\varepsilon}^p$ represent second order tensors. The strains are calculated using small deformation theory (additive strains). This representation is accurate for fatigue crack growth models where the crack tip

strains are not too large [Sehitoglu and McClung 1989 I,II]. The macroscopic plastic strain rate, $\dot{\varepsilon}^p$, is calculated from the following relationship:

$$\dot{\varepsilon}^p = \sum_{\beta=1}^{N} P^{(\beta)} \dot{\gamma}^{(\beta)} \tag{11}$$

where $\dot{\gamma}^{(\beta)}$ is the plastic shear strain rate on the active slip system β. This formula geometrically sums each contribution of shear strain rate, along the global coordinates of the strain tensor, to form the macroscopic strain rate. If one multiplies equation 10 by $P^{(\alpha)}$ one gets:

$$P^{(\alpha)}:\dot{\sigma} = P^{(\alpha)}:L^e:(\dot{\varepsilon} - \dot{\varepsilon}^p) \tag{12}$$

Combining equations 9, 11, and 12 one gets the following relationship:

$$\sum_{\beta=1}^{N} h^{(\alpha\beta)} \dot{\gamma}^{(\beta)} = P^{(\alpha)}:L^e:(\dot{\varepsilon} - \sum_{\beta=1}^{N} P^{(\beta)} \dot{\gamma}^{(\beta)}) \tag{13}$$

simplifying one gets:

$$\sum_{\beta=1}^{N} h^{(\alpha\beta)} \dot{\gamma}^{(\beta)} + P^{(\alpha)}:L^e:\sum_{\beta=1}^{N} P^{(\beta)} \dot{\gamma}^{(\beta)} = P^{(\alpha)}:L^e:\dot{\varepsilon} \tag{14}$$

or,

$$\sum_{\beta=1}^{N} (h^{(\alpha\beta)} + P^{(\alpha)}:L^e:P^{(\beta)}) \dot{\gamma}^{(\beta)} = P^{(\alpha)}:L^e:\dot{\varepsilon} \tag{15}$$

Solving this equation for $\dot{\gamma}^{(\beta)}$ and realizing that α and β will take on values from 1 to N, $\dot{\gamma}^{(\beta)}$ is calculated as:

$$\dot{\gamma}^{(\beta)} = \sum_{\alpha} \left\{ h^{(\alpha\beta)} + P^{(\alpha)}:L^e:P^{(\beta)} \right\}^{-1} P^{(\alpha)}:L^e:\dot{\varepsilon} \tag{16}$$

Using a similar summation argument, and substituting equation 16 into equation 11 gives one:

$$\dot{\varepsilon}^{P} = \sum_{\alpha\beta} P^{(\beta)} N^{-1}_{\alpha\beta} P^{(\alpha)} : L^{e} : \dot{\varepsilon} \tag{17}$$

where $N^{-1}_{\alpha\beta} = \left\{ h^{(\alpha\beta)} + P^{(\alpha)} : L^{e} : P^{(\beta)} \right\}^{-1}$

Using equation 17 allows one to write equation 10 as:

$$\dot{\sigma} = L^{e} : (\dot{\varepsilon} - \sum_{\alpha\beta} P^{(\beta)} N^{-1}_{\alpha\beta} P^{(\alpha)} : L^{e} : \dot{\varepsilon}) \tag{18}$$

$$= L^{e} : (I - \sum_{\alpha\beta} P^{(\beta)} N^{-1}_{\alpha\beta} P^{(\alpha)} : L^{e}) : \dot{\varepsilon}$$

or $\dot{\sigma} = L^{ep} \dot{\varepsilon}$ (19)

where $L^{ep} = L^{e} : (I - \sum_{\alpha\beta} P^{(\beta)} N^{-1}_{\alpha\beta} P^{(\alpha)} : L^{e})$

The constitutive equation to be used in the plastic analysis is equation 19. The summations over α and β are from 1 to 2 since this model has only two slip planes. Equation 19 relates the incremental stress tensor to the incremental strain tensor. Prior to yielding, there is no plastic flow so the incremental version of equation 2, $\dot{\sigma}_{ij} = C_{ijkl} \dot{\varepsilon}_{kl}$, is used to relate stresses and strains. This equation is assumed valid until it its bounds are violated by the yielding of a particular element. At this point, the stresses are partitioned into elastic and plastic steps and the stress state is recalculated using equations 2 and 19.

2.5 Back Stress and Active Yielding

In the simplest case, plastic flow occurs when the resolved shear stress on either slip plane reaches the critical resolved shear stress, λ_o. However, it is not realistic to simply define forward and reversed yielding at the critical resolved shear stress. As dislocations move in a real material they encounter obstacles which force them to pile up. Because of dislocation pile up a back stress is developed. Back stress is responsible for the well known Bauschinger effect in isotropic materials. Back stress development is well documented in

cyclic loading experiments. For example, Kukhlman et al. [1979] included the effect of back stress when they predicted the stress-strain behavior for Cu single crystals under cyclic loading. The incorporation of back stress is consistent with the single crystal experimental results of Mughrabi [1978], Finney [1974], and Winter [1974]. The back stress acts in the opposite direction as the direction of plastic flow. Consequently, a higher stress is needed to overcome the back stress and further move the dislocations. This increased stress state contributes to the hardening of the crystal. When the loading is reversed, according to Seeger [1957], the immediate motion of dislocations in the reverse direction does not occur. Instead, dislocation motion will occur only when the net stress on the dislocations reaches a "critical value". Since the back stress built up on the slip plane acts in the opposite direction as dislocation motion, when loading is reversed, the back stress will initially aid the movement of dislocations. The initial aid given by the back stress, causes the "critical value" at which dislocation movement occurs to be less that the critical resolved shear stress. This effectively lowers the yield stress in the reverse direction, creating a directed Bauschinger effect. If the dislocations continue to move in the reverse direction, the back stress will switch signs and start inhibiting dislocation motion. In this analysis the back stress, σ_c, will be calculated using the following relationship:

$$\sigma_c^{(\alpha)} = c\gamma^{(\alpha)} \tag{20}$$

Where c is a constant and $\gamma^{(\alpha)}$ is the current total shear strain on the slip system α. This relationship makes intuitive sense since increased plastic flow will increase the amount of back stress on a particular slip system. Subsequent yielding occurs when $\lambda^{(\alpha)} > \left|\lambda_o - \sigma_c^{(\alpha)}\right|$. Kukhlman et al. proposed a similar relationship for Cu single crystals [1979]. It should be noted that in real crystals, the back stress has a tendency to saturate. As a first approximation, the back stress here has no limiting value.

3. *Single Crystal Crack Growth and Double Slip F.E.M Formulation*

3.1 Growth Stages

Fatigue cracks have several stages of growth as they propagate through a material. Figure 3 demonstrates two important stages of crack growth. Since most of a specimens fatigue life is spent in stages I and II, engineers are most concerned with how cracks behave during these two stages. After the crack has initiated along a preferable slip direction, it begins stage I propagation. During stage I growth, or in stage II growth through large grain microstructures, the crack length is on the order of the grain size. In the early parts of stage I growth, the crack may even be contained within a single grain.

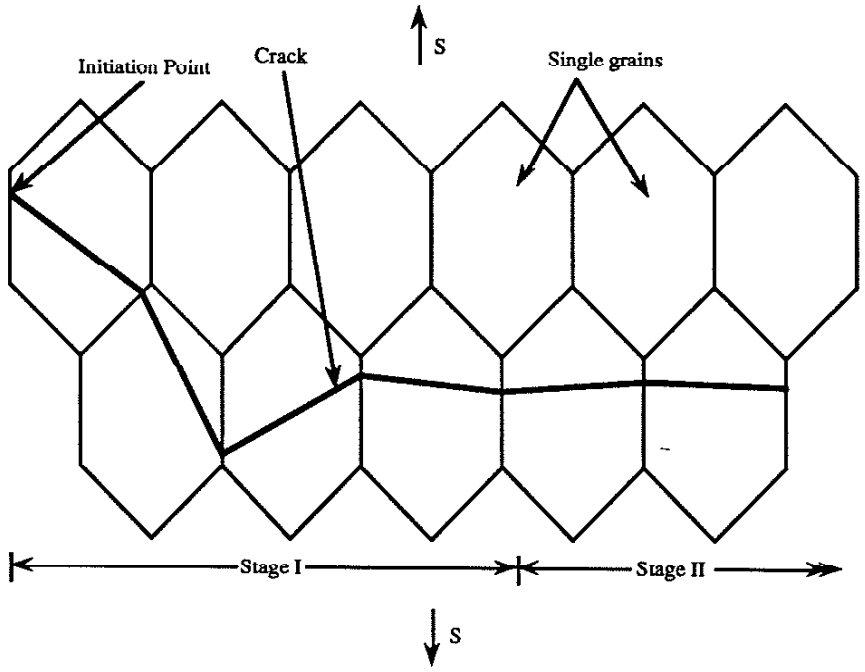

Figure 3: Demonstration plot of a fatigue crack growing through a polycrystalline material. Stage III, or the final fracture regime, is not shown here.

Cracks in this situation are referred to as "short cracks". The behavior of short cracks as they pass through different grains may be very different. Along with others, [Morris 1977, Morris and James 1983, De Los Rios et al.

1985, Tokaji et al. 1987, Liaw 1988, Larson et al. 1988, Lee and Sharpe 1988, Tanaka 1989, Miller 1991] found that short crack growth rates are highly variable. The variability is due to misorientation of different grains through which the short cracks grow. Some grains permit cracks to grow extremely fast, while others slow down crack growth considerably. In some cases they found that a crack may even arrest when it attempts to grow into an adjacent grain. Although the crack can continue to grow through cross slip or by activating secondary slip planes, they attributed this effect to the orientation mismatch between the two grains. Once a crack has grown through a significant number of grains it becomes a long, or macroscopic crack. Cracks of this nature are propagating in the stage II regime. As long as the plastic zone size with respect to the grain size is large enough, the behavior of long cracks is not as dependent on microstructure as short crack behavior. Since the crack has grown over many grains with different orientations, its profile can be macroscopically described by an average crack line. The orientation effects of individual grains and the roughness of the surface are small with respect to the overall crack length and plastic zone size, so they can be ignored. The crack growth behavior here can be described using a continuum approach. Paris [1964] pioneered the original work in this field. Since then, continuum approaches have been successfully used to describe long crack behavior. However, the variability in short fatigue cracks, or long cracks in large grain microstructures, is yet to be fully understood and quantified. In this analysis, fatigue crack growth as influenced by local slip will be modeled. The analysis applies to both stage I and stage II phases, however, initially the analysis will focus on Mode I cracks.

3.2 Mechanism of Propagation

It is well known that fatigue cracks propagate at stress intensity amplitudes much lower than their critical stress intensity value, K_{Ic}. This leads one to believe that there is a mechanism, exclusive to ductile fatigue crack growth, responsible for this phenomenon. An assortment of researchers [McEvily 1963, Laird 1967, Tomkins 1968, Pelloux 1969, Neumann 1974] have proposed, and experimentally verified, that fatigue cracks grow through crystallographic slip (dislocation motion) at the crack tip. All of the theories involve the same basic mechanism of propagation. A coarse slip

model proposed by Neumann [1974], Figure 4, does a good job illustrating how fatigue cracks propagate through local slip at the crack tip. This model, which he backed with extensive experimental evidence, is similar to the models proposed by others [McEvily et al. 1963, Laird 1967, Tomkins 1968, Pelloux 1969]. The model may be used for both mode I and mode II crack growth, and it may prove valuable to model crack growth using double slip in both regimes. Following Figure 4 during the tensile cycle, one can see that crystallographic slip occurs on alternating planes. Slip initially occurs on a single plane, then as this plane hardens slip initiates on an alternate plane. In this model, and in experiments, slip only occurs at the crack tip.

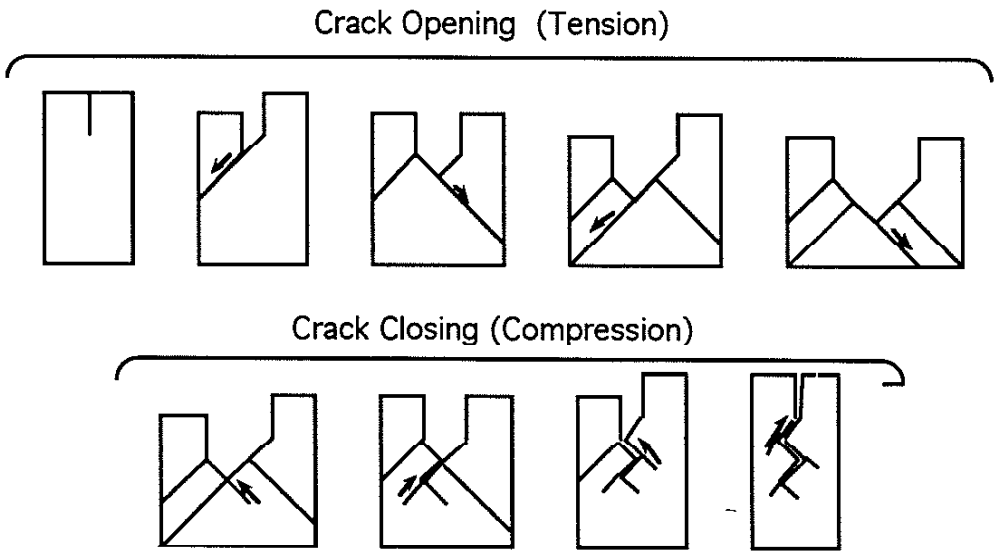

Figure 4: Coarse slip model proposed by Neumann [1974]. In this case, slip occurs at 45° angles from the crack line.

This slip causes an overall "blunting" of the crack tip. As the tension is relieved, slip in the opposite direction causes the crack to begin closing. After one complete cycle, the crack is advanced a length Δa. The amount of crack advance depends on the specimen geometry, loading conditions, and material properties. It should be noted that the slip lines in the coarse slip model are drawn far apart to better illustrate the mechanism of advance. In a real material, the slip lines are so close that they may even be indistinguishable. The final drawing in Figure 4 predicts that the crack faces should have a

rough appearance after advancing. The peaks left after crack advance are called ductile fatigue striations. Pelloux [1969] found that striations are caused by the blocking of reversed slip through oxide films. If the growth of oxide films is blocked, as in a vacuum, fatigue crack advance will still occur, but without striations. Striations are clearly visible on micrographs, and their spacing can be used to estimate crack growth rates.

3.3 Finite Element Formulation

The method used to model single crystal crack growth is similar to the one previously used to model elastic-plastic crack growth [Lalor 1986, Sehitoglu and McClung 1989 I-II]. A set of linearized equations are solved iterativly to attain the proper deformation state of the mesh. The iteration scheme is fully described by Lalor [1986]. The only difference in the iteration scheme is with the subroutine UMAT. UMAT is replaced by new routine called SMAT which relates the incremental stress, $\dot{\sigma}$, to the incremental strain, $\dot{\varepsilon}$, through the material model. SMAT also updates the linear stiffness matrix to the to accompany the current stress level. The routine uses the incremental double slip constitutive relation derived in section 2.4. By using this constitutive relationship in the finite element code, one is microscopically constraining plastic deformation to two slip planes in all four gauss points in every element in the body. To calculate macroscopic slip, or plastic deformation, microscopic slip is calculated at every gauss point in the mesh and averaged. This is similar to a real material since dislocation motion is microscopic, but when viewed over a large region slip is macroscopic.

Since the entire mesh is governed by a single law, it behaves as a single double slip grain with a crack in it. As in a real cracked single crystal, active slip occurs exclusively from the crack tip. Figure 5 demonstrates this phenomenon. In single crystals, and in the double slip model, "kink" bands develop in addition to the primary shear band [Rice 1987, Mohan et al. 1992]. For some ϕ and Θ combinations, the macroscopic slip bands which form at the crack tip closely replicate the prescribed microscopic ϕ and Θ combination. By using color post processing software, appendix A (figures a-h) takes a closer look at the experimental and F.E.M. slip bands which form at the crack tip. There are several distinct characteristics which have been

experimentally observed as a crack propagates through any particular grain [Neumann, 1974]. A few key characteristics, which are listed below, are clearly visible on the color finite element plots.

(1) Slip at the crack tip is nearly exclusively confined to two slip systems.
(2) Directly in front of the crack tip, a slip free triangular zone forms.
(3) At any moment during propagation, only the slip planes at the tip are fully active.

Figure a is a S.E.M. micrograph of slip lines experimentally observed in single copper crystals. Figures b through e in the appendix show a sequence of plots at maximum and minimum loads at the beginning and the end of the loading history of the F.E.M. fatigue crack. For these plots, Θ is 37.5° and ϕ is 0°. The macroscopic plastic zones here are formed by a microscopic

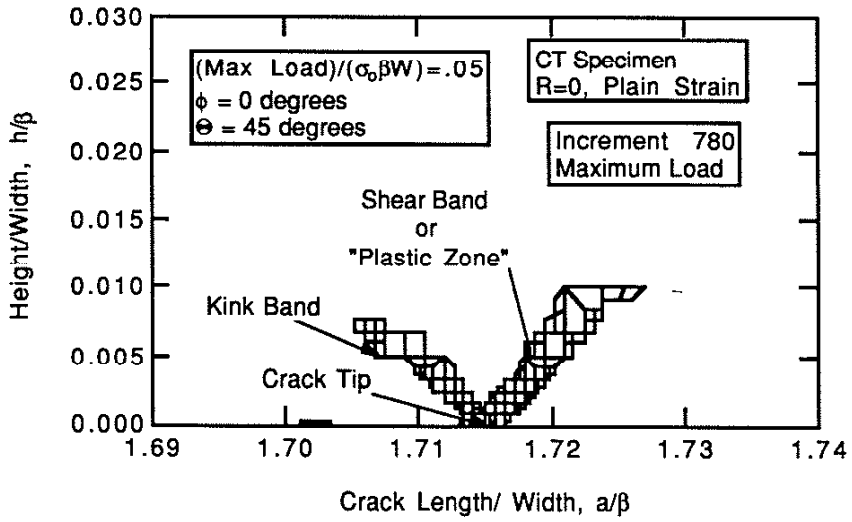

Figure 5: Plot demonstrating that slip does occur on slip bands emanating from the crack tip in the single crystal finite element program. β is the specimen width while W is the distance from the crack tip to the edge of the CT specimen.

summation of the slip strains, along both slip planes, into the global y-direction. Keeping in mind that the picture is symmetric about the x-axis, and that Θ is measured from the vertical normal, one can see that two intense

macroscopic shear bands develop around 37.5° from the vertical normal. The bands are clearer in the first two cycles where no residual plasticity is seen. However at the final cycle, two intense plastic shear bands still form exclusively at the crack tip. This correlates with the experimental evidence given statements 1 and 3. Additionally, the slip free triangular zone is clearly evident in all of the pictures. Figures f through h demonstrate the effect of changing the microscopic angle between the slip planes in the F.E.M. code. As the microscopic angle between the slip planes is increased, the macroscopic slip bands also change directions. In some cases the prescribed microscopic direction correlates with the primary direction of the macroscopic slip band at the crack tip. By changing Θ, one can change the angle of allowed microscopic or macroscopic slip between the two slip planes throughout the body. Or, by changing ϕ one can change the angle at which the crack is entering the single crystal.

The crack line boundary conditions and crack growth are also handled in a similar way [Lalor 1986, Sehitoglu and McClung 1989 I-II]. Each node along the crackline has a truss element attached to it. These truss elements have different stiffness values depending on their location and stress state. When a node is open, the truss has a stiffness value near zero, and when a node is closed, the truss has infinite stiffness. Nodes which the crack has not reached yet, have infinite stiffness throughout the entire loading history. When the crack reaches these nodes, they are given the variable stiffness. Crack advance is accomplished by "releasing" the next node in line immediately after every peak in maximum applied load. Opening and closing levels are determined by monitoring the stress level and position of the crack line truss elements.

4. Double Slip F. E. M. Considerations

4.1 Mesh Choice

Aside from the formulation of the finite element code, there are other factors that must be dealt with when modeling crack growth with double slip. The first decision to be made concerns the mesh type and fineness. In this analysis, two different meshes are used. One mesh used is the compact tension specimen, figure 6, with a fine mesh spacing, Δa, of 10 μm and a $\Delta a/W$ value of .0009. The second mesh used is the center elliptical notch

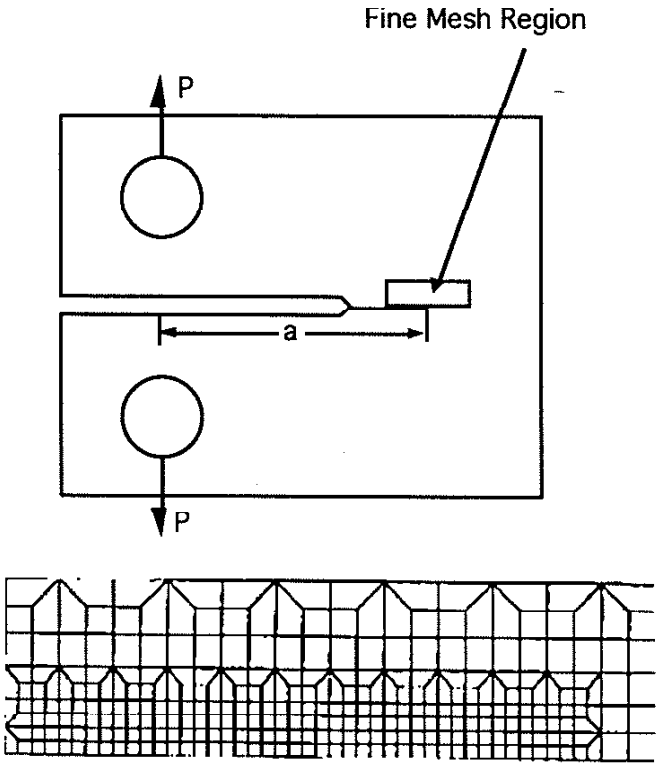

Figure 6: Compact tension specimen. Only 1/2 of the specimen was used for modeling.

specimen, figure 7. It's fine mesh region has a $\Delta a/W$ value of .0013. In this analysis, the crack is grown out of the notch stress field. This allows one to approximate the notch specimen as a center cracked specimen (CCP). Since the suggested isotropic criteria for mesh refinement could not be used [Sehitoglu and McClung 1989-I], proving that the meshes could capture the

reversed plastic zones for several slip system setups was an observational procedure. A typical reversed plastic zone has nearly 20 elements yielding. This is a sufficient number of elements to define the reversed plastic zone. One should take note that if the applied loads are reduced significantly, then the mesh may need to be refined further. Throughout this analysis, crack

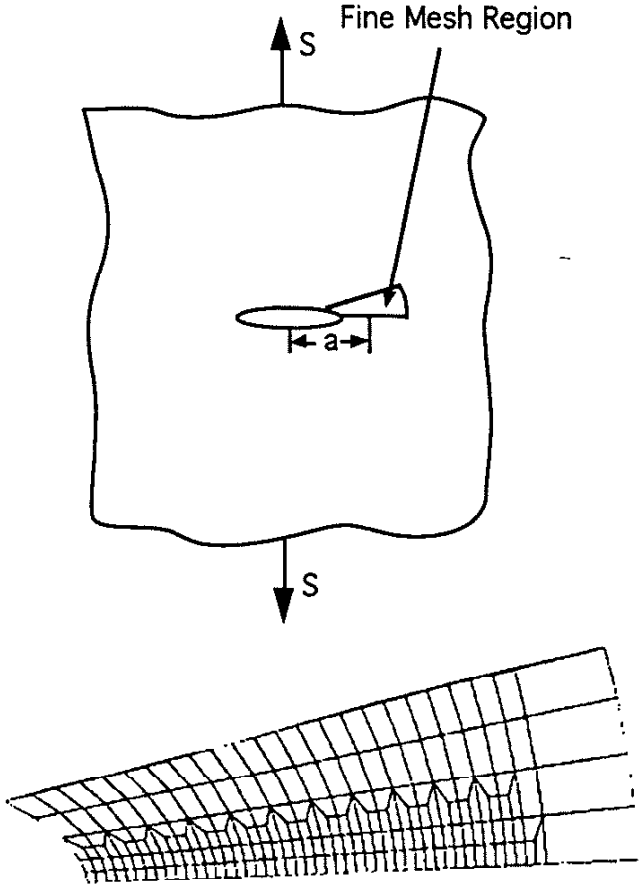

Figure 7: CCP specimen. Only 1/4 of the specimen was used for modeling.

growth in both the CT specimen and the CCP specimen will be analyzed. Since the CT specimen uses twice the CPU time, using the CCP specimen enables one to more clearly define data trends for different Θ and ϕ

combinations. However, it should be noted that both specimens exhibited *very* similar opening trends (Figure 8).

4.2 Modeling Procedure

Considerable computational effort is needed to run a single 20 cycle double slip finite element simulation. One run may take up to 1.5 CPU hours on the SGI Power Challenge super computer at the National Center for Supercomputing Applications. This fact, coupled with the large amounts of data reduction needed per run, requires the experimenter to develop a specific plan on what Θ and ϕ combinations to run. It would be insurmountable task to run every possible combination. For this F.E.M. analysis, two different variations in slip configurations will be studied. The first study will consist of keeping the angle between the slip planes constant, $\Theta = 30^{\circ}$, and changing the

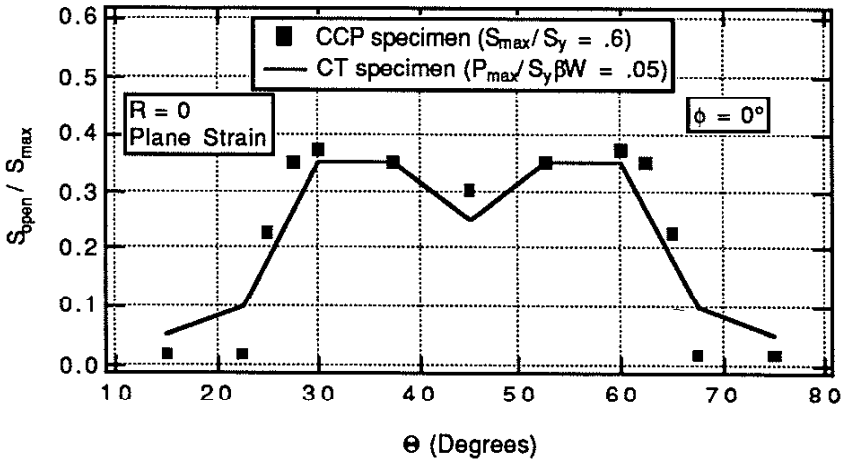

Figure 8: Opening levels as a function of Θ for both specimens. The levels are normalized by the maximum applied stress. Note Symmetry with respect to Θ = 45°.

crystallographic orientation, ϕ. The second study will focus on the effect of symmetric slip plane orientations. The crystallographic orientation, ϕ, will be kept at zero while the angle between the slip planes, Θ, is varied. The exclusive use of these two models will give one insight into fatigue crack growth parameters and rates for different double slip crystals and orientations. When Θ is varied and ϕ is kept constant, the model is

symmetric about the crack line. This is simliar to many of the experimental models show thus far. However, in real material, the slip planes which are activated may not be symmetric due to material inhomogenities or unfavorable crystallographic orientations. This effect is considered by varying ϕ while keeping Θ constant.

4.3 Material Properties

The six single crystal material constants used in this analysis, $C_{11} = 221$ GPa, $C_{12} = 134$ GPa, $C_{44} = 102$ GPa, $\lambda_o = 248$ MPa, $h = 28$ MPa, and $c = 28$ MPa are generally not changed throughout the simulation. The only value experimented with is the Koiter hardening coefficient, h. A change in h by a factor of 100 had a negligible effect on the results for all of the cases run. Even though the crystallographic properties are not varied, when analyzing crack growth on the microstructural level, it is important to understand how the overall crystal will respond to stresses and strains. As Θ or ϕ change, the stress-strain response corresponding to a constant loading direction also changes. This response can be quantified by using uniaxial material properties. To better understand the effect of crystallographic orientation and

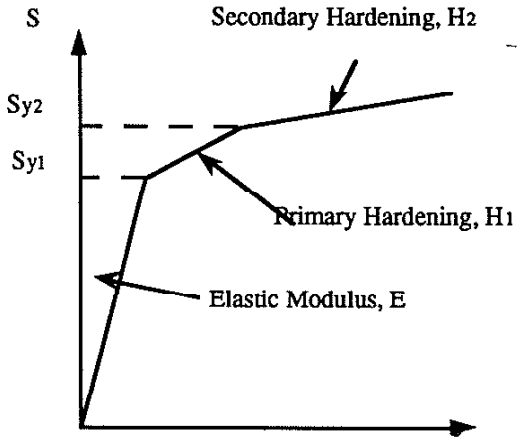

Figure 9: Uniaxial stress-strain curve with two distinct hardening regions.

slip plane direction on fatigue crack growth, it is crucial that one determines the relationship between these uniaxial material properties and model

orientation. The uniaxial material properties can be determined by loading the double slip model in the following manner: A far field uniaxial stress, S, much greater than the expected yield of the crystal is incrementally applied. Then, using the applied stresses and resulting strains, a uniaxial stress-strain (S-e) curve is plotted (Figure 9). With Koiter hardening, only three properties need to be read off of this plot: yield stress, elastic modulus, and hardening modulus. By varying ϕ and Θ, one can gain a good understanding of how

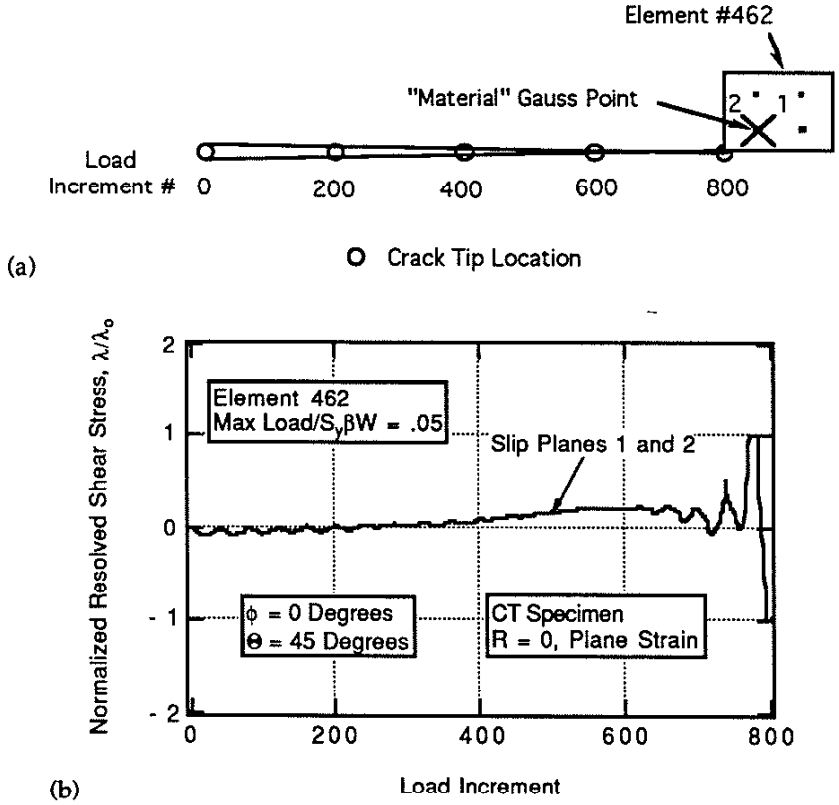

Figure 10a and 10b: (a) Schematic of the crack position versus the material point and the increment number. (b) Plot of the resolved shear stress on both microscopic slip planes throughout the loading history. In this case the resolved shear stresses on both planes are identical. Element 462 is located at the crack tip on the final cycle. β is the distance from the crack tip to the back of the specimen and W is the thickness of the specimen.

these three properties vary over orientation.

In an attempt to quantify how double slip crystals behave under applied loads, definitions for several uniaxial properties have been

developed. Some, but not all, of these definitions are specific to the double slip plane model. Since the slip model exhibits directionality, the definitions are *slightly* different than the normal uniaxial stress-strain definitions. The uniaxial elastic modulus is defined as the slope of the crystals stress-strain curve up to primary uniaxial yielding (figure 9). That is, the slope between the applied far field stress and resulting far field strain for a single crystal with slip constrained along a specific ϕ, Θ combination. The primary uniaxial yield stress, S_y, is the applied stress at which one slip plane becomes active. If both slip planes are active at primary yielding, then there is no secondary yield. However if one slip plane remains inactive at primary yield, it will become active at a higher stress called the secondary yield. Since there are two yielding points, there are also two hardening moduli. The hardening modulus, H, is defined as the slope of the crystals stress-strain curve after yielding. Between the primary and secondary yielding H is called the primary hardening modulus, and after the second slip plane becomes active H is referred to as the secondary hardening modulus. Since two slip planes are active during secondary hardening, H_2 will always be smaller than H_1.

Plots of Sy, E, and H for different Θ values are shown in Figure 11. For each of these plots, ϕ was kept at zero degrees. Since ϕ is kept at zero, the slip planes remain symmetric about the loading axis. This means that both slip planes will always activate at the same applied stress. In a cracked body the resolved shear stresses on conjugate slip planes may also be the same. Figure 10b demonstrates that when ϕ is kept at zero, the resolved shear stresses on both slip planes of an element along the crack line are similar. Figure 10a demonstrates the location of the crack tip with respect to the load increment number and the "Material Point" in element 462. A similar scheme will be used throughout the paper to look at resolved shear stress and stress-strain plots. Figure 10b plots the resolved shear stresses on the two microscopic slip planes at the gauss point shown in figure 10a. As the crack tip approaches this element, the resolved shear stresses steadily increase on both planes. By taking a look at Figure 11c one can see that the elastic modulusdoes not depend on Θ. This occurs because the elastic modulus of the crystal is governed by the crystal constants, C_{11}, C_{12}, and C_{44}. These constants are functions of ϕ (crystallographic orientation), not Θ (slip plane orientation). However, the yield stress and hardening modulus are strong functions of Θ (Figures 11a, 11b). Both curves show minimums at $\Theta = 45°$, with somewhat

stable behavior between 10° and 80°. Outside of these two bounds, the material properties begin to rise up towards infinity. This occurs because at

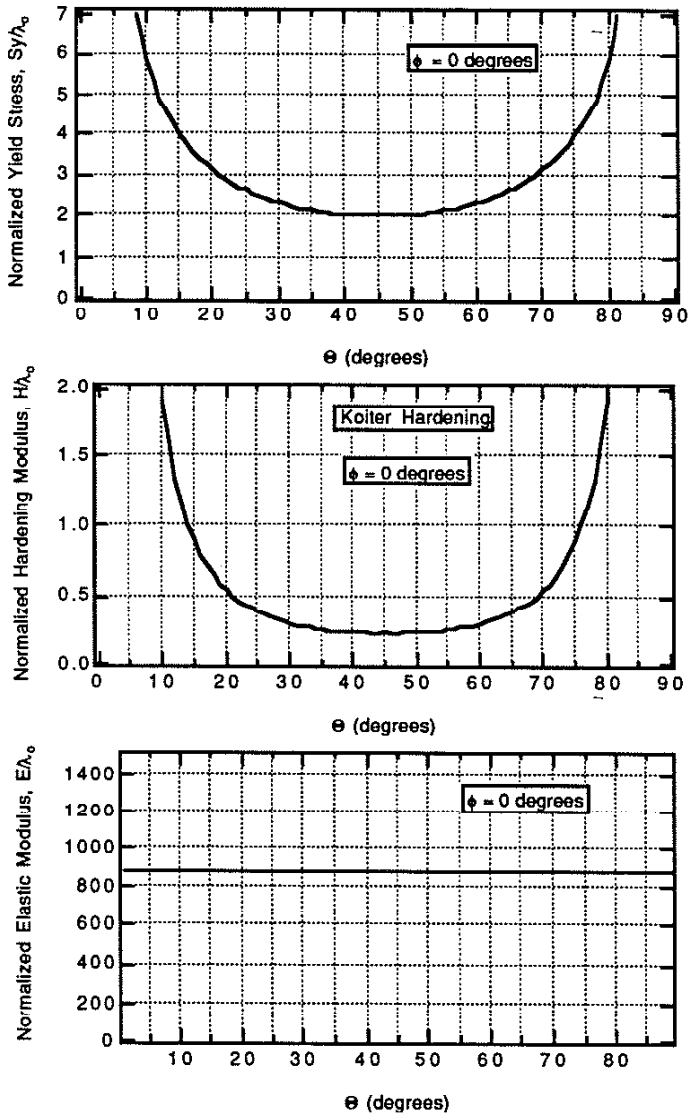

Figure 11: Variation of uniaxial material properties over Θ, when ϕ is kept at zero degrees. Yield stress - Figure 11a, Hardening modulus - Figure 11b, and Elastic modulus - Figure 11c.

the extremes, $\Theta = 0°$ or 90°, both slip planes are oriented perpendicular or parallel to the loading direction. This causes the resolved shear stress on both

slip planes to be zero. When the resolved shear stress is zero, the applied load will never be large enough to cause yielding. Hence, the uniaxial yield stress is infinite. If there is no yielding, then the hardening modulus will also be infinite. Because of the small probability of both slip planes having negligible resolved shear stresses in a real crystal, the cases outside $\Theta = 10^\circ$ and $\Theta = 80^\circ$ for $\phi = 0^\circ$ will not be analyzed.

Plots of Sy, E, and H for different ϕ values are shown in Figure 13. For each of these plots, Θ was kept at 30°. Varying ϕ while keeping Θ constant has a much different effect on material properties. Since the crystallographic

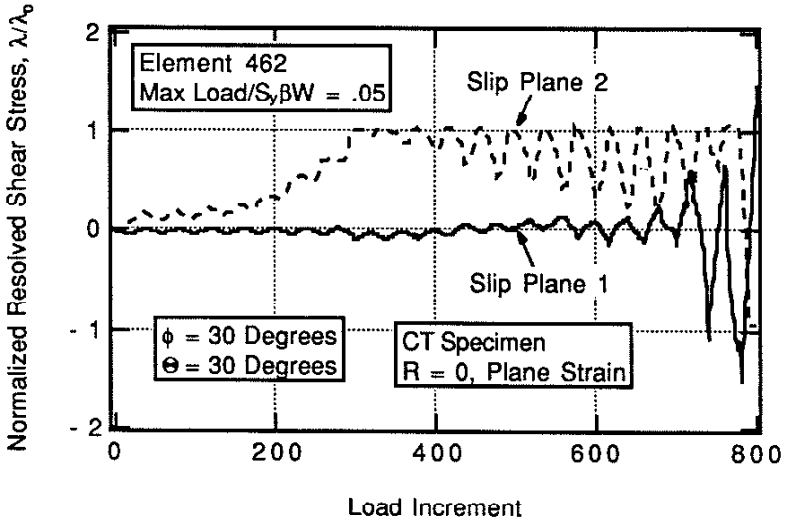

Figure 12: Plot of the resolved shear on both slip planes throughout the loading history. In this case the slip planes see two different resolved shear stresses. Element 462 is located at the crack tip on the final cycle. β is the distance from the crack tip to the back of the specimen and W is the thickness of the specimen.

orientation (ϕ) changes in this case, one sees a variation in Elastic Modulus. Figure 13c demonstrates this variation of elastic modulus over ϕ, with ϕ ranging from 0° to 90°. However, the variation of Elastic Modulus is small when it is compared to the large changes in the yield stress and the hardening modulus. By looking at Figures 13a and 13b, one can observe the variation of hardening modulus and yield stress versus ϕ. On both plots, primary and secondary property values are clearly defined. At most ϕ values the two slip planes have different resolved shear stresses, a phenomenon which also

occurs in the cracked bodies (Figure 12). This difference causes two distinct

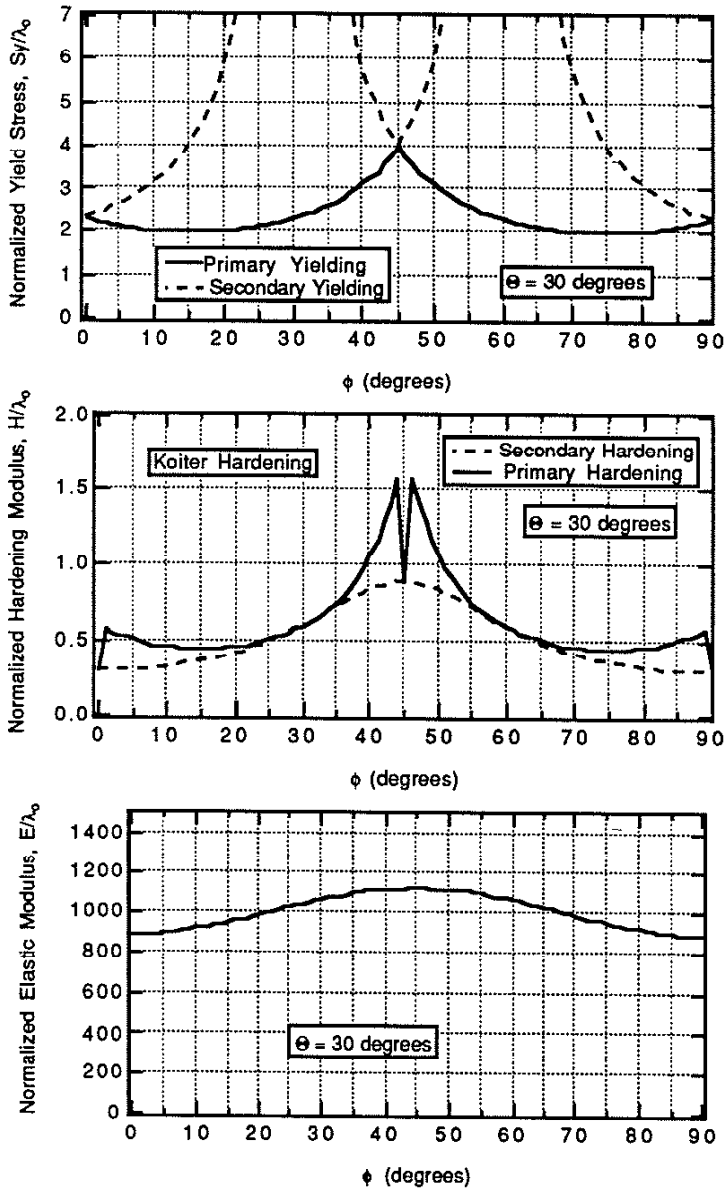

Figure 13: Variation of uniaxial material properties over phi, when Θ is kept at 30°. Yield stress - Figure 13a, Hardening modulus - Figure 13b, and Elastic modulus - Figure 13c.

yield stresses and hardening moduli. However, it should be noted that there are several angles for which one only sees primary hardening. These angles are: 0°, 30°, 45°, 60°, and 90°. For the remaining angles, it can be argued that the two separate yielding regions cause little or no modeling problems. When H_1 and H_2 take on similar values, the slope of the entire hardening region can be given by an average of the two, H_{ave}. Since the secondary yield does not cause a significant increase in plastic flow ($H_1 \approx H_2$), Sy_2 can be ignored. However, there are four regions where the primary hardening modulus is significantly higher than the secondary modulus. These regions are defined by the ϕ angle ranges: 1-5°, 40-44°, 46-50°, and 85-89° (Figure 13b). But, these very high primary hardening moduli are only active over a very narrow strain range. At the same angle ranges as the primary hardening peaks, the primary and secondary yield stresses are nearly identical (Figure 13a). This means that secondary yield will occur at a stress nearly identical to the first yield. So even though the values are much different, H_2 can effectively be used to describe the entire hardening region.

For normalization purposes, it will be necessary to find the average yield strength of a polycrystalline material containing many randomly oriented double slip crystals. Two different types of polycrystalline materials will be considered. The first material has many crystals with Θ equal to 30°, and ϕ randomly oriented between 0 and 360°. While the second has ϕ equal to 0°, and Θ randomly oriented between 10° and 80°. In 1964 Hutchinson used the self consistent method to determine the pollycrystalline behavior from the single crystal properties. However, since the properties are not needed to great precision, a simpler scheme will be used here. Hutchinson [1964] also stated that a lower bound on the polycrystalline yield stress can be found by averaging the single crystal primary uniaxial yield stresses over all possible orientations. Although this analysis was for BCC and FCC crystals, a similar averaging scheme can be used here. First, the primary uniaxial yield stresses are calculated over the respective angle ranges. Then, a weighted average is calculated using increments of one degree. The values calculated for the ϕ and Θ yield stresses are 580 MPa and 810 MPa respectively. The Θ yield stress is slightly higher because its uniaxial values tend toward infinity as Θ increases or decreases. It should be noted here that throughout the paper the uniaxial yield stresses are given by S_y, while the Hutchinson averages are denoted by σ_o.

4.4 Applied Loads

The loading in both specimens is done incrementally. The CT specimen is loaded with 20 load increments per reversal, while the CCP specimen is loaded with 50 increments per reversal. Both simulations were run for twenty cycles. For R = 0 loading, this makes the total number of increments 800 in the CT Specimen, and 2000 in the CCP specimen. Any

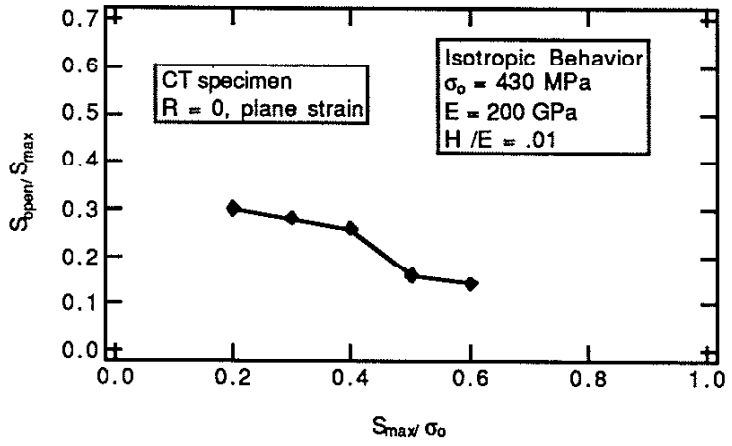

(a)

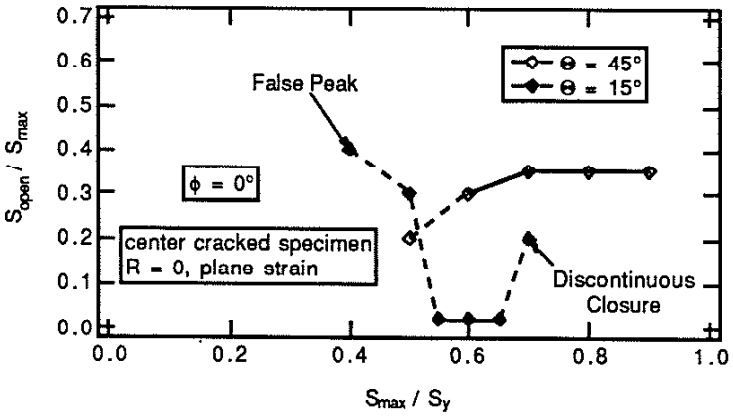

(b)

Figure 14a and 14b: Opening behaviors as a function of applied load. (a) Isotropic result [Sun 1991]. (b) Double slip result, Sy is the uniaxial yield stress for the $\Theta = 45^\circ$ and $\phi = 0^\circ$ combination, and the $\Theta = 15^\circ$ and $\phi = 0^\circ$ combination respectively.

given increment number which is used in the paper corresponds to a specific applied stress level and crack tip location during the loading history. Increasing the number of load increments per cycle was experimented with, but found to have little effect on the behavior of the model. For both specimens, the opening behavior is not a strong function of applied load. Ignoring modeling problems, Figures 14b demonstrates this concept for the double slip model using the CCP specimen. Figure 14a gives the isotropic result of closure levels under plane strain [Sun 1991]. The levels are for the CT Specimen, however the trends are similar for the CCP specimen. With figure 14a, one can see that the closure loads in the isotropic plane strain case are rather constant also. Additionally, one can compare the plane strain isotropic closure levels with the plane strain double slip levels at a given S_{max} / S_y or S_{max} / σ_o value. The applied loads in the CCP specimen were

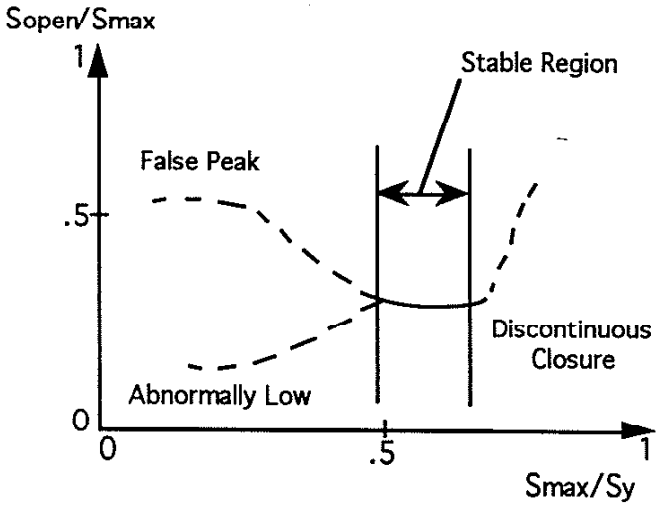

Figure 15: Demonstration plot of Sopen/Smax versus Smax/Sy showing several regions of acceptable and unacceptable behavior. Only data from the stable region will be used.

normalized according to the uniaxial yield. Because of the large variation in uniaxial yield stresses, 497 MPa to 992 MPa, this type of normalized loading was necessary. If the applied loads for a specific Θ and ϕ combination were much smaller than or close too the value of its uniaxial yield, several modeling problems arose (Figure 15). As the applied load is increased

towards the uniaxial yield, discontinuous closure begins to occur [Fleck et al, 1988]. This problem occurs when a node far from the crack tip, sometimes the furthest node, opens at a higher load than the crack tip nodes. Since the crack is not opening in a "zipper like" fashion, this causes erratic and unreasonably high opening levels. As the applied load is dropped well below the yield stress, one begins to run into mesh refinement problems. For some Θ and ϕ combinations with mesh refinement problems, "false peaks" have been observed [Sehitoglu et al. 1989-I]. While for other combinations, abnormally low opening levels were reported. Both effects are due to the inability of the mesh to pick up all of the crack line plasticity, the cause of plasticity induced closure. For the Θ=45° and ϕ= 0° combination, Figure 14 shows no evidence of discontinuous closure, but at low S_{max}/S_y values (.5) the opening level becomes questionably low. However, the Θ=15° and ϕ= 0° combination sees both discontinuous closure and the "false peak" effect.

To effectively compare the opening levels of different Θ and ϕ combinations, one needs to choose a S_{max}/S_y value which is not controlled by either of these effects for every angle combination. After observing plots similar to Figure 14 for several Θ and ϕ combinations, Smax/Sy of .6 appeared to be the most well behaved applied load to use. Nearly every single Θ and ϕ combination, with exception to one case, was well within the bounds of these two problems. Only one case underwent discontinuous closure, and all of the reversed plastic zones were sufficiently captured by the fine mesh region. Since different Θ and ϕ combinations have different uniaxial yield stresses, using a constant Smax/Sy means that one has to apply different loads to specimens with different angle combinations. However, this does not affect the opening behavior since the opening levels are not a strong function of applied load in the stable region.

4.5 Mode II Effects

In real specimens, cracks within a single grain, or several grains are rarely perpendicular to the loading direction. They usually form at some angle with respect to the loading direction along a preferred orientation. This causes the crack to see some mode II loading (shearing). As a first approximation, mode II shearing effects will be ignored. In further research, one may wish to include these effects by applying a shearing stress along the

crackline. This shear stress could be varied to match specific crack orientations with respect to loading. Investigations into this phenomenon were begun with promising results.

5. *Finite Element Results*

5.1 Mechanisms of Crack Closure in Double Slip Crystals

The mechanisms involved in isotropic plasticity induced plane strain fatigue crack closure are well understood [Fleck and Newman 1988, Sehitoglu and Sun 1989, Sehitoglu and Sun 1991, and McClung et al. 1991-II]. Plasticity induced crack closure is caused by the transfer of material along the crack face from directions in the plane of the crack face, x and z, to a direction perpendicular to the crack face, y. In plane strain, the majority of the transfer comes from the x direction since the thick body restricts deformation in the z direction. Therefore, in this plane strain analysis, the contribution from the z direction will not be heavily focused on. The excess tensile plastically deformed material left in the wake of the crack is what causes premature crack face contact. Fortunately, in single crystals, residual material is transferred through the same route as isotropic material transfer.

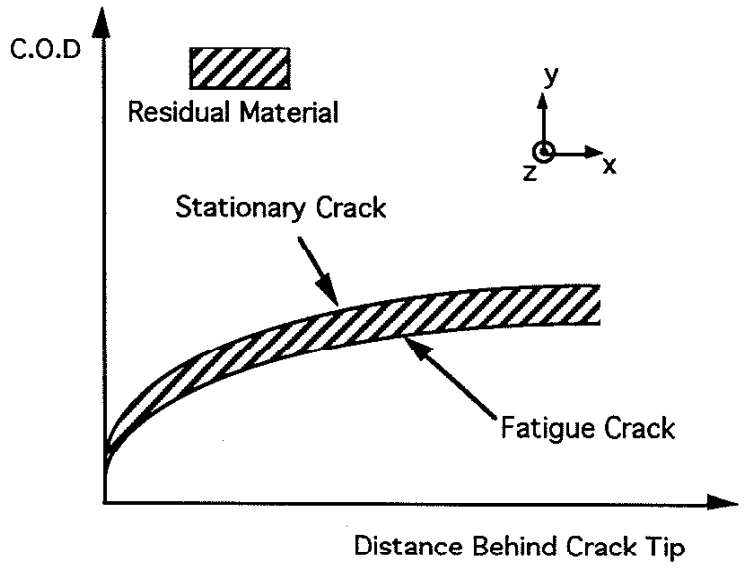

Figure 16: Plot demonstrating residual material buildup using the C.O.D. profile.

One way to visualize the amount of material which has been transferred, is to compare crack opening displacement profiles of stationary and fatigue cracks of the same length. Stationary cracks only undergo monotonic loading, hence

they do not form any residual plasticity along the crackline. Figure 16 demonstrates the effect of material transfer from the x direction to the y

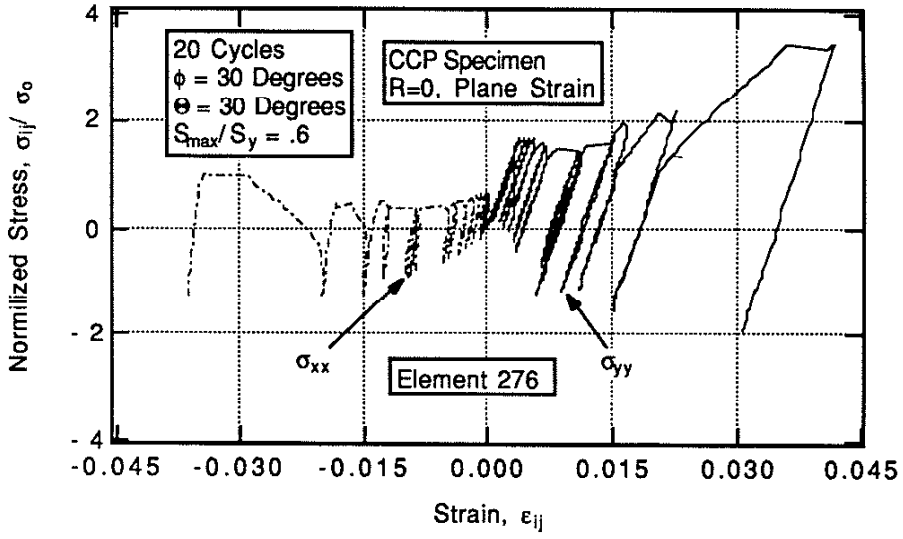

(a)

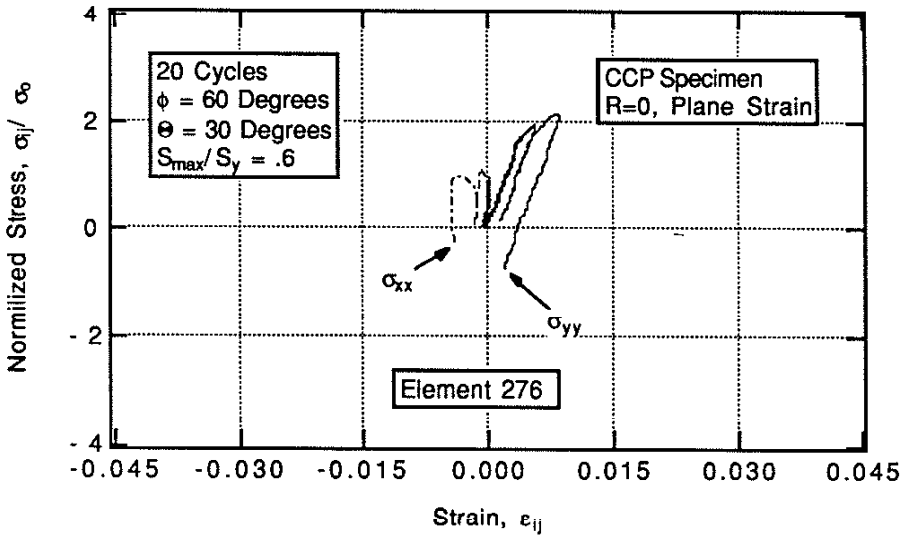

(b)

Figure 17a and 17b: Stress strain response for two different cases. Element 276 is located at the crack tip on the final cycle.

direction using a C.O.D. plot. At the same applied load, the fatigue crack clearly opens a lesser amount due to residual material built up in the y-direction. In single crystals, the exact amount of residual material transferred

perpendicular to the crackline varies greatly for different orientations. Upon unloading, the residual material from both sides of the crack will come in contact at a much higher load than the minimum. At the minimum load the crack faces will be tightly pressed together. It may take a significant far field load to first separate the faces. Both of these effects are labeled crack closure.

To quantify the transfer of material from the x-direction to the y-direction it is useful to look at the global stress-strain response of material along the crackline. To do this, the x and y global stress-strain response of an element initially far from the crack tip, and being approached by the crack tip, is monitored throughout the loading history. At the final loading cycle, the element is located at the crack tip. Since the behavior of this element is similar to all of the elements along the crackline, observing an element in this position helps the experimenters approximate of the behavior along the entire crackline. Figure 17 is a plot of the stress-strain response for two different orientations. The tracking scheme of the stress-strain response is

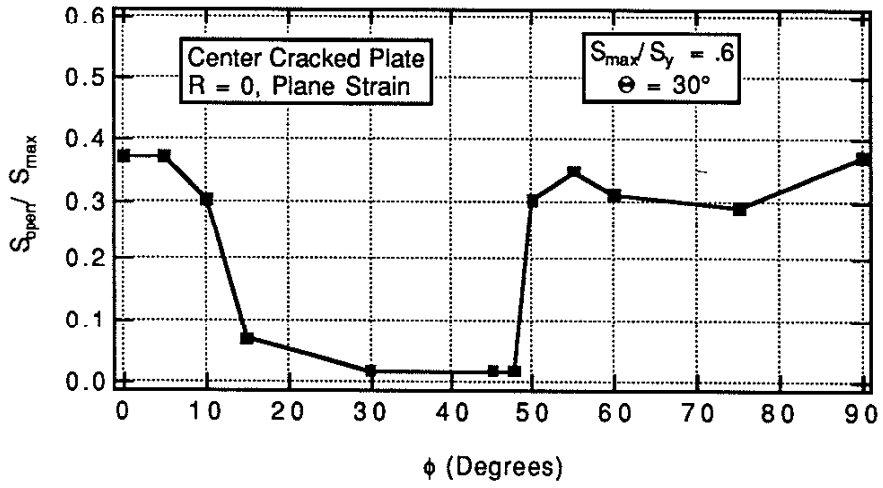

Figure 18: Plot of opening stresses versus crystallographic orientation, ϕ for the CCP specimen.

similar to the scheme used in the resolved shear stress plots. However, in this case, increment numbers are not included. The smaller hysteresis loops are at low increment numbers (element 276 is far from the crack tip) while the larger loops correspond to high increment numbers (element 276 is very

close to the crack tip). As the crack approaches this element, residual plastic strains in the positive y-direction and strains in the negative x-direction begin to accumulate. In both cases, one can see that at the final cycle significant positive residual plastic strains are formed in the y-direction, while negative residual strains are formed in the x-direction. A final measure of residual strains can be calculated by taking the distance along the horizontal axis, at zero stress, between the origin and the intersection of the final reversal. The final strain values are nearly equal and opposite in direction, indicating that the cumulative residual compressive strains in the x-direction directly contribute to the cumulative residual tensile strains in the y-direction and vice versa. Although the mechanism which causes crack closure in single crystals is quite clear, its actual effect on the closure level is yet to be explained. In single crystals the amount of residual plasticity does not solely dictate the opening level. For example, looking at Figure 17, on sees that the 30° case has significantly more residual plasticity than the 60° case. Using this observation, one may expect the 30° case to have a much higher opening level. However, looking at Figure 18 one can see that this is not the case. There are other anisotropic phenomenon which can dampen or intensify the effect of residual plasticity on opening levels. In the subsequent section, the authors will explain the factors which cause different orientations to have different opening levels.

5.2 Crystallographic Orientation Effects

By varying the microscopic crystallographic orientation of the model, ϕ, the experimenters gain a better understanding of how crack growth rates and parameters change as a crack grows through different grains. Ultimately, it turns out that varying ϕ has a pronounced effect on the opening levels of the crack. Figure 18 plots the variation of S_{open}/S_{max} over the ϕ angle range 0° to 90°. Due to the symmetry of the model, the angle ranges 90°-180°, 180°-270°, and 270°-360° take the same shape as Figure 18. The opening behavior has two distinct regions. One region has relatively high opening levels, $S_{open}/S_{max} \approx .35$, while the other region has extremely low levels, $S_{open}/S_{max} \approx .02$. Even though the closure mechanisms are similar in single crystals and isotropic materials, anisotropy causes several exclusive phenomenon to occur in single crystals. A delicate balance of these phenomenon is what causes the

drastically different opening levels for different orientations. One way to observe the mechanisms involved is to directly compare and contrast two cases with different opening levels. To help simplify the analysis, two cases with the same uniaxial material properties will be considered. The cases to be compared are $\phi = 30°$, and $\phi = 60°$ with $\Theta = 0°$ in both cases. Both cases have identical uniaxial material properties, but have drastically different opening levels. Figure 19 gives one a closer look at the setup of these orientations. The 60° case has one horizontal slip plane, and one slip plane at 30° with respect to the vertical normal. The 30° case has one vertical slip

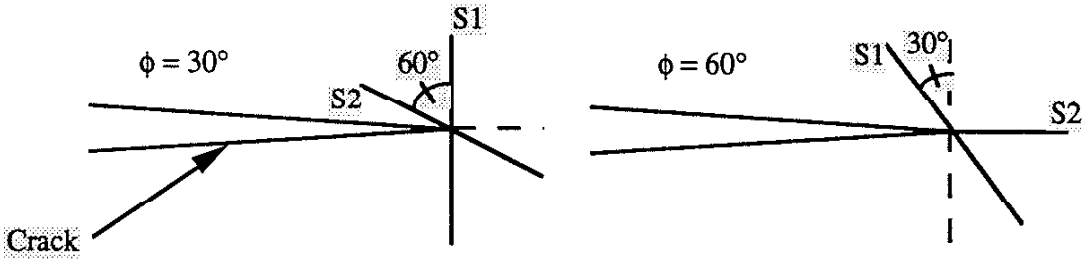

Figure 19: Microscopic slip plane orientation at the crack tip for the two phi, ϕ, cases which will be examined.

plane, and one slip plane at 60° with respect to the vertical normal. For uniaxial loading, the horizontal and vertical slip planes will see the same resolved shear stress, as will the angled planes. However, in the complicated stress field surrounding the crack tip, this symmetric resolved shear stress is not always seen.

The level at which a crack opens is directly related to its crack opening displacement, δ. Fleck and Newman [1988] stated that for an isotropic material with a fatigue crack grown a distance Δa, δ is given by:

$$\frac{\delta}{K_{max}^2 / \sigma_y E} = f\left(\frac{x}{K_{max}^2 / \sigma_y^2}, R, \frac{\Delta a}{K_{max}^2 / \sigma_y^2}, \frac{T_{max}}{\sigma_y}, \frac{\sigma_y}{E}, \nu\right)$$

where $R = K_{min}/K_{max}$, and T_{max} is the T-stress at maximum load. The T-stress is the stress parallel to the crack, and arises from the specimen geometry. For a single crystal, δ is also dependent on the material properties, specimen geometry, and distance from the crack tip. However, since the

deformation is constrained to the slip planes seeing the highest resolved shear stresses, δ is also a function of slip plane orientation. Specifically, for this model:

$$\delta = f(C_{11}, C_{12}, C_{44}, \lambda_o, x, \Delta a, T_{max}, K_{max}, R, \Theta, \phi)$$

The directionality of these properties makes it very difficult to use them in normalization. Instead of the anisotropic properties, it is useful to use the averaged uniaxial material properties for normalization. The properties, discussed in section 4.3, used to normalize the C.O.D. plots are:

$$\sigma_o = f(\lambda_o, \Theta, \phi), \quad E = f(C_{11}, C_{12}, C_{44}, \phi), \quad \text{and} \quad K_{Imax} = f(S_{max}, a)$$

Where σ_o is the Hutchinson average, E is the Voigt average, and K_{Imax} is the

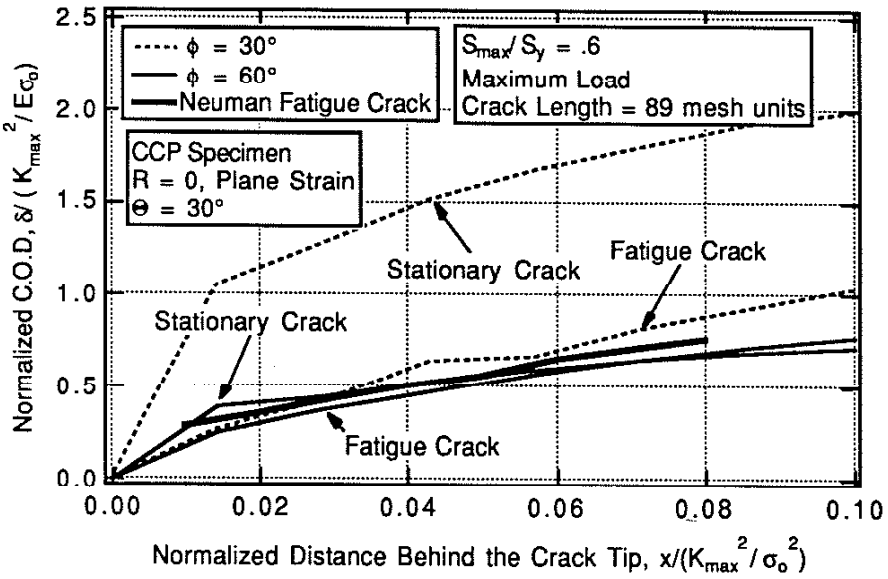

Figure 20: Plot of Normalized C.O.D. versus Normalized distance behind the crack tip.

stress intensity at maximum load. The Voigt average is discussed in section 6.3. By using these averaged properties, and Newman's normalization factors, one can compare the single crystal C.O.D. plots to polycrystalline isotropic material simulations. Also, since all of the material properties and

normalization factors are the same for these two cases, one can exclusively demonstrate the effect of different Θs and ϕs on C.O.D. plots. Figure 20 gives a comparison C.O.D. plot between the 30° case and the 60° case. The fatigue cracks were cycled 20 times from an initial crack length of 60 mesh units to a final crack length of 89, while the stationary cracks under went one cycle at a constant crack length of 89 mesh units. The first thing that one should notice is the difference between the two stationary cracks. The 30° case is open more at maximum load. Since the same load is applied to both specimens, it is apparent that the 30° case is "statically easier" to open than the 60° case. Static opening is defined here as the willingness for a crack to exhibit a large C.O.D. profile under a given applied monotonic load. However, the fatigue cracks have a smaller difference in C.O.D. profiles. This is due to the increased residual displacement left in the wake of the crack after cycling in the 30° case. This phenomenon has been previously observed in isotropic fatigue crack growth [Sehitoglu and McClung, 1989-II]. The ease in opening for the 30° case coincides with increased plastic flow at the crack tip, and increased residual displacement in the wake of the crack. Therefore, the opening level is a balance between the residual displacement and the static ease in opening. The more a particular slip orientation is willing to statically open, the more residual plasticity it will see on the crack line after cycling. However, if a crack only opens slightly under a given applied load, then the slightest amount of residual plasticity can cause it to have very high levels of closure. It follows that if a crack has a very large static opening profile under the same applied load, then it will take large amounts of plasticity to make this crack have high opening and closing levels. Following this reasoning, the increased plasticity seen in the fatigue crack profile for the 30° case cannot overcome the small crack opening profile of the 60° case even though there is minimal plasticity in the latter. This result agrees with the overall stress opening levels. The 30° case has a lower opening level than the 60° case. The difference between the fatigue C.O.D. plots given here, and Fleck and Newman's [1988] results for fatigue cracks is acceptable. The result plotted by Fleck and Newman on Figure 20 is the C.O.D. for an isotropic polycrystalline center cracked specimen. Since the isotropic polycrystalline result is essentially the average behavior of all the crystals, one would expect some orientations to see higher C.O.D. profiles while others may see lower ones. Looking at Figure 20 one can see that the Newman fatigue crack lies in

between the 30° and 60° fatigue cracks. If one were to plot more cases here, they would see a wide band of different C.O.D.'s for different orientations

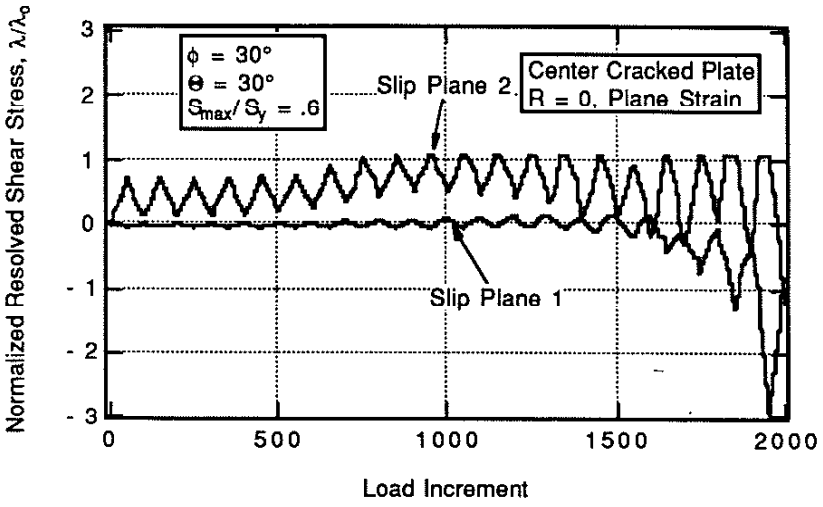

Figure 21: Normalized resolved shear stress of an element which the crack approaches, for the $\phi = 30°$ case.

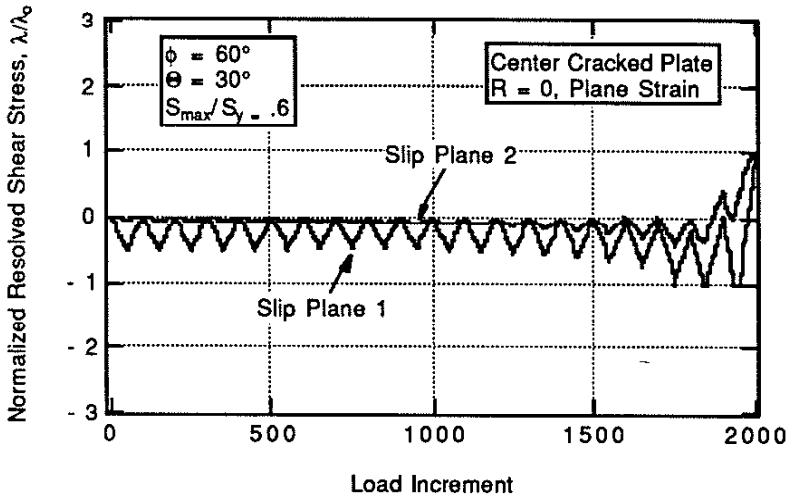

Figure 22: Normalized resolved shear stress of an element which the crack approaches, for the $\phi = 60°$ case.

with the Newman fatigue crack acting as an "average" value.

To better understand why the two cases have different C.O.D. profiles, one must look at what is happening near the crack tip as the crack advances.

One way to do this is by monitoring the resolved shear stress of an element on the crackline, which is initially far from the crack tip. The magnitude of plastic deformation along slip planes at the crack tip is a direct

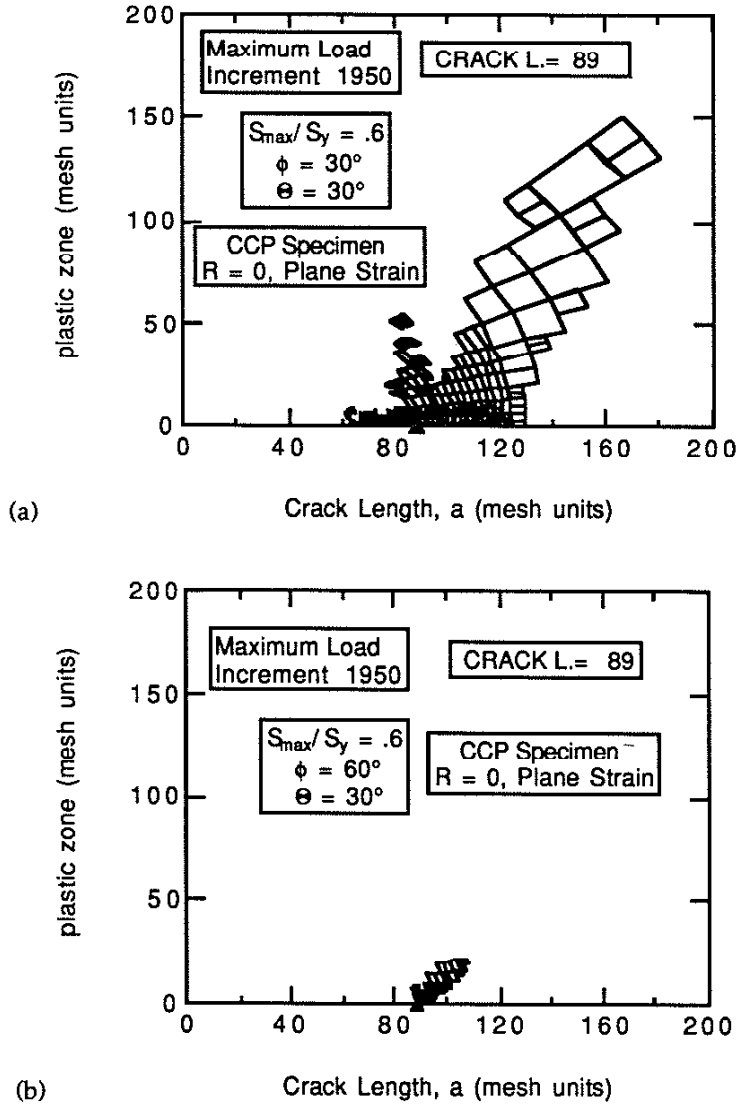

Figure 23: Plastic zones for the 30° case (a.) and the 60° case (b.).

function of the resolved shear stress on each plane. As the crack approaches this element, the resolved shear stresses will steadily increase (recall the scheme in figure 10). The rate at which they increase, along with their

magnitude, gives one a good feel for the amount of average slip occurring at the crack tip. Another words, the behavior of this microscopic element can be used as an approximation of macroscopic slip occurring from the tip. On the final loading cycle, this element is located at the crack tip. By looking at Figures 21 and 22, it is obvious that the resolved shear stress on the slip plane 2 in the 30° case reaches its critical value much earlier than slip plane 1 in the 60° case. This early yielding along the slip plane means that more plastic flow is occurring at the crack tip. For example, by looking at Figure 21, one can see that at load increment 1100 this element is yielding. This means that when this element is 10 elements away from the crack tip, it is undergoing plastic flow. If an element this far from the crack tip is yielding, then the elements near the tip are going far beyond their yield points and leaving large amounts of residual displacements. When the crack reaches its final cycle, one would expect much more residual plasticity along the crack line for the 30° case. By looking at the plastic zones for these two cases (Figures 23a and 23b) it is clear that the 30° case has more plasticity along the crack line. This residual plastic zone agrees with the residual displacement that was seen in the 30° C.O.D. plots. Besides the increased residual plasticity along the crackline, the 30° case also has a significantly larger plastic zone at maximum load.

It has been made clear that the crack in the 30° case opens "statically easier", and that its tip sees increased plasticity. However, it is still necessary

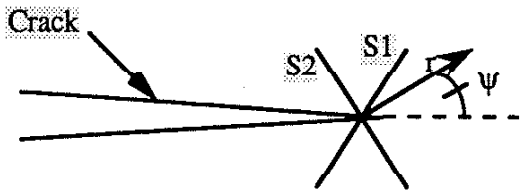

Figure 24: Geometry used in Mohans analysis. As Ψ and r change, the stresses surrounding the crack tip change. In their analysis they also included a third slip plane along the crackline.

to understand how the microscopic slip plane configuration in the 30° case causes these phenomenon. One reason that different slip plane configurations behave differently, is because of asymmetrical stress distributions around the crack tip in a single crystal. Mohan et al. [1992] provided stress distribution results for single cracked crystals undergoing

triple slip from the crack tip (Figure 24). They investigated several slip plane

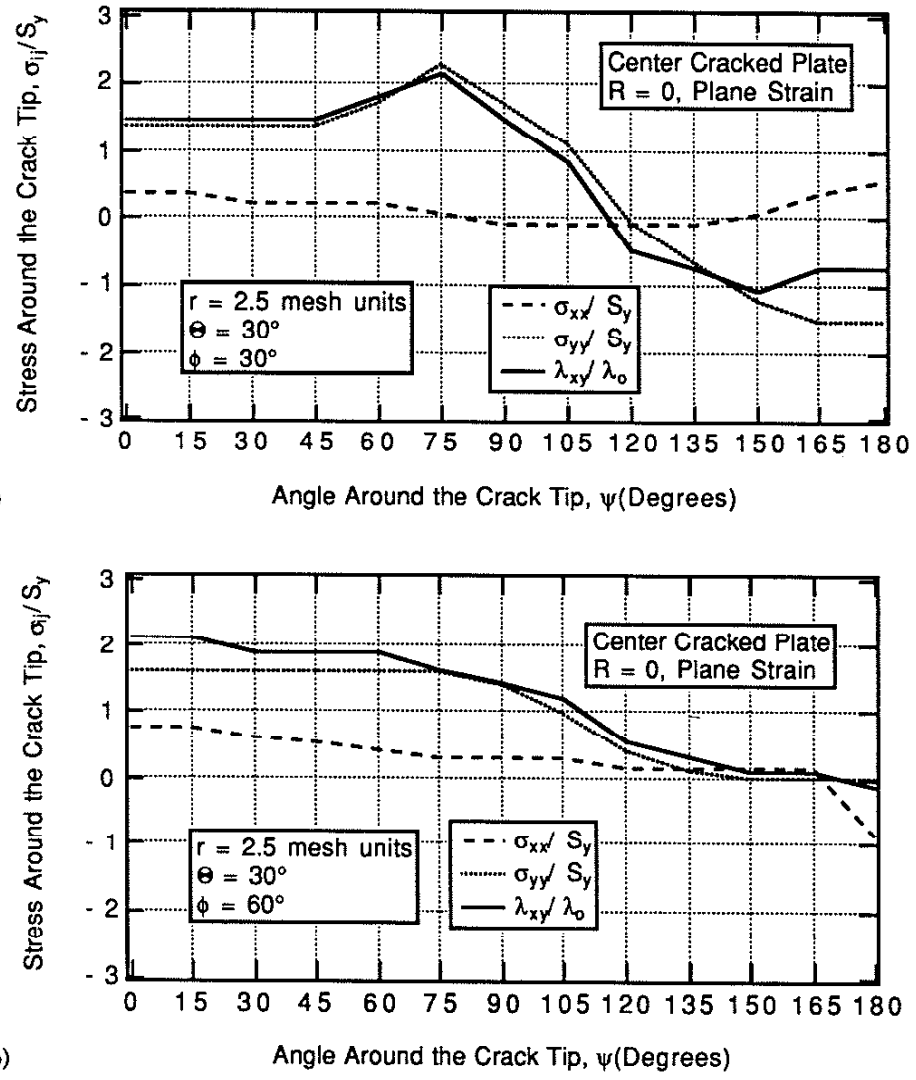

Figure 25: Stress distribution around the crack tip, using Ψ as defined in Figure 24. Plots are for the 30° case (a.) and the 60° case (b.).

orientations, and for each configuration they plotted the distribution of normal and shear stresses for all angles surrounding the crack tip. For different slip plane orientations they found that the normal and shear stresses tended to peak out at different angles. The peak values of the macroscopic stresses were not always along the prescribed microscopic slip plane direction.

This type of behavior was also observed here (Figure 25a and 25b). One can see that the stresses are highly variant with respect to the angle measured from the crackline. One interesting difference in Figures 25a and 25b is the peak seen at 75°. The stresses in the 30° case all peak out at 75°. Looking at Figure 23a, one can clearly see that a large zone of plastic deformation does develop at this angle. This peak in stresses and strains is what causes the crack to open "statically easier" in the 30° case. This 75° peak is caused by slip along the vertical slip plane. Figure 21 demonstrates that the vertical slip plane, slip plane 1, becomes highly active when this element is at the crack tip (Increment 1950). The vertical slip plane lies along a zone where slip is "preferred". This zone, Figure 26, is an area where slip wants to occur. It's

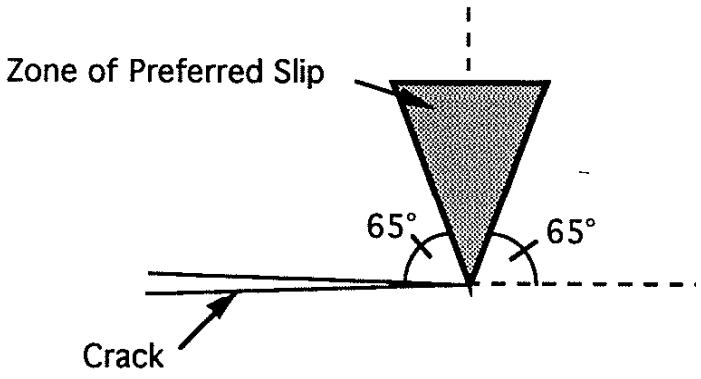

Figure 26: Plot of preferred slip zone at the crack tip for Mode I loading. Macroscopic slip wants to occur in this direction.

location is similar to the Mode I plastic zone for an isotropic material, where macroscopic deformation is not constrained along specific crystallographic planes. If either slip plane of a given orientation lies along this zone, then it may be statically easy to open due to increased plastic flow in the direction of a slip plane. In turn, it will also see more residual plasticity along the crackline. Another words, if microscopic slip is allowed on or near a plane where the crack wants to macroscopically deform, then the crack is going to see an increased amount of plasticity. This increased plastic flow in turn causes the opening profile of some cases to be larger at any given load. All of the orientation cases studied follow this rule relatively well. For example, the cases which have *neither* slip plane in the zone are; ϕ equal to 0°, 5°, 50°,

55°, 60°, and 75°. All of which have relatively small stationary crack opening displacements. The bounds of the zone are only approximate. It should be noted here that presence in the zone does not exclusively dictate the slip behavior. Macroscopic slip can appear to occur along directions other than prescribed slip directions. In Figure 23b one can see that a small plastic zone develops around 45° from the crackline. However, looking at Figure 19, one can see that the 60° case does not have any microscopic slip planes oriented along that direction. The zone in this case is caused by microscopic slipping along directions which are not parallel to the principal direction of the zone. The non-parallel microscopic slipping adds up in a direction which is macroscopically preferred by the crack. Hence, this zone is much smaller than a zone formed when the microscopic slip and macroscopic slip have similar orientations. Although these "artificial" plastic zones are negligible in many of the orientation cases, they play an important role when both slip planes are symmetric about the crack face.

5.3 Slip Plane Orientation Effects

In this section, the effect of slip plane orientation, Θ, on crack opening levels will be studied. Since the crystallographic orientation, ϕ, will be kept at zero, the slip planes remain symmetric about lines perpendicular and parallel to the crack line. The behavior of the model in this state is similar, but not exactly the same, as the previous section. The symmetry causes some different phenomenon to occur. Looking back at Figure 8, one can see how the crack opening levels vary with different Θ values. The plot has two interesting features. As seen in the orientation study, the opening plot is divided into two regions: a high opening region and a low opening region. Additionally, the Θ variation plot has a very interesting symmetry at 45°. Intuitively, this symmetry may not seem justifiable. However, its existence will be thoroughly explained.

Since the opening levels are symmetric at 45°, slip planes which are microscopically oriented nearly vertical (Θ = 15°) have the same effect as slip planes which are oriented nearly horizontal (Θ = 75°). This result may seem odd since the preferred Mode I macroscopic slip zone (Figure 26) appears nowhere near the microscopic slip planes oriented at 75°. One may expect the 75° case to have less plasticity than the 15° case. For a single slip plane this

reasoning was found valid, but when two symmetric slip planes are involved the situation is different. Keeping in mind that the macroscopic shear is the summation of microscopic shear, it is crucial that one understands how two

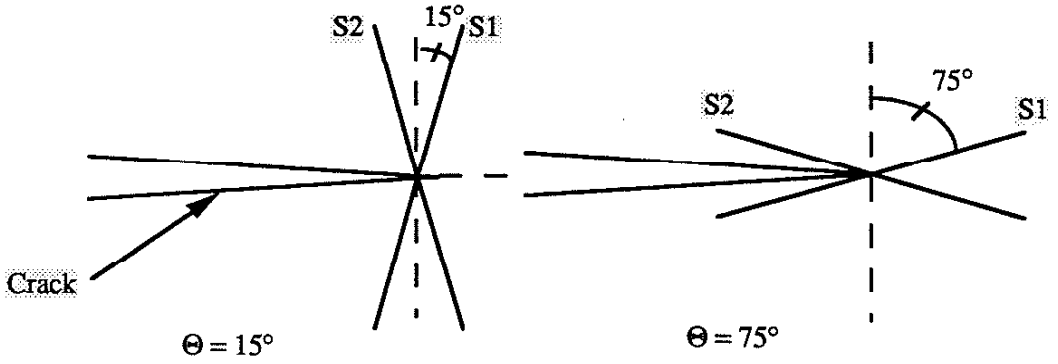

Figure 27: Microscopic slip plane orientation at the crack tip for the two Θ, cases which will be examined.

different microscopic cases can yield the same macroscopic result. To do this, two specific Θ cases are compared and contrasted. Figure 27 takes a look at the cases that will be studied here. Even though both cases have different microscopic slip configurations, the crack sees the same opening levels for both cases. They have the same opening levels because the microscopic slip along individual planes adds up to yield the same macroscopic plastic zone (Figure 28). Both of the macroscopic plastic zones in Figure 28 form in the "preferred" direction discussed in section 5.2. For the 15° case, this makes intuitive sense since the both microscopic slip planes are oriented along the zone. However, the 75° case has microscopic slip planes which appear to be out of the zone. Even though one may expect a smaller zone to form in this case, a significant one does form. The zone which forms here is "artificial" in nature. That is, it is formed by microscopic slipping which is not parallel to the general direction of the zone. This effect was observed in most of the orientation cases, but was deemed negligible. However, in these symmetric cases, the microscopic non parallel slipping adds up to create a significant macroscopic plastic zone in the preferred direction.

To better understand how the two microscopically different cases sum to yield the same macroscopic slip, one need to observe the microscopic slip

behavior of an individual element. The approach used here is the same as

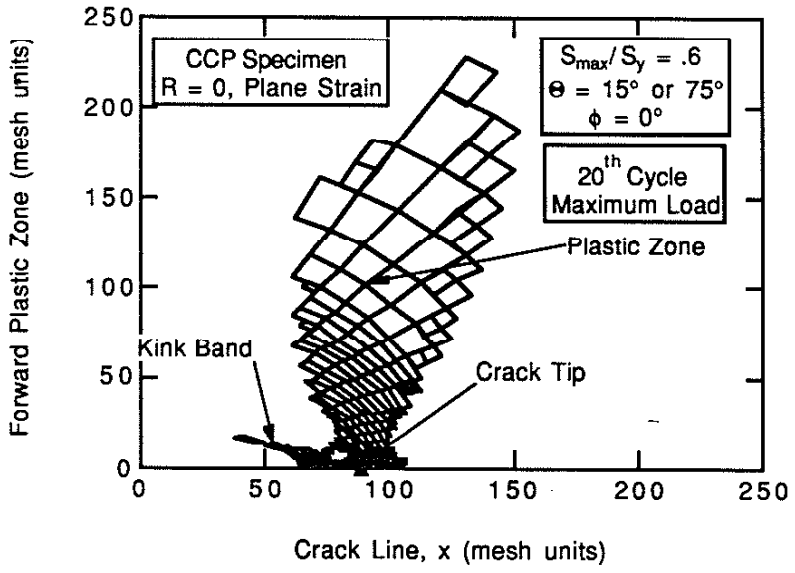

Figure 28: Plastic zone, or macroscopic slip band, for both Θ cases. The zones are exactly the same.

the one used in section 5.2. By monitoring the resolved shear stresses on both slip planes for an element initially far from the crack tip, one can essentially observe the behavior of the crack as it advances. Figure 29 plots the microscopic resolved shear stress on both slip planes for an element which is at the crack tip on the final cycle. Looking at Figure 29, one can see that a very interesting phenomenon occurs. Even in the complex stress state at the crack tip, the two slip planes for the different cases see complimentary resolved shear stresses. That is, slip plane 1 in the 15° case sees the same resolved shear stress as slip plane 2 in the 75° case, and slip plane 2 in the 15° case sees the same resolved shear stress as slip plane 1 in the 75° case. This resolved shear stress symmetry between slip planes is only seen when the slip planes are symmetric about the crack line. Another words, when ϕ is 0°, 90°, 180°, or 270°. When this symmetry is seen between slip planes, the microscopic slip will sum to the same macroscopic slip. Additionally, the macroscopic slip will occur close to the preferred slip direction (Figure 26). It should be noted that the symmetry is caused by the mathematical nature of the model. The

symmetric double slip model causes the cancellation of some sine and cosine

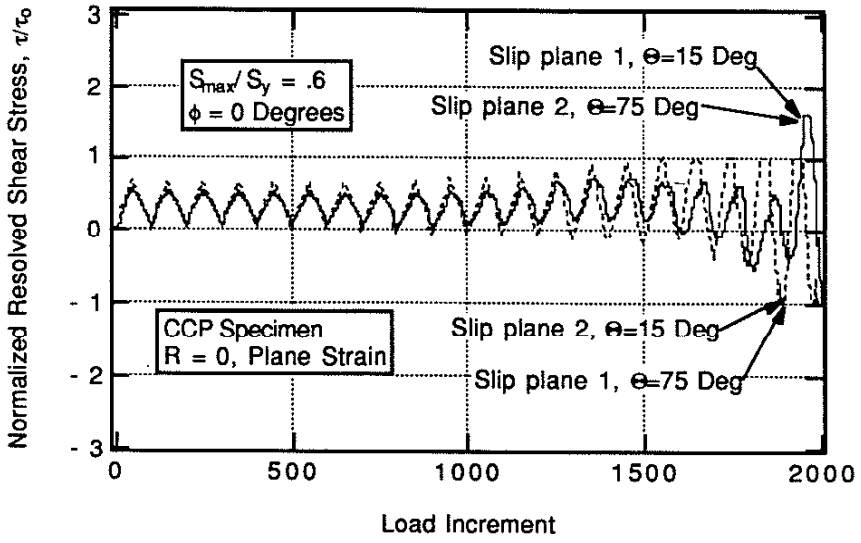

Figure 29: Normalized resolved shear stress of an element which the crack approaches, for the 15° and the 75° case.

terms used in the Schmid orientation tensor. The term cancellation arises when summing the plastic strain contribution from each slip plane, along the global directions, into the macroscopic strain tensor. In a real material, this effect may not be seen. Additionally, the crystal lattice is not allowed to rotate. If this effect is included, then the slip planes will rotate with respect to each other as they plastically deform.

Now that the symmetry of Figure 8 is understood, an explanation of the different opening levels for different Θ values is needed. As the slip planes are moved closer together, $\Theta \rightarrow 0°$ or $\Theta \rightarrow 90°$, the opening levels begin to drop off. To explain this trend, two cases will again be compared. Because the plot is symmetric about 45°, only the left side will be used to explain the results. Since both sides are macroscopically the same, the reasoning for the right sides drop in opening levels is similar. The cases which will be compared are Θ = 15°; ϕ = 0° and Θ = 30°; ϕ = 0°. It should be noted here that the applied loads for the CCP specimen are different for these two cases. Although this does not affect the opening levels (See section 4.4 and note that in Figure 8, the CT specimen has the same applied loads for all

of the orientations), the difference in some of the plots may be slightly exaggerated. However, it has been investigated and the differences in plastic

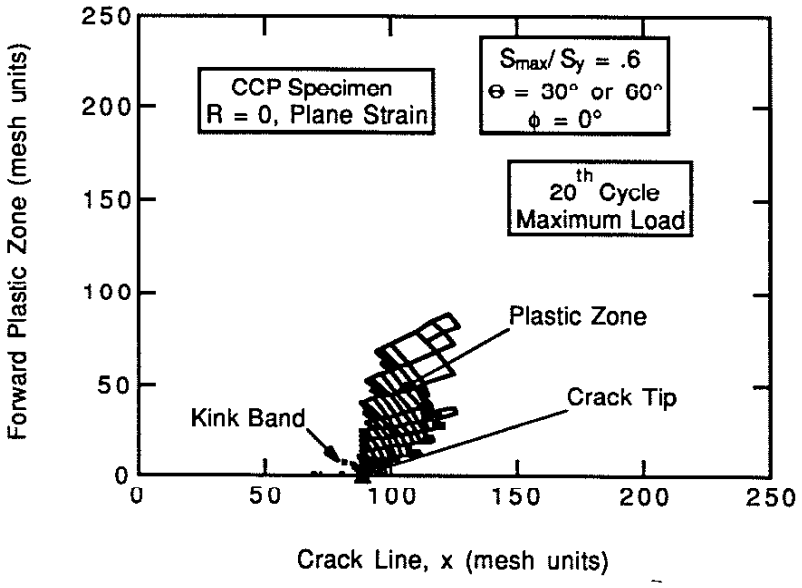

Figure 30: Plastic zone, or macroscopic slip band, for the $\Theta = 30°$ and $\Theta = 60°$ cases. The zones are exactly the same.

zone plots, and resolved shear stress plots still exists at the same applied loads. Even though the differences may not be as large at the same applied load, the opening levels are affected in the same way.

As in the orientation cases, the opening level is a balance between residual plasticity along the crackline and static ease in opening. As the slip planes are moved more vertical, or horizontal, increased plasticity is seen. This can be observed by comparing Figures 28 and 30. The 30° case has much less plasticity than the 15° case. The smaller degree of plasticity in the 30° and 60° cases is again a result of the macroscopic shear zone. The 15° and 75° cases are allowing more slip in the zone than other two cases. The increased plastic flow in the 15° and 75° cases affects the crack opening profiles in the same manner as previously discussed (Figure 31). The C.O.D. plots in Figure 31 are normalized by the maximum applied stress intensity. This factor helps to alleviate any differences in the plots caused by different applied loads. As expected, the case with a larger plastic zone (15°) is statically easier to open.

Surprisingly, the difference in crackline plasticity between these two cases is negligible. The coupling of these two facts is what causes the 15° case to have much lower opening loads. A general trend in C.O.D. plots was found for the

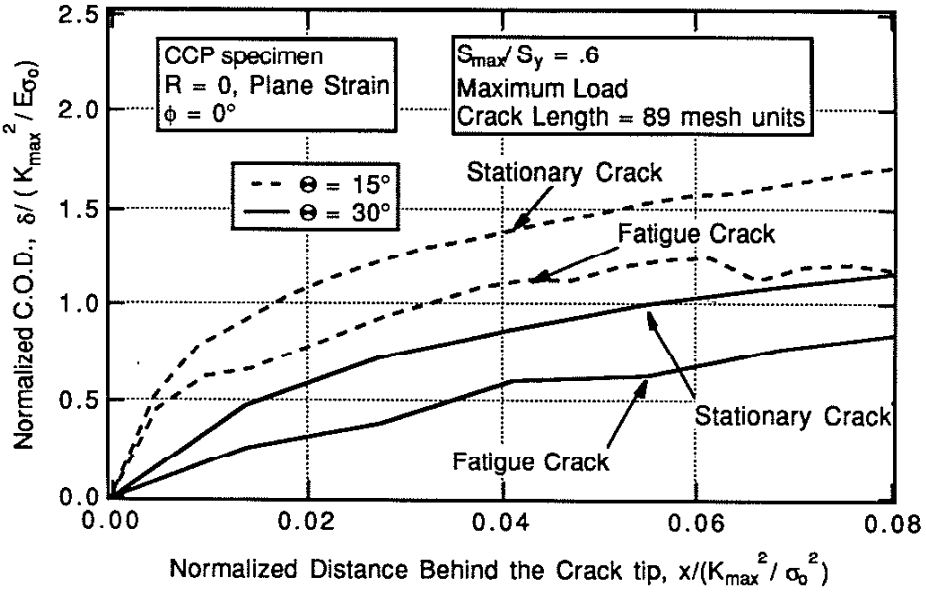

Figure 31: Plot of normalized C.O.D. versus normalized distance behind the crack tip.

Θ variation cases. As the slip planes approached the vertical ($\Theta \rightarrow 0°$) or horizontal ($\Theta \rightarrow 90°$) extremes, the stationary and fatigue C.O.D. plots increased. The trend can be observed in appendices B and C. Although the increase was more prominent for different applied loads, the trend still existed at the same applied load. In appendix B one can see that at the same applied load, the C.O.D. plots for the CT Specimen still exhibited the same trend as CCP specimen. This trend is responsible for the variation in opening levels for different Θ cases (Figure 8).

6. Discussion

6.1 Crack Growth Rate Variability Due to Closure Stress

Variability in microstructurally short crack growth data due to closure stress differences within grains has been documented by Morris [1977] and Morris and James [1983]. Figure 32 demonstrates the experimental variation seen in growth rate data for 7075-T6 Al. At any given stress intensity value, the crack growth rate spans a wide range of values. In the short crack regime, between 2 and 5 $MPa\sqrt{m}$, the scatter due to closure stress differences is particularly large. At 2 $MPa\sqrt{m}$ the experimental maximum growth rate is nearly 5 times the minimum growth rate. Morris and James attributed this variation to differences in closure stresses for short cracks as they grow within

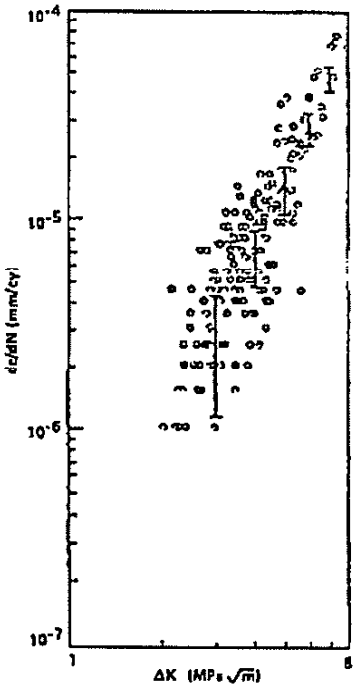

Figure 32: Growth rate data for 7075 Al [Morris and James 1983]. The error bars represent the scatter obtained form a computer simulation of growth rate using closure stress.

a grain. The error bars represent the scatter which they predicted with a statistical computer simulation using closure stress differences. In the shortcrack regime Morris and James's model predicts the scatter ratio,

$\frac{da}{dN}(\max)/\frac{da}{dN}(\min)$, to be around 4. Aside from closure variations *within* grains, the experimenters here also attribute the actual experimental scatter to closure differences *between* grains with different orientations. Since grains of different orientations exhibit vastly different opening levels (Figure 18), microscopically short cracks may have many different opening levels for the same loading conditions. By using a modified crack growth law one can quantify, or set bounds on, the variability of crack growth rates due to different closure stresses in different grains. Through a simple calculation, using the maximum and minimum closure levels from section 5.2, one can predict the expected da/dN scatter. The maximum growth rate will occur when the closure stresses are extremely low, while the minimum growth rate will occur when the closure levels are extremely high. Using the definition of effective stress intensity range, and plugging in the maximum ($S_{open}/S_{max} \approx .35$) and minimum ($S_{open}/S_{max} \approx .02$) opening levels form section 5.2, one gets the following effective stress ranges:

$$\Delta\sigma_{eff(max)} = .98\sigma_{max} \qquad \Delta\sigma_{eff(min)} = .65\sigma_{max}$$

Now, one can calculate the maximum and minimum stress intensity ranges using the maximum and minimum effective stress ranges:

$$\Delta K_{eff(max)} = Y(.98\sigma_{max}\sqrt{\pi a}) \qquad \Delta K_{eff(min)} = Y(.65\sigma_{max}\sqrt{\pi a})$$

For a typical crack growth exponent of m, the ratio $\frac{da}{dN}(\max)$ over $\frac{da}{dN}(\min)$ can be written as;

$$\frac{\frac{da}{dN}(\max)}{\frac{da}{dN}(\min)} = \frac{C(Y(.98\sigma_{max}\sqrt{\pi a}))^m}{C(Y(.65\sigma_{max}\sqrt{\pi a}))^m}$$

Which reduces to;

$$\frac{\frac{da}{dN}(\max)}{\frac{da}{dN}(\min)} = \frac{(.98)^m}{(.65)^m}$$

One should note here that this scatter ratio is not constant. The ratio is highly dependent on the crack growth exponent, m (Figure 33). Near the threshold regime, where the slope of the growth curve (m) is higher, the ratio may be higher since the m is higher. In Figure 32, the average slope of the data is around 4. From Figure 33 this gives one a scatter ratio of 5. Given that the

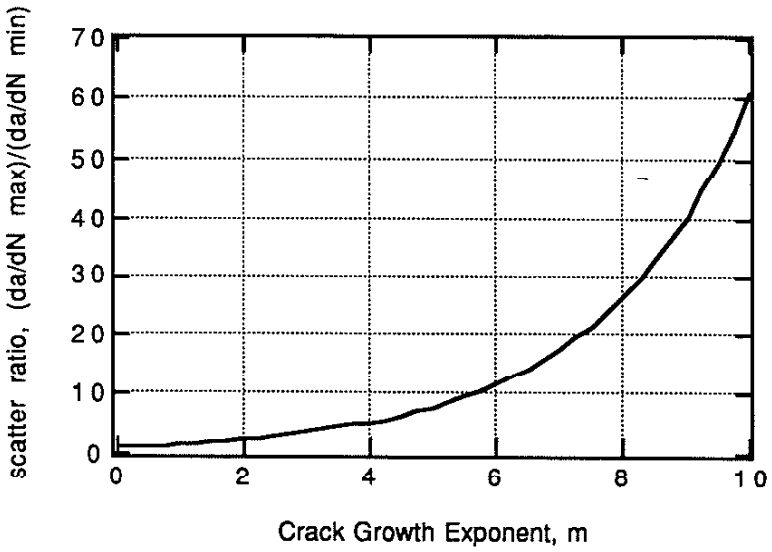

Figure 33: Dependence of the scatter ratio, $\frac{da}{dN}$(max) over $\frac{da}{dN}$(min), on the crack growth exponent, m.

ratio $\frac{da}{dN}$(max) over $\frac{da}{dN}$(min) is nearly 5, a microscopically short crack is capable of growing through one grain, with a preferred orientation, 5 times faster than a similar grain with an unpreferred orientation. This growth rate scatter prediction is due solely to closure stress differences *between* grains. This ratio of crack growth rates is very close to the actual experimental scatter. Although this simulation only considers plasticity induced closure, the expected scatter should be similar when other mechanisms of closure are introduced.

6.2 Crack Growth Rate Variability Due to Grain Boundaries

In addition to variability due to closure levels, short crack variability has also been attributed to "grain boundary effects" [Lankford 1982, De Los

Rios et al. 1985, Tokaji et al. 1987, Liaw 1988, Larson et al. 1988, Lee and Sharpe 1988, Tanaka 1989, Miller 1991]. Along with many others, the researchers cited here have observed a common phenomenon in short fatigue crack growth. Figure 34 is a reproduction of a typical short crack growth curve. The short cracks not only grow faster, but the growth rates experience several peaks and valleys. Many researchers have attributes this variability to "grain boundaries". They have found that crack growth rates slow down, or even become zero, as a crack approaches a new grain. Once a significant number of grains have been grown through, and the plastic zone spans several grains, this effect is less significant. On a similar note, Lankford [1982] and Tokaji et al. [1987] noted that grain boundaries are simply adjoining grains with different crystallographic orientations. They concluded that it is not a mysterious "grain boundary" which causes crack slowdown and arrest, but rather a difference in crystallographic slip orientations between grains.

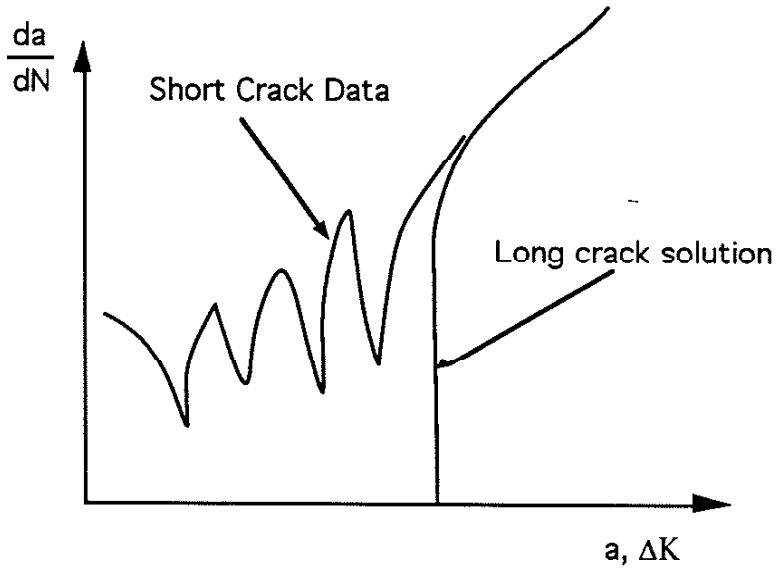

Figure 34: Typical short crack growth curve compared to the long crack solution.

Lankford [1982] and Tokaji et al. [1987] both found that crack growth was not affected when two adjacent grains had similar crystallographic orientations. Slowdown and arrest only occurred when a grain of unpreferred orientation followed a preferred grain. The slowdown effect is not exclusively a closure

effect. Since crack growth is accomplished through plastic flow at the crack tip, the amount of crack tip plasticity and crack tip opening displacement which a grain permits for a constant loading condition is crucial. As the orientation of the grain with respect to the loading is changed, these parameters may change.

Using the results in section 5.2 this slowdown and or arrest of crack growth can be reasoned. For example, consider the setup given in Figure 35. Assume that the loading is perpendicular to the crack face, and that it stays that way until it reaches grain B. This crack is growing relatively easily through grain A. The orientation (ϕ = 30°) of grain A, with respect to the crack face and loading, allows large amounts of crack tip plastic flow and large crack opening displacements. Since cracks propagate through plastic slip at the tip and the propagation rate is proportional to the C.O.D. [Pelloux, 1969], this increased plastic flow and C.O.D. means that this grain is oriented in a

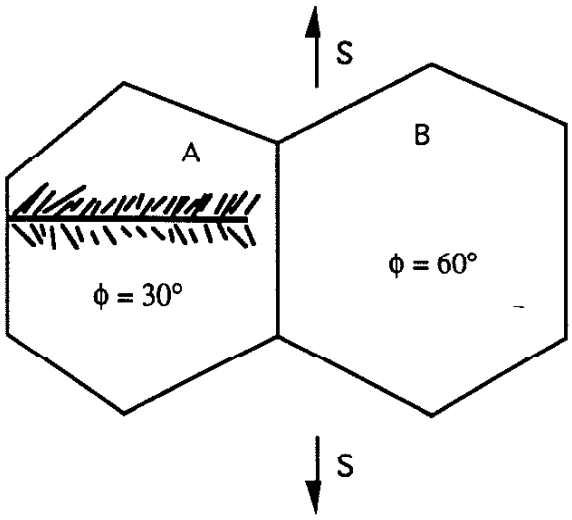

Figure 35: Crack growth through two grains of a material. Θ is kept at 30° in both cases.

preferred direction. Additionally, since closure levels in the ϕ = 30° case are low, the tip is hardly shielded. As the crack grows through grain A, and the crack tip approaches grain B, crack tip plasticity and C.O.D. is reduced. The reduction is caused by the orientation of grain B. For the given loading conditions, the ϕ = 60° grain does not allow plastic flow in the preferred

direction. In turn, the crack tip opening displacement becomes smaller. Plastic flow, or dislocation motion, at the crack tip may even be abruptly stopped near the boundary if the misorientation between grains is large enough. This effect becomes more prominent as the crack gets closer to the boundary. The restriction will essentially slow the crack while it is still growing in grain A. Additionally, when the crack reaches grain B, it may be forced to change directions into a more preferred growth direction. It is even possible for the crack to arrest if a preferred direction is not easily initiated in grain B. This crack slowdown and possible halting is what causes the highly variable crack growth rates in microstructurally short cracks (Figure 34). In future research the F.E.M. model may be revised to include several grains. This will help to quantify the effect of neighboring grains on fatigue crack growth parameters.

6.3 Strain Range Variability Ahead of the Crack Tip

One parameter used to characterize a fatigue crack is the strain range ahead of the crack tip. A plot of strain range versus distance from the crack tip can be done along the crack line to demonstrate the increased strain that material near the crack tip sees. And when used correctly, crack tip strain ranges can help give insight into the fatigue behavior an life of different materials [Chan, 1993]. The strain ranges may become very high in magnitude. McClung and D.L Davidson [1991-I] reported that near tip strain ranges could reach levels of ten times the yield strain, for an applied far field load that is 85% of the yield stress.

A common normalization scheme has been developed to compare experimental and finite element strain range plots [McClung et al., 1991-I]. Since finite element analysis provides easy access to a wealth of information near the crack tip, F.E.M. results can help give a better understanding of fatigue crack growth. That is, only if the F.E.M. results match experimental results. McClung and Davidson used this scheme to look at strain ranges for short and long cracks. He found that the finite element results did an excellent job predicting strain ranges for long cracks, but were quite deficient for short cracks (Figure 36). The short crack data exhibited high variability from experiment to experiment. And, the finite element simulation served as a lower bound for these experimental results. This is a definite

shortcoming of traditional F.E.M. analysis since the cracked bodies are seeing much higher strains than predicted. He reasoned that since the short cracks are smaller than the average grain size, microstructural effects come into play. This is because the experimental data was taken from several different

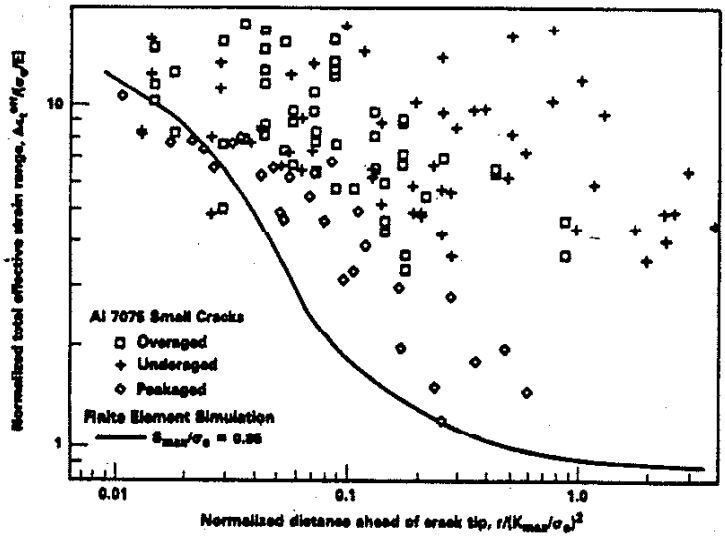

Figure 36: Plot of effective strain ranges ahead of the crack tip for small fatigue cracks [McClung and Davidson, 1991].

specimens under the same testing conditions. For different specimens with a short crack, the grain containing the crack may be oriented differently. This different orientation causes vastly different strain ranges for a given applied load and crack length. However, this difference can be properly estimated using the double slip finite element simulation. By applying the same far field load, varying the crystal orientation, and keeping the angle between the slip planes constant, the experimental setup can be simulated.

Before plotting the strain distributions for the double slip F.E.M. simulation, a normalization scheme similar to the one used by McClung and Davidson is implemented. The effective strain range is calculated using the same procedure. At each gauss point along the crack line, the strains $\Delta\varepsilon_{xx}, \Delta\varepsilon_{yy}$, and $\Delta\gamma_{xy}$ are calculated for the final reversal. Then using the plane strain Mohr's circle solution, the corresponding two principal strains are

calculated at each gauss point. Finally, the plane strain total effective strain range is calculated using the following equation:

$$\Delta\varepsilon_t^{eff} = \frac{2}{\sqrt{3}}(\Delta\varepsilon_1^2 + \Delta\varepsilon_1\Delta\varepsilon_2 + \Delta\varepsilon_2^2)$$

The next step is to deal with the normalization factors. The strain range is normalized by the yield strain, (σ_o / E), and the distance ahead of the crack tip is normalized by the factor $(K_{max} / \sigma_o)^2$. The maximum stress intensity calculation is trivial since it only depends on the applied stress and the crack length. Since the crack is grown sufficiently far from the notch, crack length > .1 notch width, one can include the notch width into crack length calculations. This allows one to use the center cracked plate stress intensity solution. For a finite width body, the stress intensity is given by:

$$K_I = C\sigma_{app}\sqrt{\pi a}$$

Where C is the finite width correction factor for this geometry. For the mesh width used here, this factor turns out to be negligible. The values of σ_{app}, and a are taken from the top of the final reversal to calculate K_{max}. However, a decision is necessary on what values to use for the yield stress and elastic modulus. The experimental results are normalized using the average isotropic material constants for aluminum. To best mimic this situation, one needs to imagine that the cracked grain being analyzed with the crystal plasticity F.E.M. program is one grain inside of an externally loaded large body. This body is made up of many more similar grains of different orientation. The averaged material properties of this large body are the properties needed for normalization. Using these properties will enable one to predict upper and lower bounds on the strain ranges by varying the orientation of the crack tip grain.

There are several theories developed for predicting multi-granular isotropic properties from single crystal properties. Given the crystal elasticity constants, C_{11}, C_{12}, and C_{44}, Voigt has determined an average elastic modulus for a given isotropic material made up of many of these grains. The grains are oriented in random directions. His governing equation is:

$$E = \frac{(C_{11} - C_{12} + C_{44})(C_{11} + 2C_{12})}{(2C_{11} + 3C_{12} + C_{44})}$$

The value of the crystal elasticity constants for the simulation are: C_{11} = 221 GPa, C_{12} = 134 GPa, and C_{44} = 102 GPa. The Voigt average elastic modulus calculated from these constants is 203 GPa. A reasonable yield stress average to use is the Hutchinson ϕ average, σ_o. Using E and σ_o as normalization factors for a loaded single crystal enables one to replicate the effect of loading different isotropic specimens with short cracks.

Sample results of these runs are shown in Figure 37. It is clearly shown

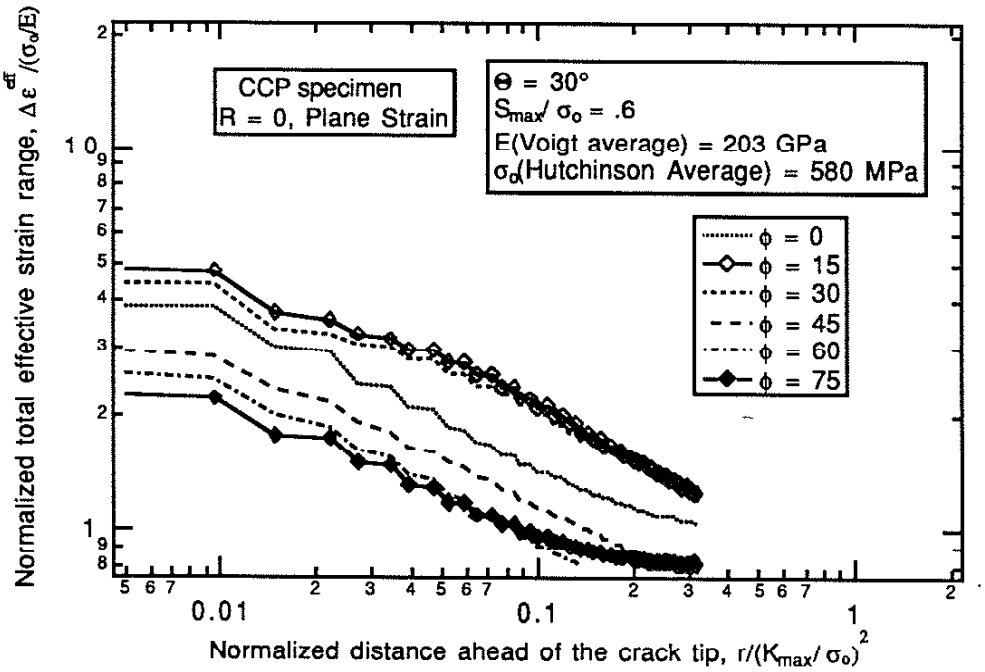

Figure 37: Plot of effective strain ranges ahead of the crack tip for the final loading cycle in the CCP specimen. The ranges are taken from fatigue cracks at the peak of their 20th cycle.

that for the same applied load, different crystal orientations exhibit different effective strain ranges. From the plot, one also notices that upper and lower bounds on the strain range are formed. Since it is not realistic to run cases at every angle, cases have been run at increments of 15°. The behavior in between the increments is assumed to be relatively smooth. For the cases

run, ϕ = 75° provides a lower bound on the strain ranges while ϕ = 15° dictates the upper bound. The difference between them is about a factor of two. It should be noted here that in addition to the high variability in strain ranges, McClung et al. [1991-I] reported much higher strain ranges away from the tip for short cracks. They attributed this to the fact that the crystals containing the short crack may be fully plastic. At this time, the single crystal mesh could not be run fully plastic. If the load for the single crystal program was increased from Smax/Sy = 0.6 to a load near Smax/Sy = 1.0, then the maximum and minimum strain ranges would do a much better job serving

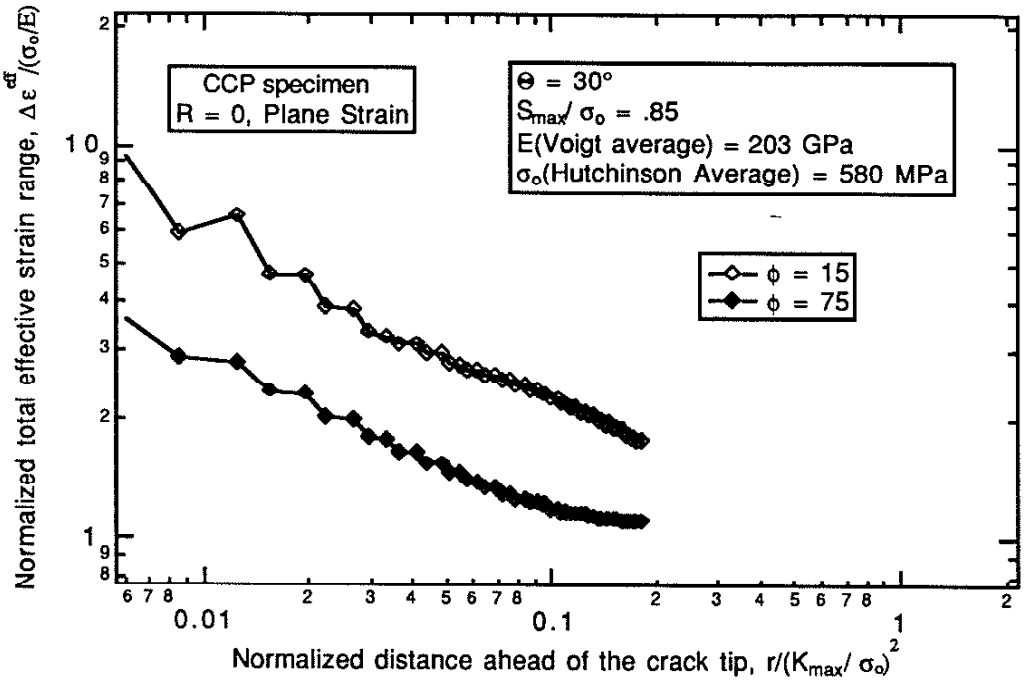

Figure 38: Plot of effective strain ranges ahead of the crack tip for the CCP specimen. The ranges are taken from stationary cracks of the same crack length as the cracks in Figure 36.

as upper and lower bounds for the experimental results that McClung documented. The highest far field load allowed by the program for *one cycle* was Smax/Sy = .9. Using this information, the bounds for the extreme cases, ϕ = 15° and ϕ = 75°, were run for one cycle at the same crack length as the fatigue cracks in Figure 37. The experimenters found that the strain ranges for the fatigue and stationary cracks were similar. The results are plotted in

Figure 38. Although the ranges are increased, and still exhibit great variability, they still drop off quickly as one moves away from the crack tip. The average slope of the experimental data (Figure 36) is less than the average slope of the single crystal plots (Figure 37 and 38). The difference in average slopes is attributed to the limitations on the applied loads in the program. The ranges are expected to follow the experimental results closer if the mesh could be loaded at greater far field loads.

The following example should further illustrate the variability concept. Take two center cracked specimens with microstructurally short cracks, both loaded with the same far field stress. Specimen one's crack is in a grain oriented at 15° with respect to the crack line, and specimen two's crack is in a grain oriented at 75°. According to Davidson's experimental work, one may see a large variation in effective strain ranges near the crack for these two *macroscopically* similar specimens with short cracks. And we also know that traditional finite element simulations predict that there should be no variability between these specimens. However, the crystal plasticity strain range plots (Figure 37 and 38) predict the variability in ranges. The crack tip in specimen one has a much higher strain range than the crack tip in specimen two. This effect is due solely to varying the microscopic orientation of the grain.

7. Conclusions

(1) The elastic-plastic double slip finite element model does an excellent job simulating fatigue crack growth through a real single crystal. Given a single finite element mesh, with plastic deformation microscopically constrained on two slip directions throughout the mesh, the finite element model forms macroscopic slip bands exclusively at the crack tip. The slip bands which form here have many of the same characteristics as the bands which an assortment of researchers have experimentally observed. These bands are the cause of fatigue crack propagation at stress intensities below K_{Ic}.

(2) As the crystallographic orientation of a single crystal, or grain, with respect to the crackline is changed, many fatigue crack growth parameters change. Different grain orientations have been found to exhibit different degrees of plasticity, display different static and fatigue crack C.O.D.'s, and ultimately have different degrees of crack closure.

(3) The different degrees of closure seen for different crystallographic grain orientations can provide justification for the higher variability seen in short fatigue crack growth rates, or in long cracks growing through large grain structures. Since both types of cracks grow through grains, they encounter grains with different orientations. Since grains of different orientation have been shown to exhibit different degrees of crack closure and plasticity, the driving forces in fatigue crack growth, the rate at which cracks grow through different grains will vary. Using closure differences between grains, the crack growth rate may be expected to vary by nearly a factor of five.

(4) Besides variability in growth rates, experimentalists have also blamed microstructural effects on the strain range variability seen in microstructurally short cracks (cracks contained within single grains). Aside from being incapable of predicting this variability, traditional finite element methods unfortunately under predict the strain ranges in these cracks. However, by varying the crystallographic orientation of this finite element model, the variability in strain ranges can be predicted.

(5) As the angle between the microscopic slip directions, with respect to the crackline is changed, many fatigue crack growth parameters change. Different slip configurations have been found to exhibit different degrees of plasticity, display different static and fatigue crack C.O.D.'s, and ultimately have different degrees of crack closure.

(6) Macroscopic slip usually occurs in a preferred direction. The preferred direction is along a direction similar to the isotropic plastic zone. If microscopic slip does not add up in the macroscopically preferred direction then the cracks sees minimal plasticity and is "statically" difficult to open.

(7) The mechanism of macroscopic material transfer, which causes premature crack face contact, is the same in double slip crystals and multi-granular isotropic materials. Residual material is transferred from directions lying in the plane of the crack face to a direction perpendicular to the crack face. In plane strain the majority of the material comes from the direction along the crackline.

(8) The two different specimens studied (CT specimen and Center Cracked Specimen) essentially produced the same results. Primarily, the crack opening levels for different Θ and ϕ combinations are the same.

(9) At a constant applied load ratio, $S_{max} / S_y = .6$, the opening levels (.02 - .35) in the plane strain double slip model fell both above and below the isotropic plane strain result (.1).

References

Adams, N. J. I., "Fatigue Crack Closure at Positive Stresses", *Eng. Fract. Mech.*, **4**, 543-554, (1972).

Asaro, Robert J., McHugh, P.E., Varias, A.G., Shih, C.F. "Computational Modeling of Microstructures", *Elsevier Science Publications*, 295-318, (1991).

Asaro, Robert J. "Micromechanics of Crystals and Polycrystals", *Advances in Applied Mechanics*, **23**, 1-115, et. John W. Hutchinson. (1983).

Asaro, Robert J., "Geometrical Effects in the Inhomogeneous Deformation of Ductile Single crystals", *Acta Metallurgica*, **27**, 445-453, (1978).

Bassani, John L., Wu, Tien-Yue, and Laird, Campbell. "Latent Hardening in Single crystals I. Theory and experiments.", *Proc. R. Soc. Lond.*, **435**, 1-19, (1991).

Elber, W., "The Significance of Fatigue Crack Closure.", *Damage Tolerance in Aircraft Structures*, ASTM STP 486, 230-242, (1971).

Chan, *Mett. Trans.*, (1993).

Fleck, N. A. and Newman, J. C., Jr., "Analysis of Crack Closure Under Plane Strain Conditions", *ASTM STP 982*, 319-341, (1988).

Finney, J., PhD. thesis, University of Pennsylvania, 1974.

De Los Rios, E. R., Hussain J. Mohamed and K. J. Miller, "A Micro-Mechanics Analysis For Short Fatigue Crack Growth", *Fatigue Fract. Engng Mater. Struct.*, **8**, 49-63, (1985).

Hosford, William F., "The Mechanics of Crystals and Textured polycrystals" Oxford University Press, (1993).

Hutchinson, J. W. "Plastic Deformation of BCC Polycrystals", *J. Mech. Phys. Solids*, **12**, 25-33, (1964).

Koiter, W. T., "Stress-Strain relations, uniqueness and variational theorems for elastic plastic materials with a singular yield surface." *Quart. Appl. Math.*, **11**, 350 (1953).

Kukhlman-Wilsdorf, D. and C. Laird, "Dislocation Behavior in Fatigue, II. Friction Stress and Back Stress as Inferred from an Analysis of Hysteresis Loops" *Material Science and Engineering*, **37**, 111, (1979).

Laird, C., "The Influence of Metallurgical Structure on the Mechanisms of Fatigue Crack Propagation.", ASTM STP 415, 131-180, (1967).

Liaw, P.K "Overview of Crack Closure at Near -Threshold Fatigue Crack Growth Levels", *Mechanics of Fatigue Crack Closure*, ASTM STP 982, J.C. Newman, Jr. and W. Elber, Eds., American Society for Testing and Materials, Philadelphia, 62-92, (1988).

Lalor, Paul L. "Mechanics Aspects of Crack Closure". *Masters Thesis, University of Illinois..* Report **133**, (1986).

Lankford, J., "The Growth of Small Fatigue Cracks in 7075-T6 Aluminum", *Fatigue of Engineering Materials and Structures.*, **5**, 233-248, (1982).

Larson, J.M., Williams, J.C., and Thompson, A. W., "Crack Closure Effects on the growth of Small Surface Cracks in Titanium-Aluminum Alloys", *Mechanics of Fatigue Crack Closure*, ASTM STP 982, J.C. Newman, Jr. and W. Elber, Eds., American Society for Testing and Materials, Philadelphia, 149-167, (1988).

Lee, J.J. and Sharpe, W.N. "Closure Measurements on Short Fatigue Cracks", *Mechanics of Fatigue Crack Closure*, ASTM STP 982, J.C. Newman, Jr. and W. Elber, Eds., American Society for Testing and Materials, Philadelphia, 270-278, (1988).

McClung, R. C. and D. L. Davidson, "High Resolution Numerical and Experimental Studies of Fatigue Cracks", *Engn. Fracture Mech.*, **39**, 113-130, (1991-I).

McClung, R.C., Thacker, B.H., and Roy, S. "Finite Element Visualization of Fatigue Crack Closure in Plane Stress and Plane Strain", *Inter. J. of Fracture.*, **50**, 27-49, (1991-II)

McEvily, A. J. and Boettner R. C., "On Fatigue Crack Propagation In F.C.C Metals", *Acta Metallurgica*, **11**, 725-742, (1963).

Miller, K J., "Metal Fatigue--past, current, and future", *Proc Instn Mech Engrs*, **205**, (1991).

Mohan, R. , M. Ortiz, and C. F. Shih, "An Analysis of Cracks in Ductile Single Crystals-II. Mode I Loading", *J. Mech. Phys. Solids.*, **40**, 315- 337, (1992).

Morris, W. L. , "A Comparison of Microcrack Closure Load Development for Stage I and Stage II Cracking Events for Al 7075-T651", *Metallurgical Transactions A* , **8**, (1977).

Morris, W. L. and James, M. R., "Statistical Aspects of Fatigue Failure Due to Alloy Microstructure", *ASTM STP 811*, 179-206, (1983).

Mughrabi, H. "The Cyclic Hardening and Saturation Behavior of Copper Single Crystals". *Material Science and Engineering*, **33**, 207, (1978).

Neumann, P. "New Experiments Concerning the Slip Process at Propagating Fatigue Cracks-I", *Acta Metallurgica*, **22**, 1155-1165, (1974).

Paris, Paul C., "The Fracture Mechanics Approach to Fatigue". *Fatigue an Interdisciplinary Approach* , Proceeding, 10th Sagamore Army Materials Research Confrence, 107-132, (1964).

Pelloux, R. M. N, "Mechanisms of Formation of Ductile Fatigue Striations", *Transactions of the ASME*, **62**, 281-285, (1969).

Rice, James R. "Tensile Crack Tip Fields In Elastic-Plastic Crystals", *Mechanics of Materials.*, **6**, 317-335, (1987)

Ritchie, R. O., Suresh, S., and Moss, C. M., "Near-Threshold Fatigue Crack Growth in Cr-1Mo Pressure Vessel Steel in Air and Hydrogen.", *J. Eng. Mats. and Techn.* , **102**, 293-299, (1980).

Seeger, *In Dislocation and Mechanical Properties of Crystals.*, Wiley, 243,
(1957).

Sehitoglu, H. and R. C. McClung, "On the Finite Element Analysis of Fatigue Crack Closure-1. Basic Modeling Issues", *Engn. Fracture Mech.* **33**, 237-252, (1989).

Sehitoglu, H. and R. C. McClung, "On the Finite Element Analysis of Fatigue Crack Closure-2. Numerical Results", *Engn. Fracture Mech.* **33**, 253-272, (1989).

Sehitoglu, H. and Sun, Wei, "Mechanisms of Crack Closure in Plane Strain and in Plane Stress", *Third International Conference on Biaxial/Multiaxial Fatigue*, Stuttgart, FRG (1989).

Sehitoglu, H. and Sun, Wei, "Modeling of Plane Strain Fatigue Crack Closure", *J. Eng. Materials Tech.*, **113**, 31-40, (1991).

Taylor, G. I. Plastic Strain in Metals. *J. Inst. Met.* **62**, 307-325, (1938a).

Taylor, G. I. "Analysis of plastic strain in a cubic crystal". *In: Stephen Timoshenko 60th Anniversary Volume.* Macmillan, New York, (1938b).

Tanaka, K. "Mechanics and Micromechanics of Fatigue Crack Propagation" *Fracture Mechanics: Perspectives and Directions (Twentieth Symposium), ASTM STP 1020.* R.P. Wei and R.P. Gangloff, Eds., American Society for Testing and Materials, Philadelphia, 151-183, (1989).

Tokaji, K., Ogawa, T., Osako, S., Harada, Y., "The Growth Behavior of Small Fatigue Cracks; The effect of Microstructure and Crack Closure", *Fatigue 87'*, Vol I, 313-322, (1987).

Tomkins, B. "Fatigue Crack Propagation-An Analysis". (1968)

Winter, A.T. *Philos. Mag.*, **30**, 719, (1974).

Appendix A: Plastic Zone Plots

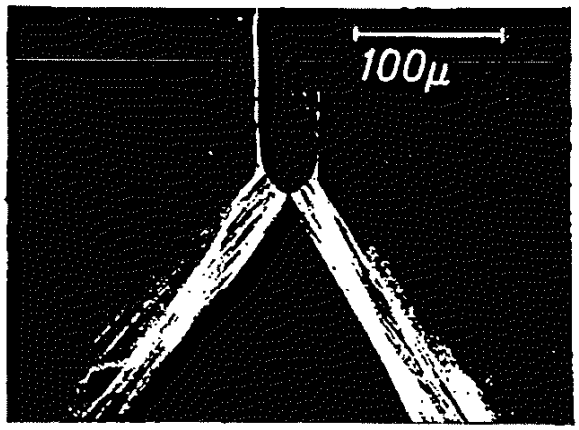

Figure a: SEM micrograph of slip lines in copper crystals from Neumann [1974]. Previous slip lines were etched out to demonstrate that slip occurs exclusively at the crack tip. Note that two macroscopic slip planes at the tip are active, and that a slip free triangular zone forms.

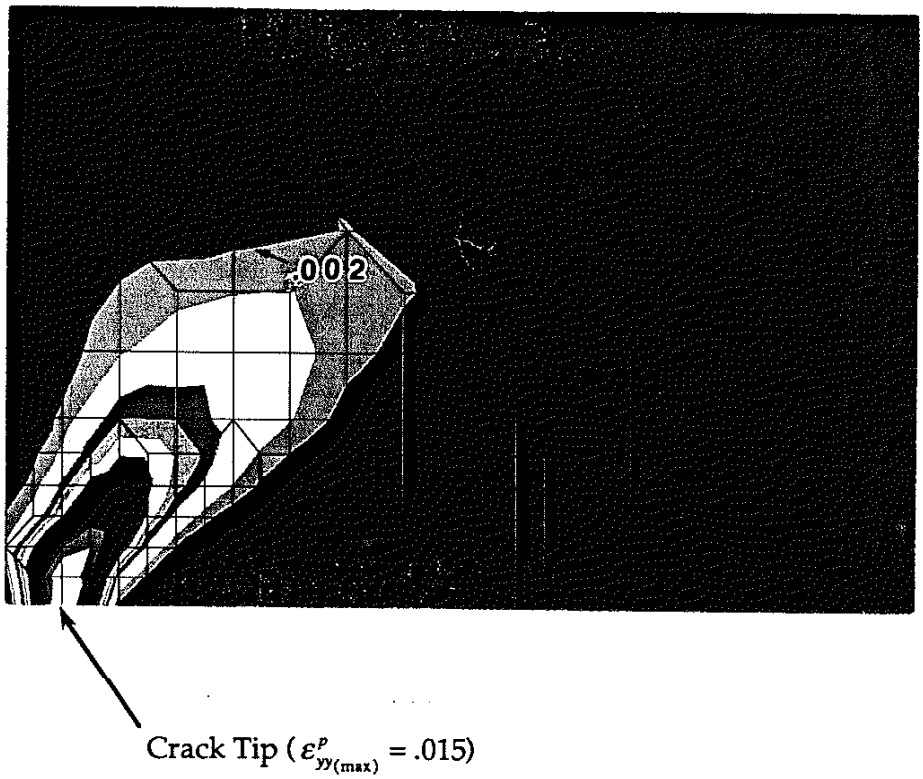

Figure b: Plastic zone plot for the case where Θ = 37.5° and ϕ = 0°. The plot is for the CT specimen at maximum load (Increment 20/800). Note that two slip planes at the tip are active (recall crack line symmetry), and that a slip free triangular zone forms ahead of the crack tip. The outermost contour represents a plastic strain of .002, and the maximum strain is .015.

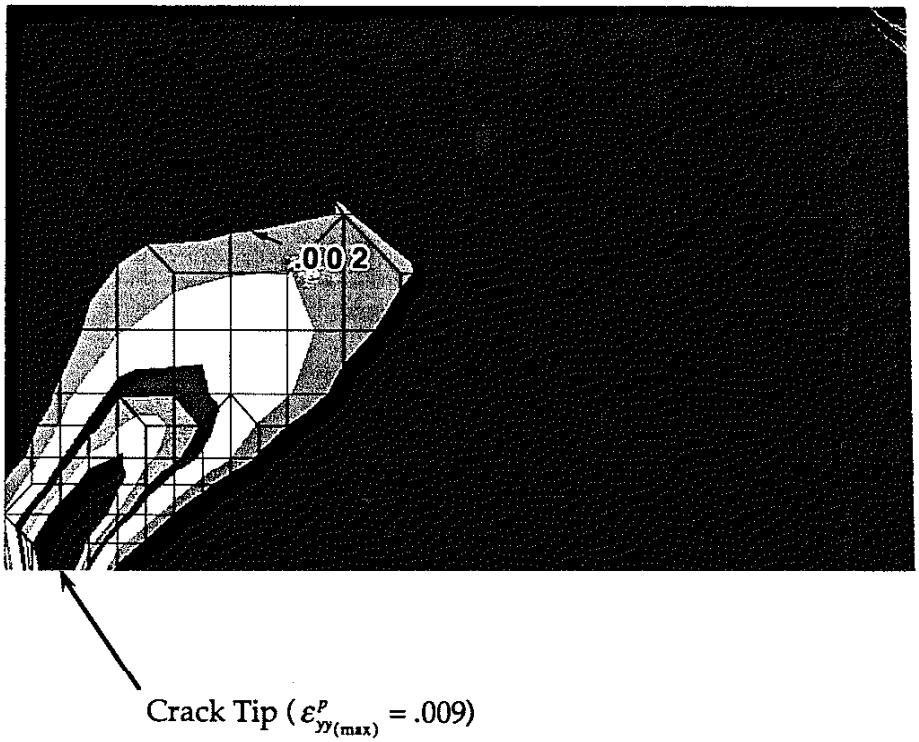

Figure c: Plastic zone plot for the case where Θ = 37.5° and ϕ = 0°. The plot is for the CT specimen at minimum load (Increment 40/800). Note that two slip planes at the tip are active (recall crack line symmetry), and that a slip free triangular zone forms ahead of the crack tip. The outermost contour represents a plastic strain of .002, and the maximum strain is .009.

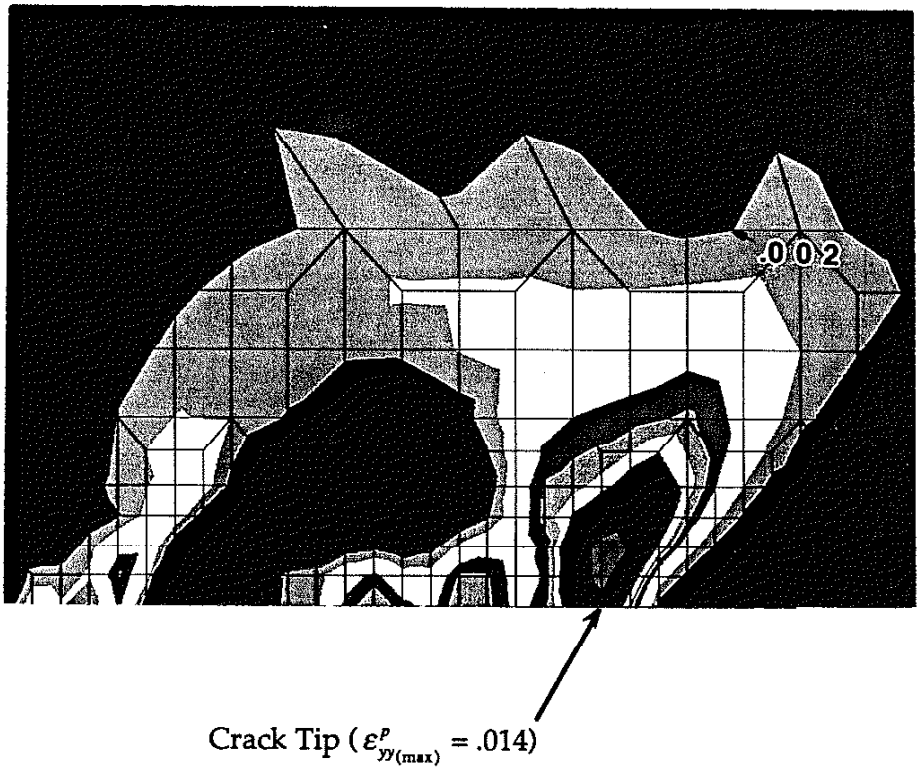

Figure d: Plastic zone plot for the case where $\Theta = 37.5^{\circ}$ and $\phi = 0^{\circ}$. The plot is for the CT specimen at maximum load (Increment 780/800). Note that two slip planes at the tip are active (recall crack line symmetry), and that a slip free triangular zone forms ahead of the crack tip. The outermost contour represents a plastic strain of .002, and the maximum strain is .014.

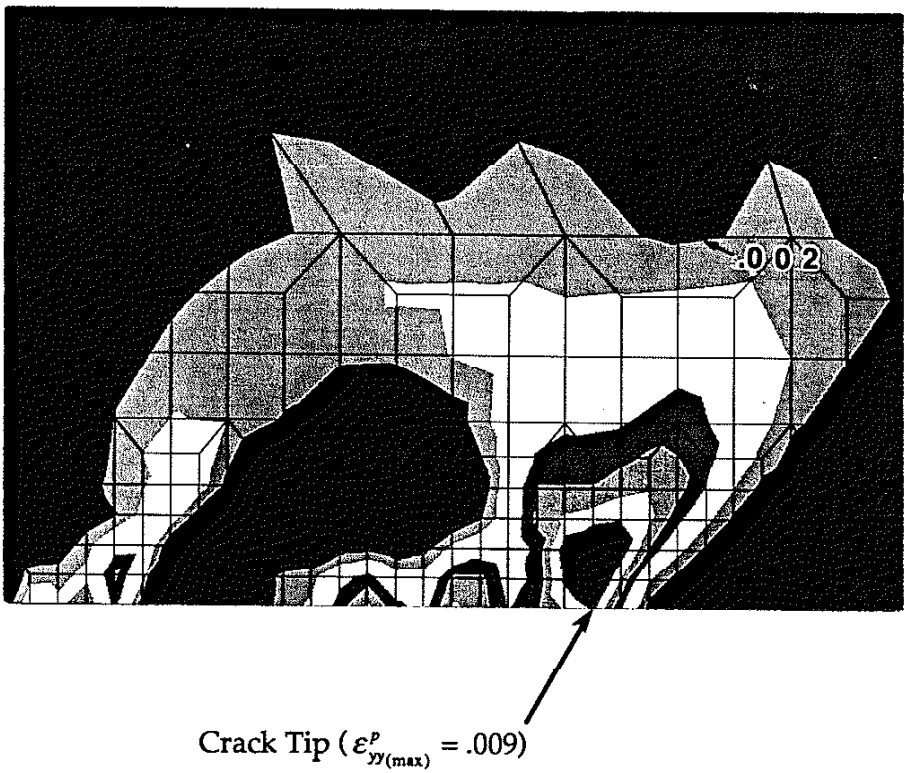

Figure e: Plastic zone plot for the case where $\Theta = 37.5°$ and $\phi = 0°$. The plot is for the CT specimen at minimum load (Increment 800/800). Note that two slip planes at the tip are active (recall crack line symmetry), and that a slip free triangular zone forms ahead of the crack tip. The outermost contour represents a plastic strain of .002, and the maximum strain is .009.

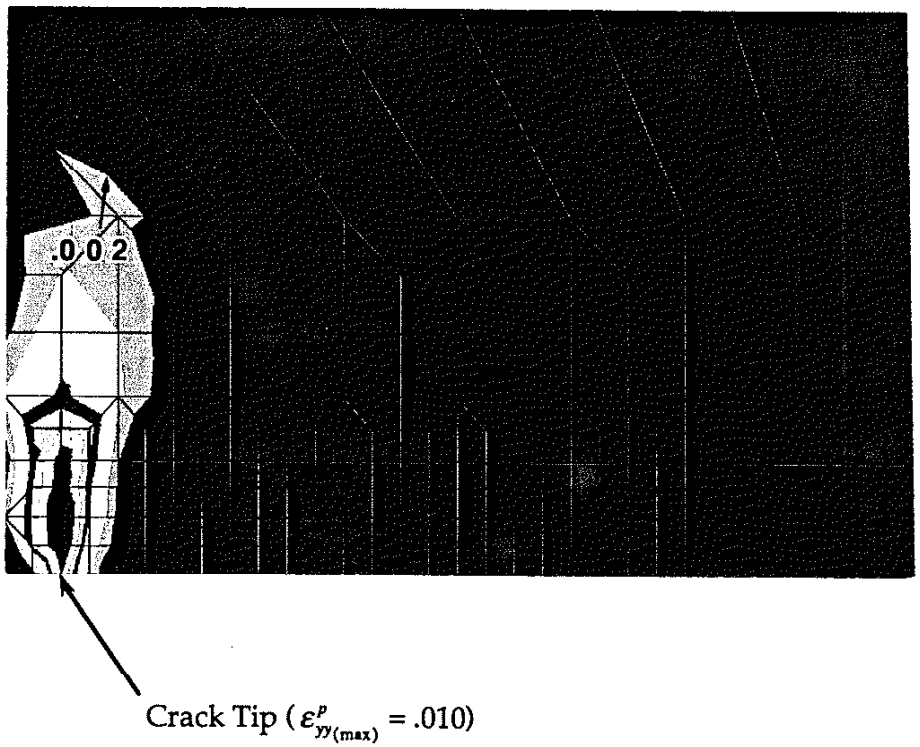

Figure f: Plastic zone plot for the case where $\Theta = 12^{\circ}$ and $\phi = 0^{\circ}$. The plot is for the CT specimen at maximum load (Increment 20/800). Note that two slip planes at the tip are active (recall crack line symmetry). The slip free triangular zone is not as clear since the slip planes are nearly vertical. The outermost contour represents a plastic strain of .002, and the maximum strain is .010.

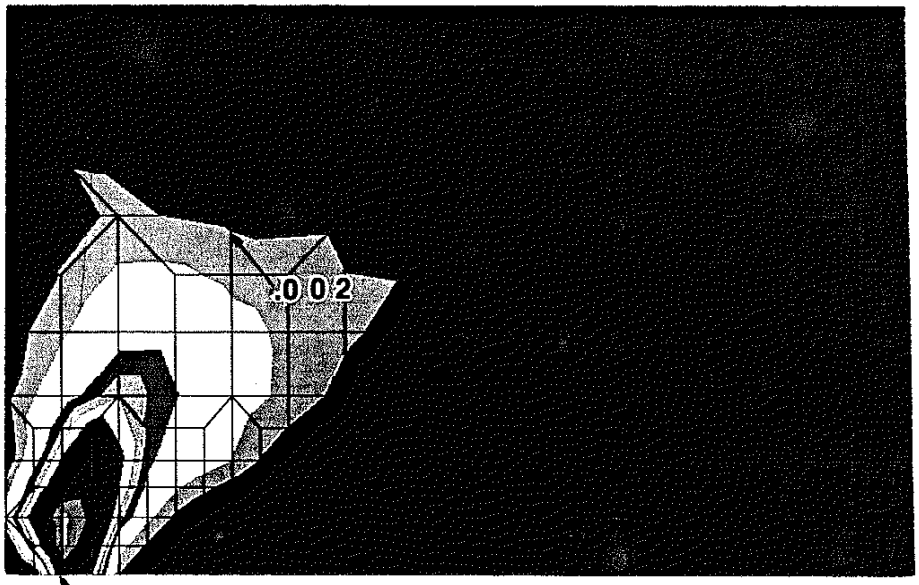

Figure g: Plastic zone plot for the case where $\Theta = 30^{\circ}$ and $\phi = 0^{\circ}$. The plot is for the CT specimen at maximum load (Increment 20/800). Note that two slip planes at the tip are active (recall crack line symmetry), and that a slip free triangular zone forms at the crack tip. The outermost contour represents a plastic strain of .002, and the maximum strain is .015.

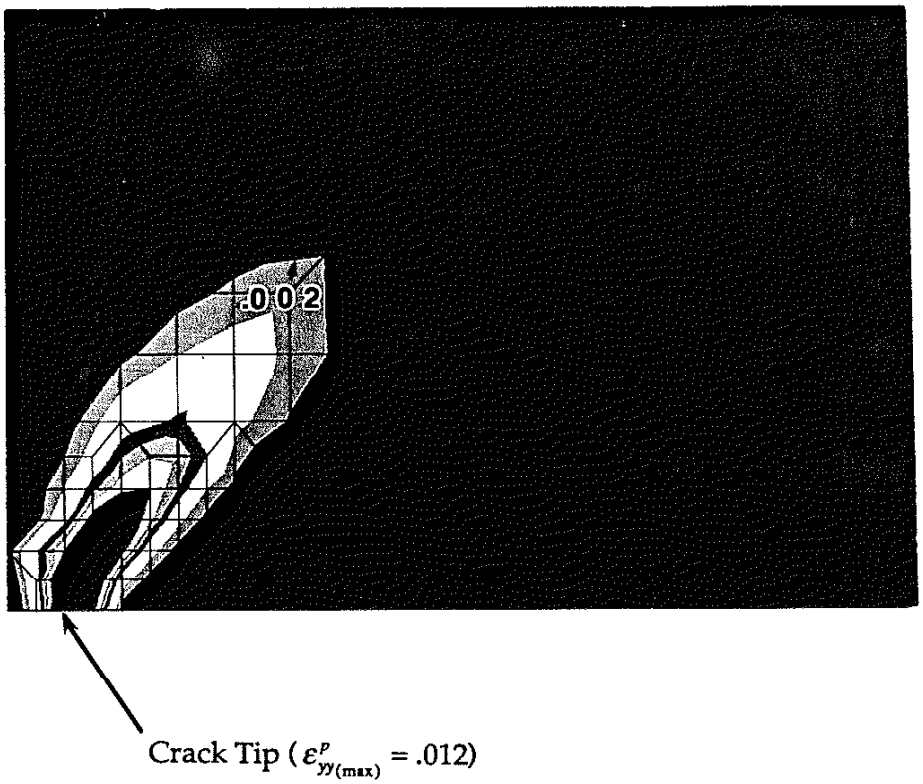

Figure h: Plastic zone plot for the case where Θ = 45° and ϕ = 0°. The plot is for the CT specimen at maximum load (Increment 20/800). Note that two slip planes at the tip are active (recall crack line symmetry), and that a slip free triangular zone forms ahead of the crack tip. The outermost contour represents a plastic strain of .002, and the maximum strain is .012.

Appendix B: Additional CT Specimen Plots

B.1 Crack opening displacements

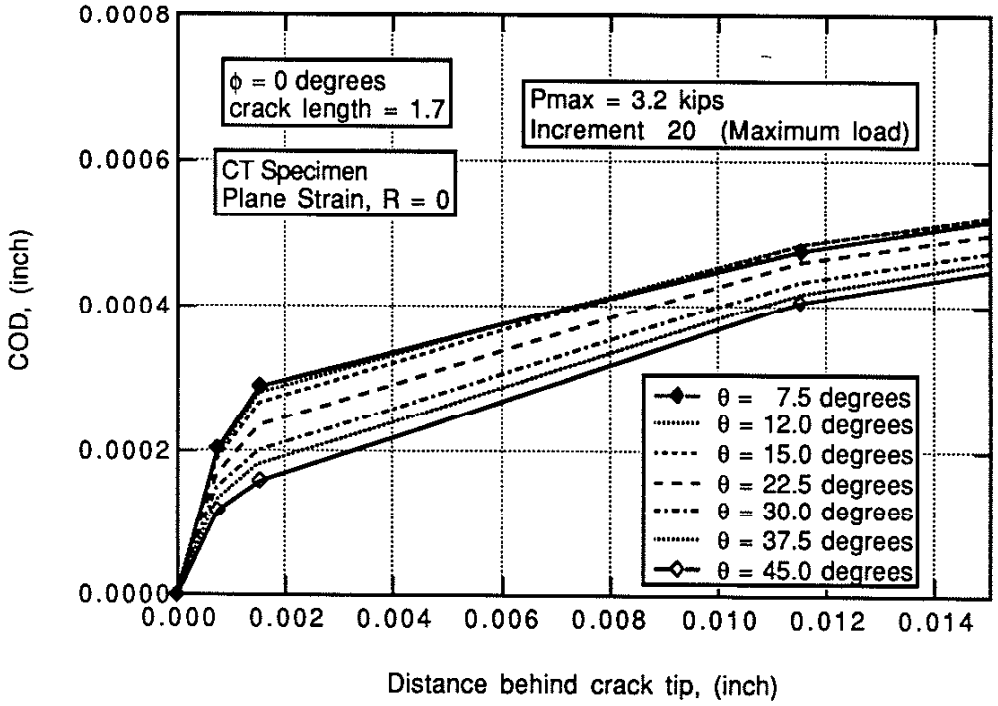

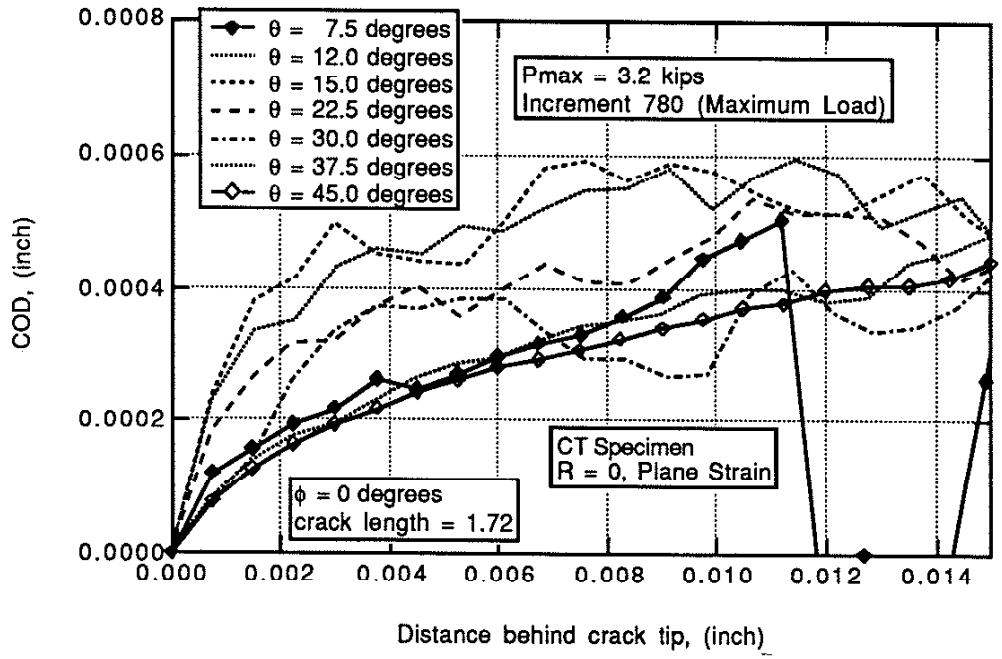

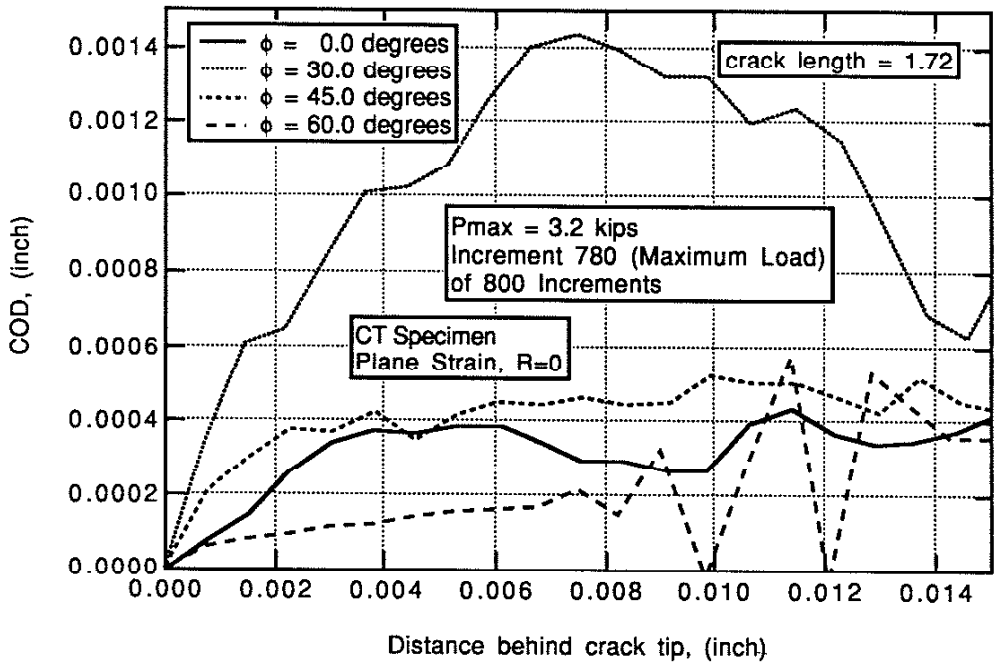

B.2 Stress Strain Plots

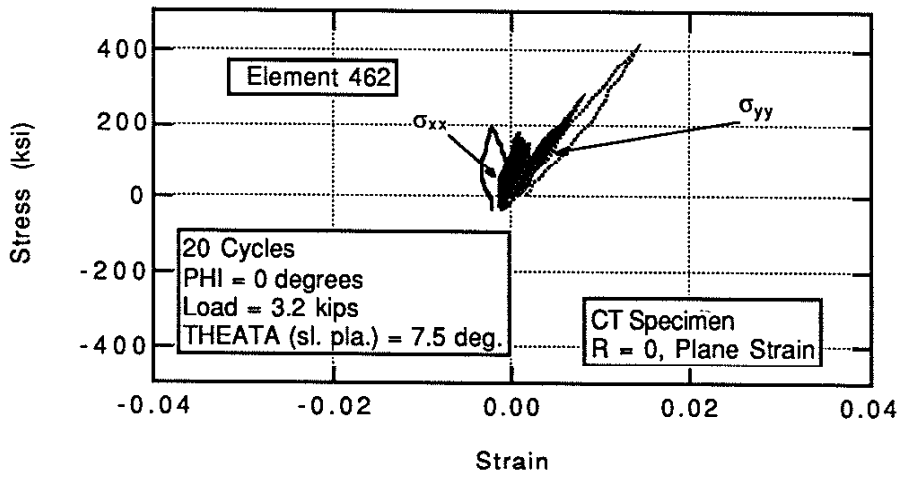

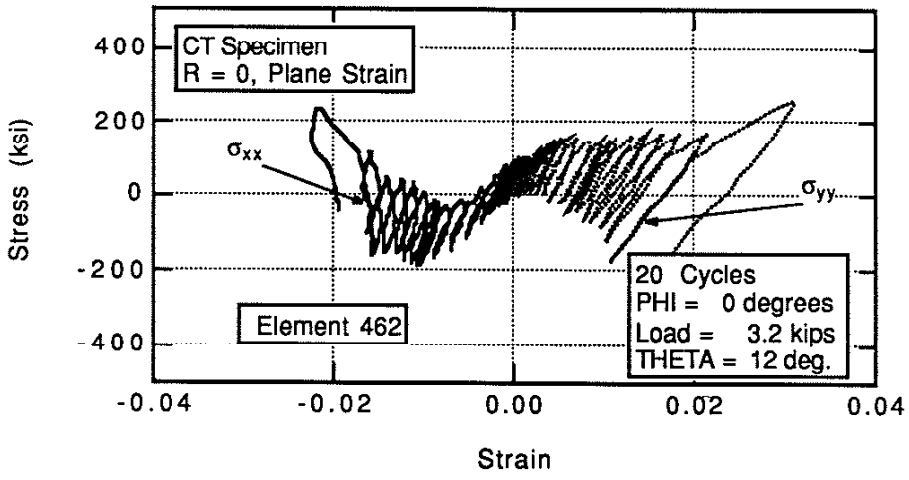
CT Specimen
R = 0, Plane Strain
σ_{xx}
σ_{yy}
20 Cycles
PHI = 0 degrees
Load = 3.2 kips
THETA = 12 deg.
Element 462
400
200
0
-200
-400
-0.04
-0.02
0.00
0.02
0.04
Stress (ksi)
Strain

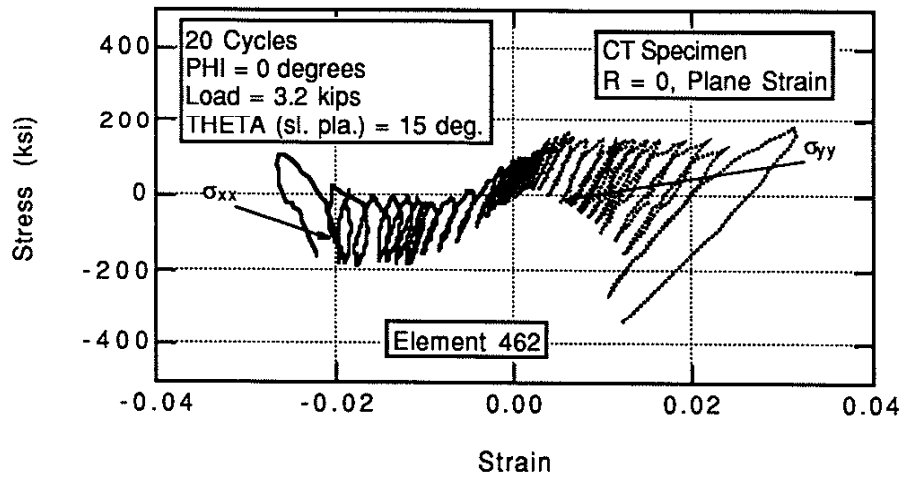
20 Cycles
PHI = 0 degrees
Load = 3.2 kips
THETA (sl. pla.) = 15 deg.
CT Specimen
R = 0, Plane Strain
σ_{xx}
σ_{yy}
Element 462
400
200
0
-200
-400
-0.04
-0.02
0.00
0.02
0.04
Stress (ksi)
Strain

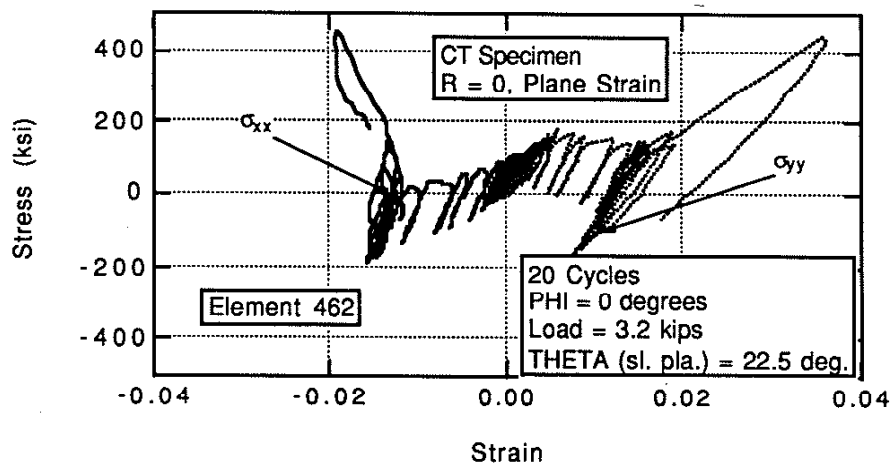
CT Specimen
R = 0, Plane Strain
σ_{xx}
σ_{yy}
Element 462
20 Cycles
PHI = 0 degrees
Load = 3.2 kips
THETA (sl. pla.) = 22.5 deg.
400
200
0
-200
-400
-0.04
-0.02
0.00
0.02
0.04
Stress (ksi)
Strain

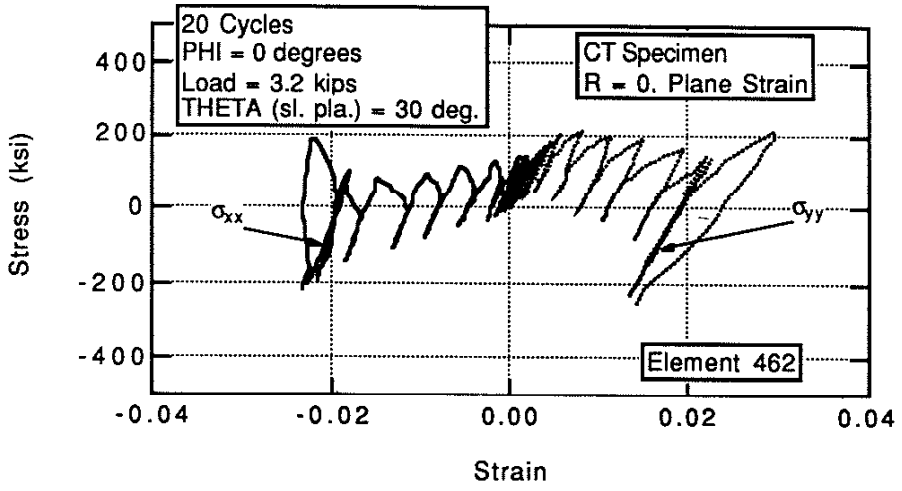
20 Cycles
PHI = 0 degrees
Load = 3.2 kips
THETA (sl. pla.) = 30 deg.
CT Specimen
R = 0. Plane Strain
Element 462
σ_{xx}
σ_{yy}
Stress (ksi)
Strain
400
200
0
-200
-400
-0.04
-0.02
0.00
0.02
0.04

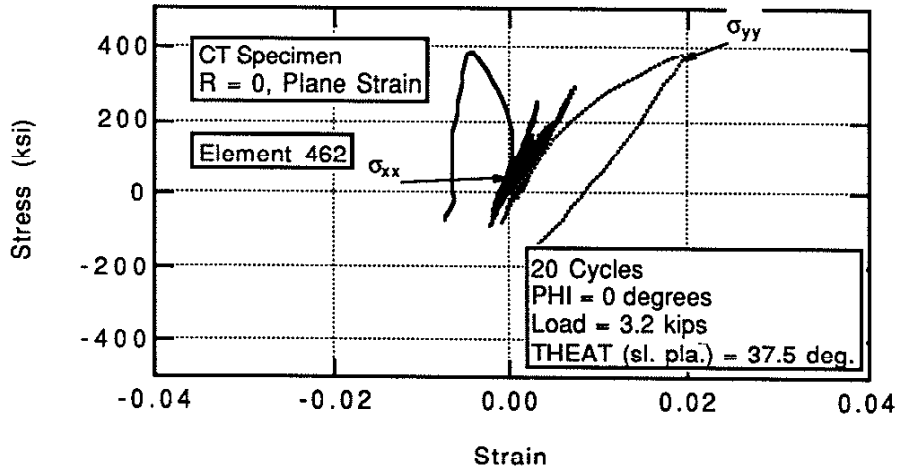
CT Specimen
R = 0, Plane Strain
Element 462
σ_{xx}
σ_{yy}
20 Cycles
PHI = 0 degrees
Load = 3.2 kips
THEAT (sl. pla.) = 37.5 deg.
Stress (ksi)
Strain
400
200
0
-200
-400
-0.04
-0.02
0.00
0.02
0.04

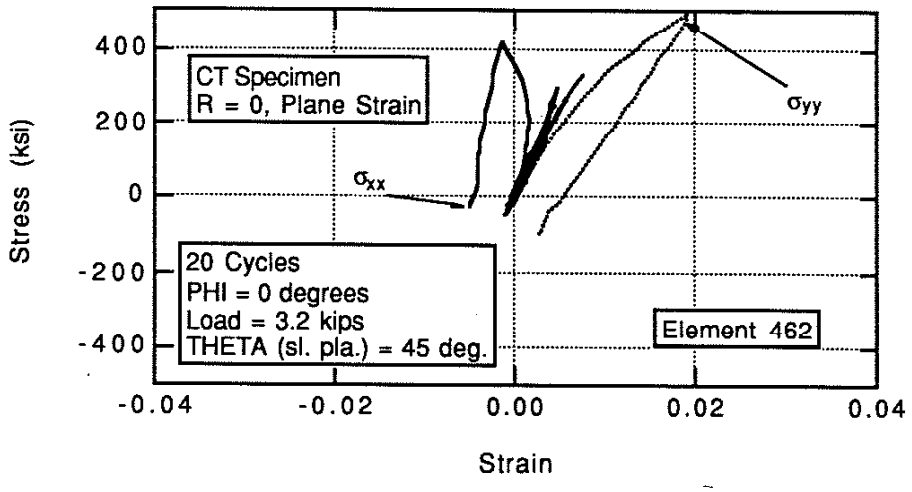
CT Specimen
R = 0, Plane Strain
σ_{xx}
σ_{yy}
20 Cycles
PHI = 0 degrees
Load = 3.2 kips
THETA (sl. pla.) = 45 deg.
Element 462
Stress (ksi)
Strain
400
200
0
-200
-400
-0.04
-0.02
0.00
0.02
0.04

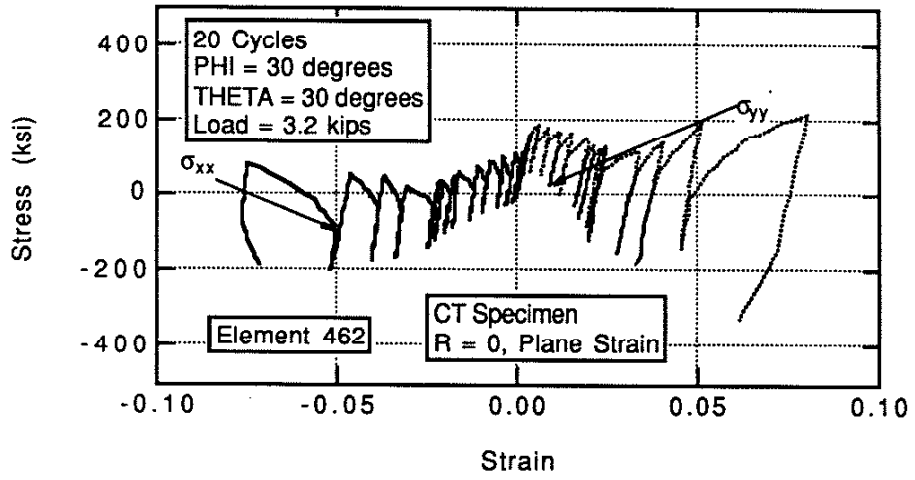
20 Cycles
PHI = 30 degrees
THETA = 30 degrees
Load = 3.2 kips
σ_{xx}
σ_{yy}
Element 462
CT Specimen
R = 0, Plane Strain
400
200
0
-200
-400
-0.10
-0.05
0.00
0.05
0.10
Stress (ksi)
Strain

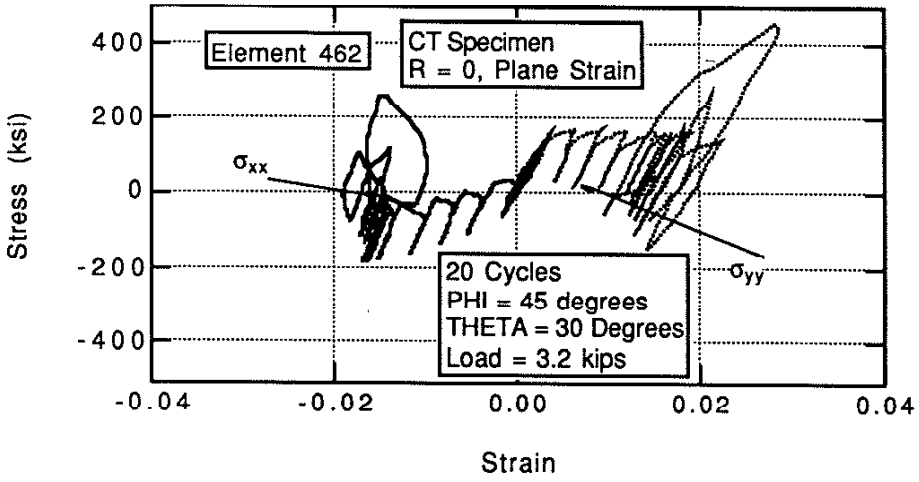
Element 462
CT Specimen
R = 0, Plane Strain
σ_{xx}
σ_{yy}
20 Cycles
PHI = 45 degrees
THETA = 30 Degrees
Load = 3.2 kips
400
200
0
-200
-400
-0.04
-0.02
0.00
0.02
0.04
Stress (ksi)
Strain

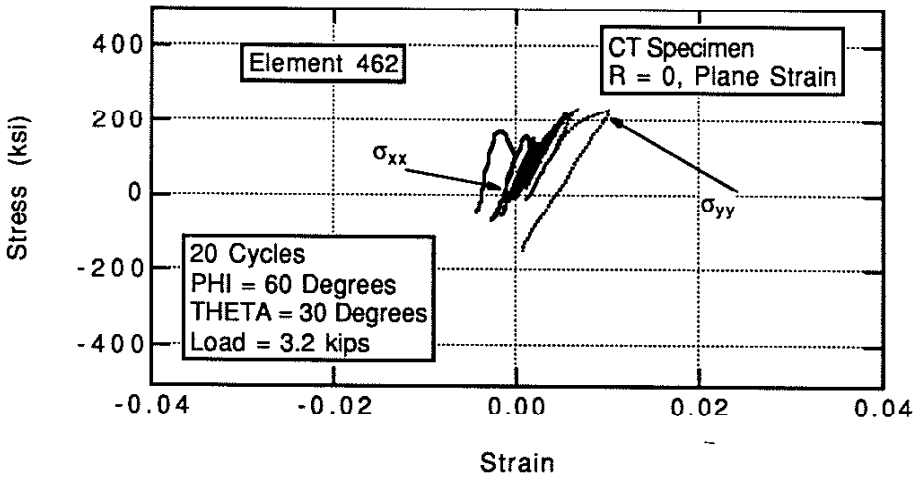

B.3 Plastic Zones

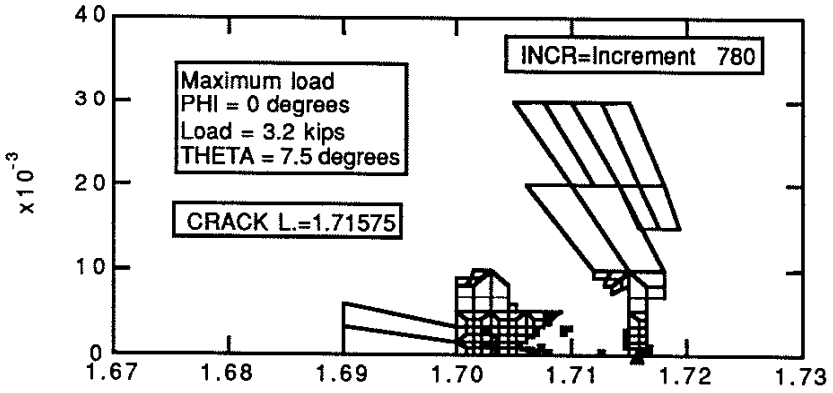

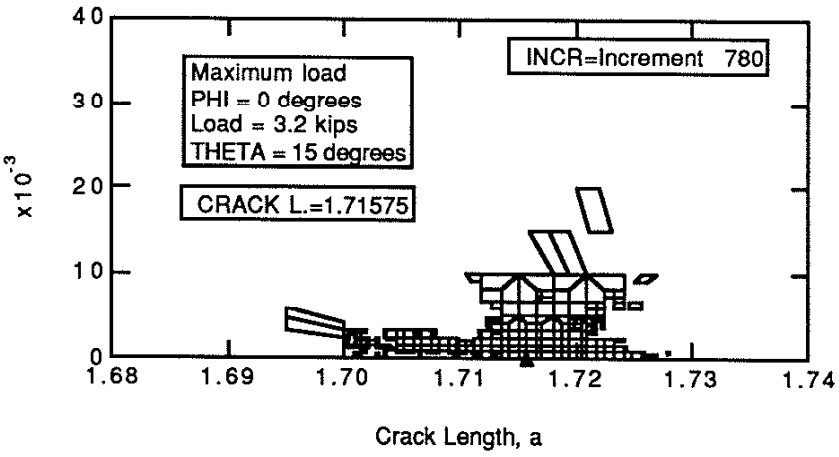

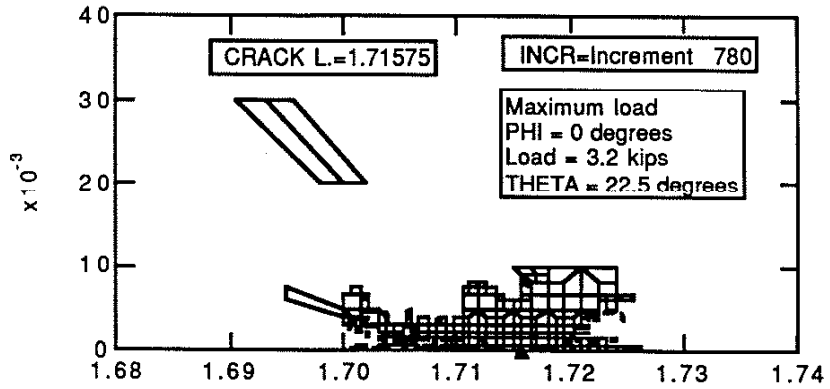
CRACK L.=1.71575
INCR=Increment 780
Maximum load
PHI = 0 degrees
Load = 3.2 kips
THETA = 22.5 degrees
x10^-3
40
30
20
10
0
1.68
1.69
1.70
1.71
1.72
1.73
1.74
Crack Length, a

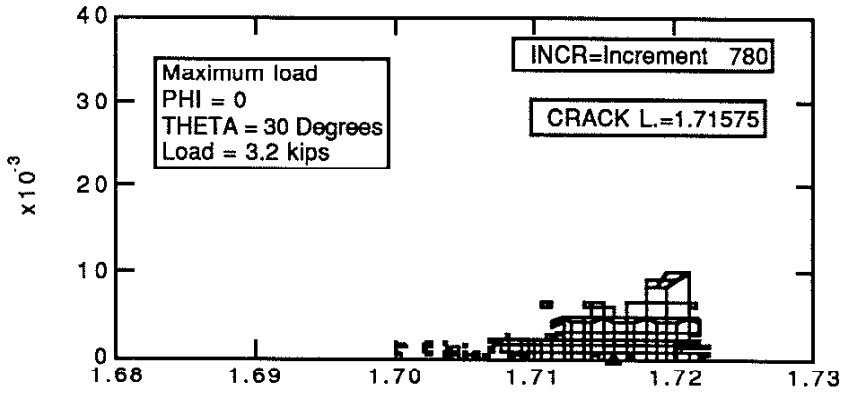
Maximum load
PHI = 0
THETA = 30 Degrees
Load = 3.2 kips
INCR=Increment 780
CRACK L.=1.71575
x10^-3
40
30
20
10
0
1.68
1.69
1.70
1.71
1.72
1.73
Crack Length, a

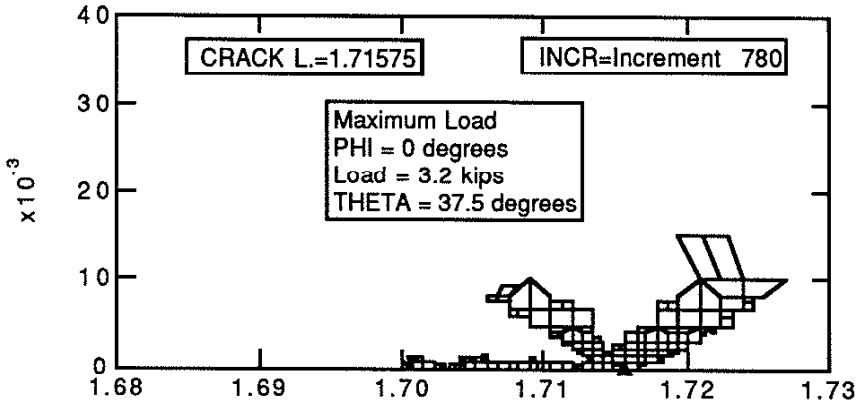
CRACK L.=1.71575
INCR=Increment 780
Maximum Load
PHI = 0 degrees
Load = 3.2 kips
THETA = 37.5 degrees
x10^-3
40
30
20
10
0
1.68
1.69
1.70
1.71
1.72
1.73
Crack Length, a

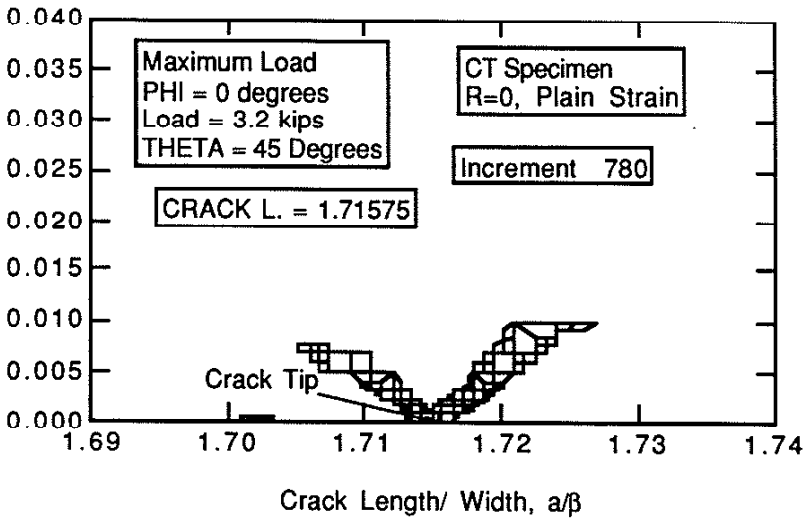
0.040
0.035
0.030
0.025
0.020
0.015
0.010
0.005
0.000
1.69
1.70
1.71
1.72
1.73
1.74
Maximum Load
PHI = 0 degrees
Load = 3.2 kips
THETA = 45 Degrees
CT Specimen
R=0, Plain Strain
Increment 780
CRACK L. = 1.71575
Crack Tip
Crack Length/ Width, a/β

Appendix C: Additional CCP Specimen Plots

C.1 Crack Opening Displacements

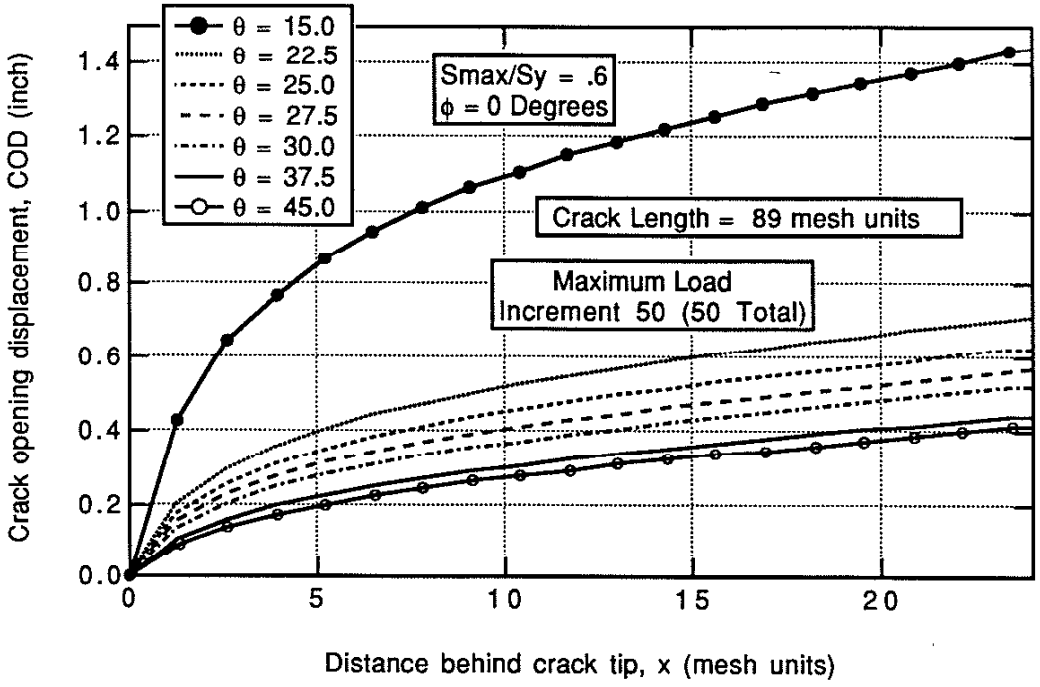

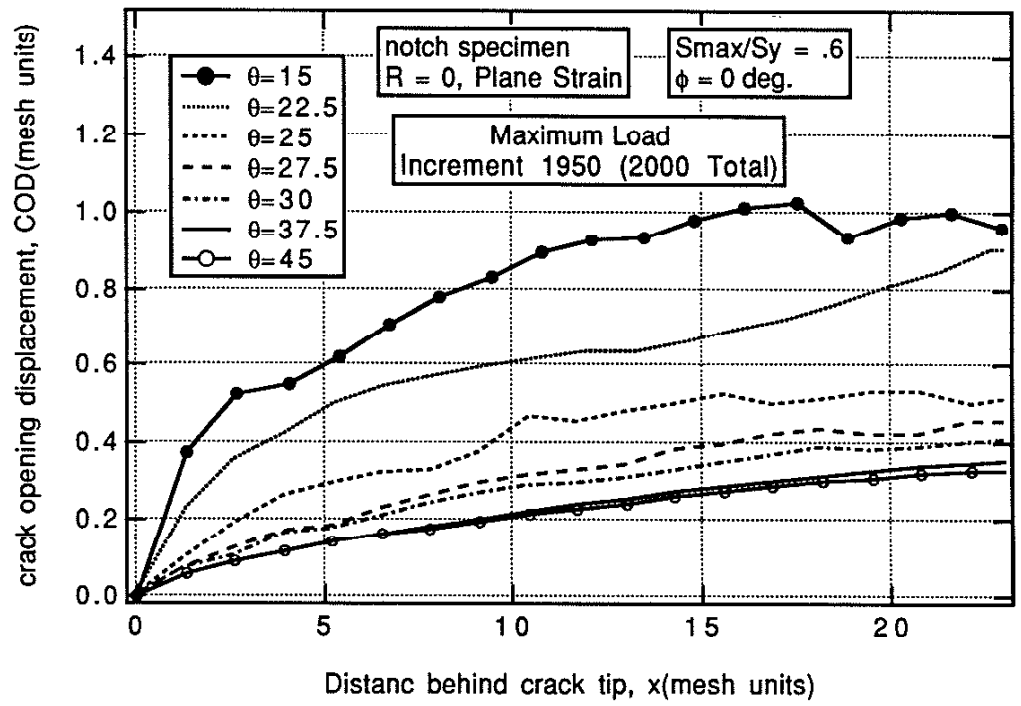

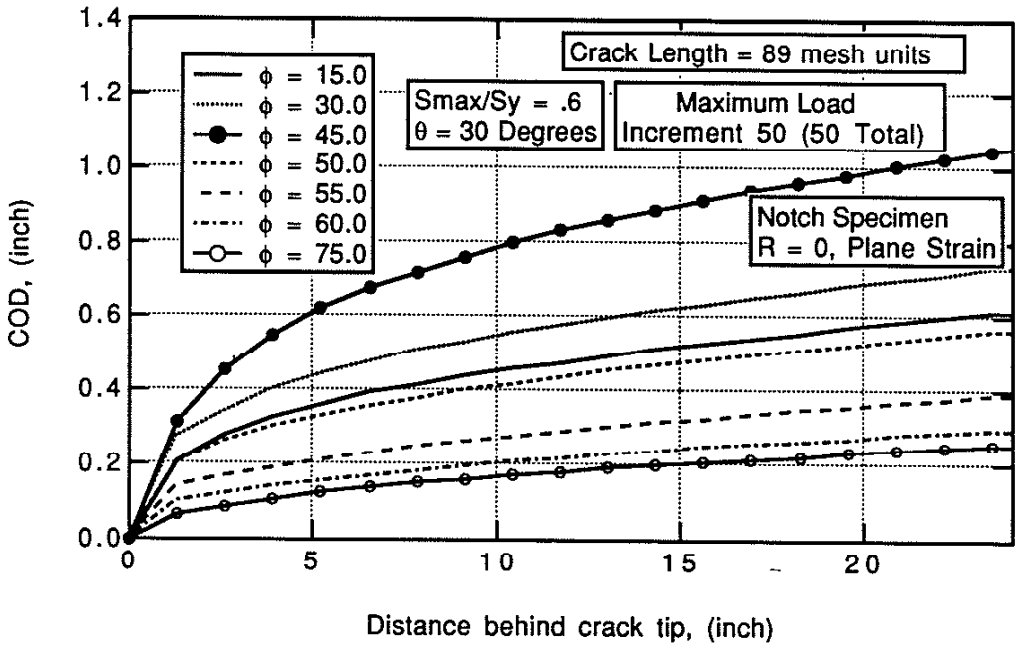
Crack Length = 89 mesh units
ϕ = 15.0
ϕ = 30.0
ϕ = 45.0
ϕ = 50.0
ϕ = 55.0
ϕ = 60.0
ϕ = 75.0
Smax/Sy = .6
θ = 30 Degrees
Maximum Load
Increment 50 (50 Total)
Notch Specimen
R = 0, Plane Strain
COD, (inch)
Distance behind crack tip, (inch)

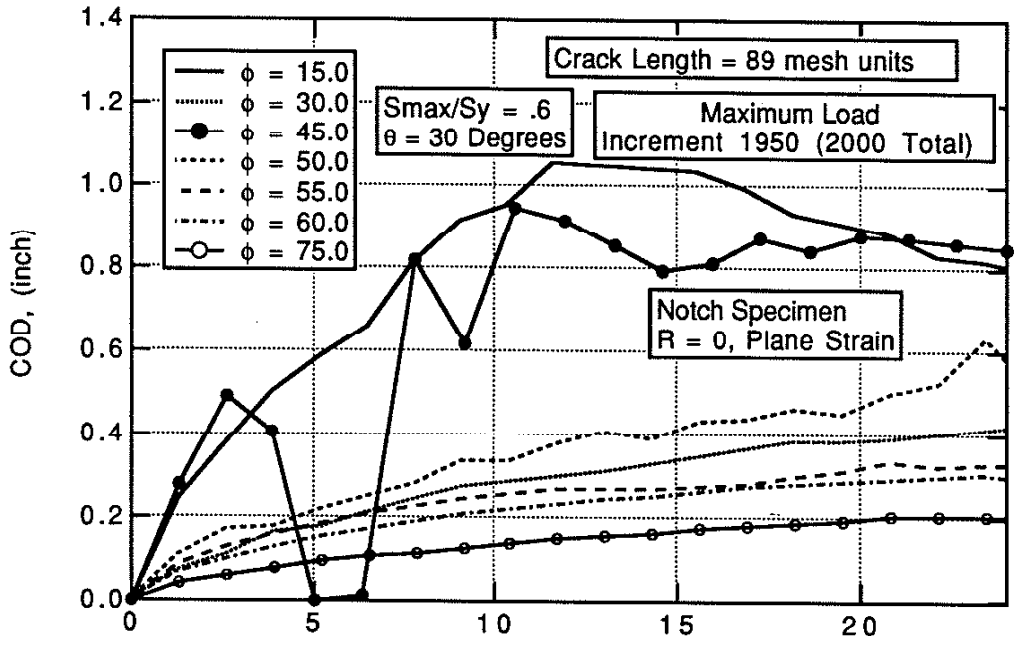
Crack Length = 89 mesh units
ϕ = 15.0
ϕ = 30.0
ϕ = 45.0
ϕ = 50.0
ϕ = 55.0
ϕ = 60.0
ϕ = 75.0
Smax/Sy = .6
θ = 30 Degrees
Maximum Load
Increment 1950 (2000 Total)
Notch Specimen
R = 0, Plane Strain
COD, (inch)
Distance behind crack tip, (inch)

C.2 Stress Strain Plots

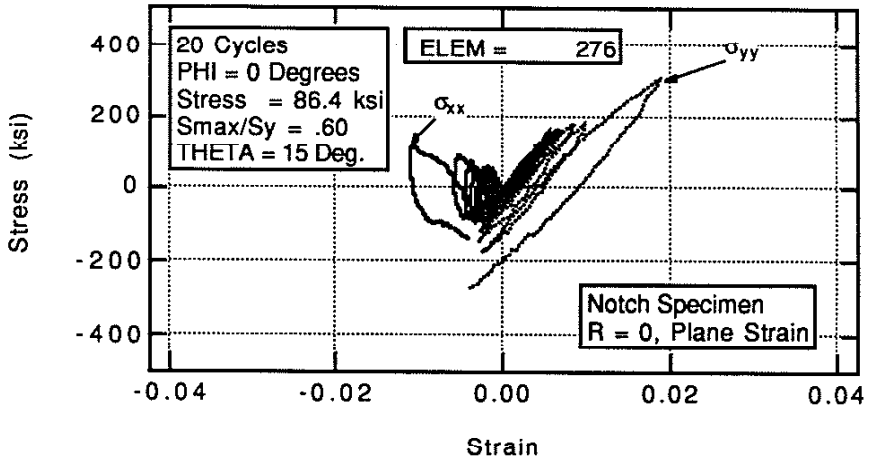

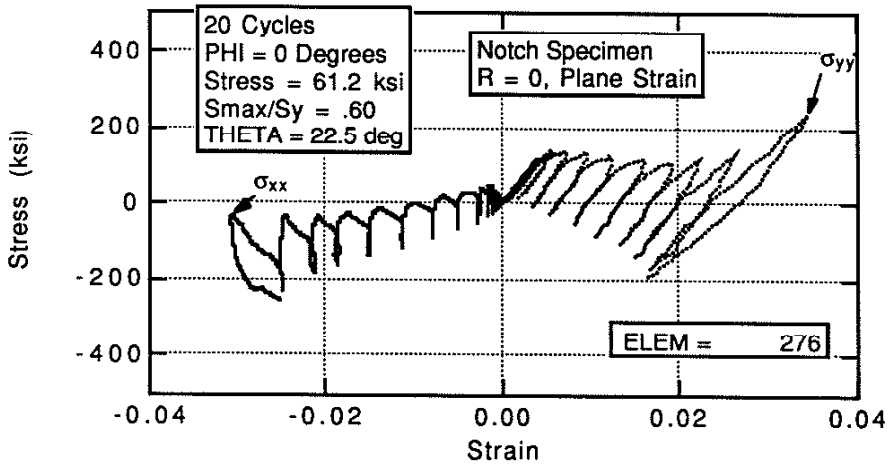

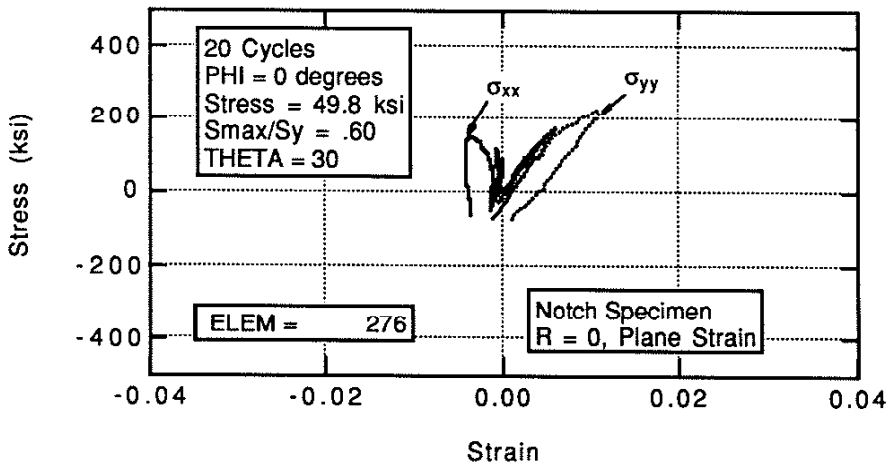

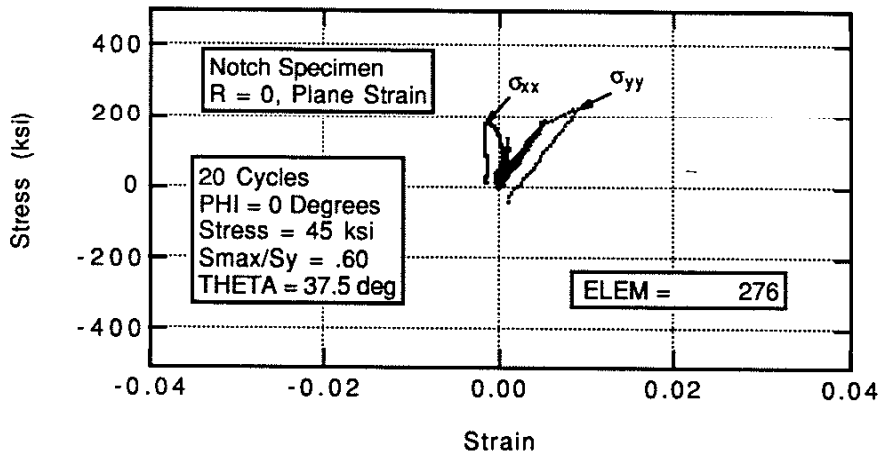
Notch Specimen
R = 0, Plane Strain
20 Cycles
PHI = 0 Degrees
Stress = 45 ksi
Smax/Sy = .60
THETA = 37.5 deg
ELEM = 276
σxx
σyy
Stress (ksi)
Strain
400
200
0
-200
-400
-0.04
-0.02
0.00
0.02
0.04

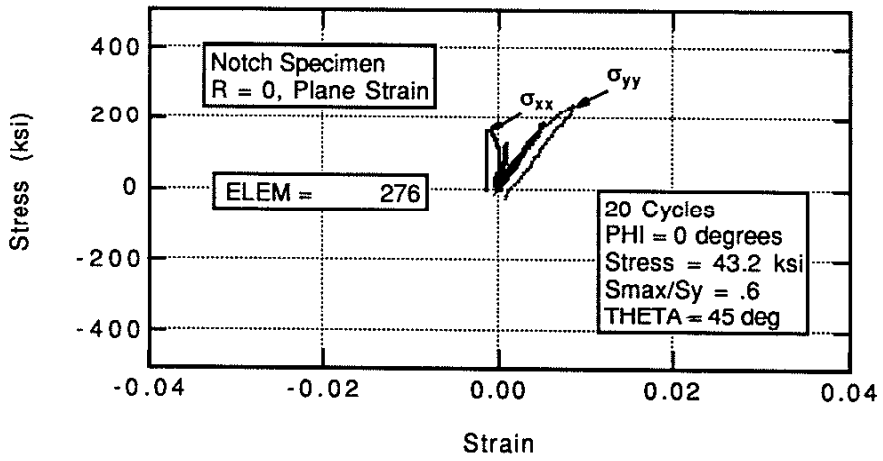
Notch Specimen
R = 0, Plane Strain
ELEM = 276
20 Cycles
PHI = 0 degrees
Stress = 43.2 ksi
Smax/Sy = .6
THETA = 45 deg
σxx
σyy
Stress (ksi)
Strain
400
200
0
-200
-400
-0.04
-0.02
0.00
0.02
0.04

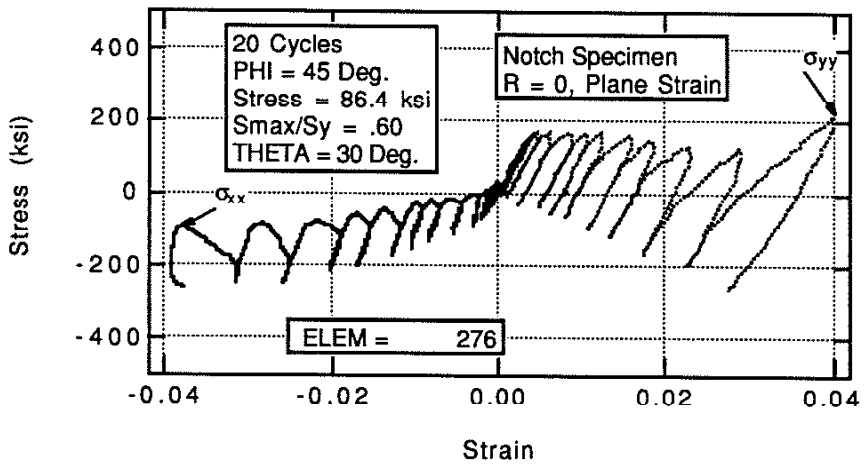
20 Cycles
PHI = 45 Deg.
Stress = 86.4 ksi
Smax/Sy = .60
THETA = 30 Deg.
Notch Specimen
R = 0, Plane Strain
ELEM = 276
σxx
σyy
Stress (ksi)
Strain
400
200
0
-200
-400
-0.04
-0.02
0.00
0.02
0.04